

# **The Role of Protein Aggregation in Huntington's Disease**

**Claire Martina Didszun**

This thesis was submitted for the degree of Doctor of Philosophy  
at the University of Leicester in April 2009.

The experimental work was carried out at the Medical Research Council  
Toxicology Unit in Leicester between October 2001 and March 2005.

## Abstract

Huntington's disease (HD) is a hereditary progressive neurodegenerative disorder characterised by chorea, general motor impairment, psychiatric disturbances and dementia, leading to death within 10 to 20 years of onset. It is caused by a (CAG)<sub>n</sub> trinucleotide repeat expansion in the gene *IT15* that is translated into a prolonged polyglutamine tract in the protein huntingtin. This mutation leads to the self-association of huntingtin to form aggregates in the brains of affected people.

Work in Professor Nicotera's group at the MRC Toxicology Unit identified expression changes in Rab11, a protein involved in endosomal recycling, in a cell culture model of HD. The aim of this thesis was to investigate whether endosomal recycling is affected in this model. Monitoring the trafficking of labelled transferrin by Western blotting and live-cell imaging showed rapid uptake of transferrin into all cells, but a significantly reduced rate of clearance in cells containing huntingtin aggregates, which was associated with the accumulation of transferrin in the endosomal recycling compartment (ERC). This finding demonstrates an aggregate-specific lesion in the exit of cargo from the ERC in the absence of cell death. As endosomal recycling is essential for correct neuronal function, this process provides a mechanism whereby protein inclusions may contribute to the cognitive and motor deficits seen in HD.

A second project focused on purification of aggregates to determine if they could sequester material important for cellular function. Many attempts to purify the aggregates in their intact globular form revealed their highly unspecific affinity towards other proteins, which renders purification methods very susceptible to artefacts. The large globular aggregates could, however, be dispersed by SDS-treatment into fibrils of approximately 10 nm diameter, which were subsequently purified and visualised by electron microscopy.

## **Acknowledgements**

Above all, I am obliged to Prof. Pierluigi Nicotera for allowing me to work in his group and providing the most excellent research facilities. Moreover I would like to thank him for giving me the opportunity to participate in various scientific courses and meetings.

I am extremely grateful to Dr. Paul Richards for his supervision of my work and his patience and support over the last difficult years.

Furthermore, I am indebted to Dr. David Rubinsztein for kindly giving us the cell lines on which this work has been carried out.

I would like to acknowledge the work that Anna Simpson and Barbara Horley have contributed to this project. My special thanks go to Anna Simpson for her creative technical help, invaluable proof-reading services, constant moral support, good humour and friendship.

Moreover, I would like to express my gratitude to Dr. Chris Guerin and Dr. Kenneth Young for their excellent advice on confocal microscopy and siRNA techniques. Many thanks also to Dr. David Dinsdale who carried out the electron microscopy work in this project.

I am grateful for the opportunity to participate in several scientific meetings which were part of the EU concerted action 'Early pathogenetic markers for slow neurodegenerative diseases'.

Finally, I would like to offer my deepest thanks to my friends and family who never stopped caring for me and supporting me during these years with long telephone conversations, emails, visits, postcards, letters and chocolate packages.

# Table of Contents

## 1 Introduction

### 1.1 Huntington's Disease

#### 1.1.1 Genetics

#### 1.1.2 Pathology

#### 1.1.3 Huntingtin

### 1.2 Pathogenic Mechanisms in Huntington's Disease

#### 1.2.1 Loss-of-function Mechanisms

#### 1.2.2 Gain-of-function Mechanisms

### 1.3 Endosomal Recycling

### 1.4 Aims

## 2 Material and Methods

### 2.1 Materials

#### 2.1.1 Antibodies

#### 2.1.2 Transferrin

#### 2.1.3 Chemicals

### 2.2 Methods

#### 2.2.1 Cell Culture

#### 2.2.2 Collagen IV Coating

#### 2.2.3 SDS-PAGE

#### 2.2.4 Western Blotting

#### 2.2.5 Filter Retardation Assay

#### 2.2.6 MTS Viability Assay

#### 2.2.7 Immunocytochemistry

#### 2.2.8 Transferrin Recycling

#### 2.2.9 Live Cell Imaging

#### 2.2.10 Rab11 Overexpression

#### 2.2.11 Rab11 siRNA

#### 2.2.12 Density Gradient Centrifugation

#### 2.2.13 Solubilisation of Aggregates

#### 2.2.14 2-Dimensional Electrophoresis

#### 2.2.15 Immunomagnetic Separation

### 3 Results

#### 3.1 PC12 Cell Culture Model of Huntington's Disease

##### 3.1.1 Aggregate Formation

##### 3.1.2 Cell Viability and Apoptosis

#### 3.2 Effects of GFP-HttEx1 Aggregates on Endosomal Recycling

##### 3.2.1 Endosomal Recycling, ERC and Rab11

##### 3.2.2 Uptake of Transferrin

##### 3.2.3 Extrusion of Transferrin

##### 3.2.4 Flux of Transferrin through the ERC

##### 3.2.5 siRNA Silencing of Rab11a and Rab11b

##### 3.2.6 Effect of Rab11 Silencing on Transferrin Recycling

##### 3.2.7 Immunocytochemistry of Microtubules

#### 3.3 Purification of GFP-HttEx1 Aggregates

##### 3.3.1 Gradient Centrifugation

##### 3.3.2 Immunomagnetic Separation

##### 3.3.3 Purification of Fibrils

### 4 Discussion

#### 4.1 Effect of Huntingtin Aggregates on Endosomal Recycling

#### 4.2 Purification of Huntingtin Aggregates

### 5 References

## Abbreviations

AMPA	$\alpha$ -amino-3-hydroxyl-5-methyl-4-isoxazole-propionate
AP-2	adaptor protein 2
ASK1	apoptosis signal-regulating kinase 1
BDNF	brain-derived neurotrophic factor
BSA	bovine serum albumin
CBP	CREB binding protein
CHIP	C-terminal Hsp70-interacting protein
CNS	central nervous system
CRE	cyclic AMP response element
CREB	cyclic AMP response element binding protein
Da	Dalton
DMEM	Dulbecco's modified Eagle medium
DMSO	dimethylsulfoxide
DMT1	divalent metal transporter 1
DNA	deoxyribonucleic acid
Dox	doxycycline
DRPLA	dentatorubral pallidoluysian atrophy
DTT	dithiothreitol
ec	extracellular
EDTA	ethylenediamine tetraacetic acid
EEA1	early endosomal antigen 1
EGFP	enhanced green fluorescent protein
EHD1	Eps15-homology domain protein
ERC	endocytic/endosomal recycling compartment
FACS	fluorescence-assisted cell sorting
FCS	fetal calf serum
FM	full medium
GAP	GTPase activating protein
GAPDH	glyceraldehyde 3-phosphate dehydrogenase
GDF	GDI displacement factor
GDI	Rab GDP dissociation inhibitor

GDP	guanosine diphosphate
GEF	guanine nucleotide exchange factor
GFP	green fluorescent protein
GTP	guanosine triphosphate
h	hour
HA	hemagglutinin
HAP1	huntingtin associated protein 1
HEAT	motif found in huntingtin, elongation factor 3, A subunit of protein phosphatase 2, target of rapamycin 1
HD	Huntington's disease
HDAC	histone deacetylase
HEPES	4-(2-hydroxyethyl)-1-piperazineethanesulfonic acid
HIP-1	huntingtin interacting protein 1
HIP1R	HIP-1 related protein
Hippi	HIP-1 protein interactor
3-HK	3-hydroxykynurenine
HRP	horseradish peroxidase
Hsp	heat shock protein
Htt	huntingtin
ic	intracellular
ICC	immunocytochemistry
IGF-1	insulin-like growth factor 1
MALDI	matrix-assisted laser desorption ionization
MAP2K6	mitogen-activated protein kinase kinase 6
MAP3K5	mitogen-activated protein kinase kinase 5
min	minute
MTOC	microtubule organizing centre
mTOR	mammalian target of rapamycin
MTS	3-(4,5-dimethylthiazol-2-yl)-5-(3-carboxymethoxyphenyl)-2-(4-sulphophenyl)-2H-tetrazolium
NGF	nerve growth factor
NGS	normal goat serum
NII	neuronal intranuclear inclusions
NMDA	N-methyl-D-aspartate

3-NP	3-nitropropionic acid
NRSE	neuron restrictive silencer element
NRSF	neuron restrictive silencer factor
PAA	polyacrylamide
PAGE	polyacrylamide gel electrophoresis
PARP	poly (ADP-ribose) polymerase
PBS	phosphate buffered saline
PC12	rat phaeochromocytoma cell line
PCR	polymerase chain reaction
PFA	paraformaldehyde
PGC-1 $\alpha$	peroxisome proliferator-activated receptor $\gamma$ coactivator 1 $\alpha$
PKB	protein kinase B
PolyQ	polyglutamine
QA	quinolinic acid
Rab11BP	Rab11 binding protein
Rab11-FIP	Rab11-family interacting protein
RE-1	repressor element-1
REST	repressor element -1 transcription factor
RILP	REST/NRSF-interacting LIM domain protein
RNA	ribonucleic acid
ROI	region of interest
ROS	reactive oxygen species
RT	room temperature
rTetR	reverse Tet repressor
SBMA	spinobulbar muscular atrophy
SCA	spinocerebellar ataxia
SDS	sodium dodecylsulfate
SFM	serum-free medium
SGK	serum- and glucocorticoid-induced kinase
siRNA	short interfering RNA
Sp1	specificity protein 1
TBP	TATA binding protein
TEMED	tetramethylene diamine
Tf	transferrin

TGN	trans-Golgi network
TRE	Tet responsive element
TrkA	tropomyosin-related kinase A receptor tyrosine kinase
UCHL1	ubiquitin carboxy-terminal hydrolase L1
UPS	ubiquitin-proteasome system
wt	wild-type
YAC	yeast artificial chromosome

# 1 Introduction

## 1.1 Huntington's Disease

Huntington's disease (HD) is a hereditary progressive neurodegenerative disorder which leads to death within 10 to 20 years of onset. The disease usually commences in mid-life with symptoms that include chorea, general motor impairment, psychiatric disturbances and cognitive deterioration. The choreiform involuntary movements of the proximal and distal muscles are most characteristic of the disease, however these are often missing in juvenile-onset HD, which starts before the age of 20 and progresses more rapidly. Juvenile-onset patients more often suffer from rigidity, bradykinesia, dystonia, tremor and epileptic seizures (for reviews see Hayden, 1981, and Harper, 1991).

The disease is named after George Huntington, who published his article 'On Chorea' in 1872, in which he described the clinical symptoms of the disease and its autosomal-dominant pattern of inheritance. The disease had been described before (Waters, 1848; Lyon, 1863), but Huntington's article was so comprehensive that it became the authoritative text and the disease was accordingly named 'Huntington's chorea' or 'Huntington's disease'.

Huntington's disease belongs to a class of hereditary neurodegenerative disorders, the polyglutamine diseases, which are caused by a (CAG)<sub>n</sub> trinucleotide repeat expansion in the mutant gene that translates into a polyglutamine tract in the respective protein. In Huntington's disease the affected gene is *IT15*, which encodes the protein huntingtin, and the CAG repeat is located in the first of 67 exons (The Huntington's Disease Collaborative Research Group, 1993). Eight other diseases have been identified as polyglutamine diseases, including the spinocerebellar ataxias (SCA) types 1, 2, 3, 6, 7 and 17, spinobulbar muscular atrophy (SBMA) and dentatorubral pallidoluysian atrophy (DRPLA). The polyglutamine diseases share the adult onset of symptoms and the progressive neurodegeneration, but the affected brain regions and, consequently, the clinical phenotypes differ. No homology between the mutant genes besides the CAG repeat has been observed. The CAG repeat is in all disease genes a

highly polymorphic region and shows a common expansion threshold of approximately 40 repeats above which disease occurs (with the exception of spinocerebellar ataxia 6, where the threshold is only 20 repeats). (For reviews on polyglutamine diseases see Gusella and MacDonald, 2000, and Zoghbi and Orr, 2000.)

The prevalence of Huntington's disease is 4-8 in 100,000 in European and North American populations (Harper et al., 1992). So far, there is neither a cure for the disease nor an effective treatment.

### **1.1.1 Genetics**

In the region of Lake Maracaibo in Venezuela, the incidence of Huntington's disease is much higher than in the usual population. These 'Venezuelan kindreds' have been part of a long-term research project organised by the Hereditary Disease Foundation and have contributed greatly to the discovery of the disease gene and to the elucidation of the disease genetics (Wexler et al., 2004). In 1983, the disease mutation was mapped to the short arm of chromosome 4 (Gusella et al., 1983), followed by the cloning of the gene 10 years later through a multicentre effort (The Huntington's Disease Collaborative Research Group, 1993). The gene was named *IT15* for 'interesting transcript 15' and the protein it encodes was named huntingtin.

The huntingtin gene contains 6 to 35 CAG repeats in the normal population and 36 to 120 repeats in people with HD, in rare cases even more, but the most common adult-onset disease is caused by 40 to 50 repeats. The disease shows full penetrance in individuals with 40 or more CAG repeats, whereas reduced penetrance is only observed in individuals with intermediate repeat lengths between 36 and 39 (Andrew et al., 1993; Duyao et al., 1993; Snell et al., 1993; Rubinsztein et al., 1996). There is an inverse correlation between the length of the CAG repeat and the age of disease onset, which leads to an earlier onset of symptoms with increasing CAG repeat length (Fig. 1). As a consequence, the age of disease onset varies from childhood to old age (Andrew et al., 1993; Duyao et al., 1993; Snell et al., 1993).

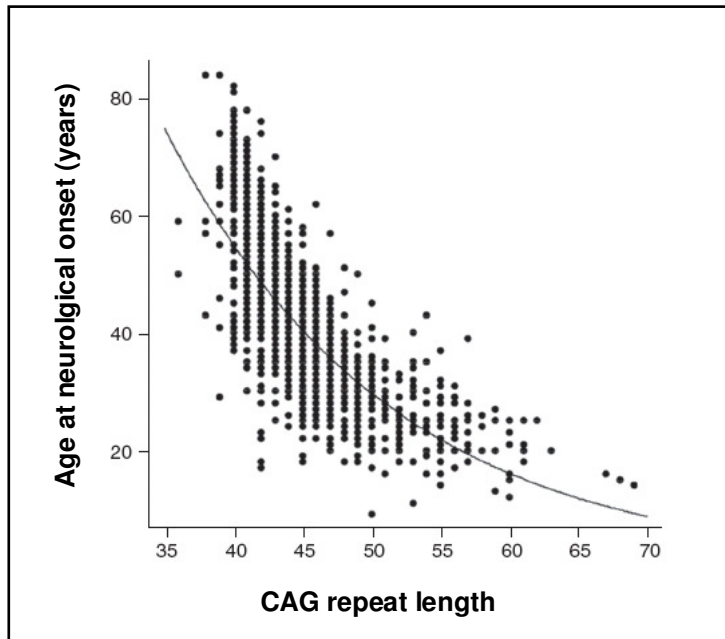


Fig. 1: Correlation between CAG repeat length and age of onset in HD.  
 The plot is taken from a review article by Gusella and MacDonald, 2009, and shows data points from 1,200 HD subjects of known age of neurological onset. For each individual, the measured CAG repeat length in blood DNA is plotted against age at neurological onset. The line represents the best-fit simple logarithmic regression to the data.

The CAG repeat length accounts for approximately 50-70% of the variance in age of onset (Andrew et al., 1993; Duyao et al., 1993; Rubinsztein et al., 1997; Wexler et al., 2004). The wide range of results from these studies may be due to different genetic backgrounds in the studied cohorts of HD patients and to the range of repeat lengths in each cohort, because the correlation is found to be weaker for shorter repeat lengths (Duyao et al., 1993; Wexler et al., 2004). Thus, there is a large variation in age of onset observed for any specific number of repeat units, especially in the lower range.

The variation of HD with respect to age of onset and to the clinical manifestation of the disease indicates that other factors, either genetic or environmental, influence the disease process. Studies in the Venezuelan kindreds suggest that approximately 40% of the remaining variance in age of onset (i.e. not accounted for by CAG repeat length) can be attributed to genetic factors (Wexler et al., 2004). Genetic modifiers of HD are genes whose natural polymorphisms in the

human population modify the pathogenic process (for a review see Gusella and MacDonald, 2009). Therefore, many genes suspected to play a role in HD have been examined for genetic variation in humans and these variants have been tested for an effect on the disease.

During the last 12 years, several genes have been linked to a variation in age of onset. Among these are the genes for the GluR6 kainate receptor and the glutamate receptor subunits NR2A and NR2B, which are involved in glutamatergic transmission (Rubinsztein et al., 1997; MacDonald et al., 1999; Arning et al., 2005), the genes for the transcriptional coactivator CA150 and the transcription factor p53 (Holbert et al., 2001; Chattopadhyay et al., 2005), the ubiquitin carboxy-terminal hydrolyse L1 (UCHL1) (Naze et al., 2002), the genes for ASK1, MAP2K6 and caspase-activated DNase, which are involved in apoptosis (Chattopadhyay et al., 2005; Arning et al., 2008), the huntingtin-associated protein HAP1, which has a function in axonal transport (Metzger et al., 2008), and the gene for PGC-1 $\alpha$ , a transcriptional regulator of mitochondrial function (Tahezadeh-Fard et al., 2009; Weydt et al., 2009). Other studies did not replicate the association of some of these genes with the age of onset in HD, including the genes for GluR6, NR2A, CA150, UCHL1, p53 and caspase-activated DNase (Metzger et al., 2006; Andresen et al., 2007). Differences in cohort sizes, methods of analysis and the distribution of genetic polymorphisms in the studied cohorts may be the cause of these inconsistent results.

Another genetic characteristic of Huntington's disease is the phenomenon of anticipation, i.e. the reduction in the age of onset with successive generations, caused by the increase in repeat length during transmission. The expanded CAG repeat is unstable in more than 80% of the transmissions from one generation to the next, including both expansions and contractions in maternal and paternal transmissions. However, very large increases in repeat length occur during paternal transmission (Duyao et al., 1993). The lower allele in heterozygotes (i.e. the allele with the normal CAG repeat) is stable during transmission and has no effect on the age of onset (Rubinsztein et al., 1997; Wexler et al., 2004).

Individuals with juvenile onset Huntington's disease (onset  $\leq$  20 years) carry alleles with 44 to 120 repeats or more (Andrew et al., 1993; Telenius et al., 1993). Given that very large increases in repeat length occur during paternal transmission, juvenile onset patients usually inherit the disease from their father (Ridley et al., 1988; Telenius et al., 1993). The instability in the male germ line is reflected in the large variation of repeat size in sperm (Duyao et al., 1993; Telenius et al., 1995). However, the repeat expansion is not restricted to the germ line, but also somatic mutations were observed in several studies on post-mortem HD brain, and, moreover, the somatic CAG repeat instability was reported to mirror the selective vulnerability in Huntington's disease (Telenius et al., 1994; Shelbourne et al., 2007). Evidence from mouse models of HD suggests that DNA repair pathways are involved in the generation of expanded CAG repeats and that different repair proteins are responsible for germ line expansion and somatic expansion of the CAG repeat (Manley et al., 1999; Kovtun and McMurray, 2001; Wheeler et al., 2003; Owen et al., 2005; Dragileva et al., 2009).

Huntington's disease displays an autosomal dominant pattern of inheritance. Initially it was believed that the disease is a case of perfect dominance, i.e. that the phenotype of homozygotes is indistinguishable from that of heterozygotes (Wexler et al., 1987). Although this remains apparently true with respect to the age of onset, the clinical course of the disease has been observed to be more severe in homozygous patients (Squitieri et al., 2003).

### **1.1.2 Pathology**

Huntington's disease is predominantly a disease of the central nervous system, but the protein is ubiquitously expressed and also peripheral abnormalities have been observed. For example, innate immune activation has been detected in the peripheral plasma many years before disease onset (Bjorkqvist et al., 2008). Inflammatory processes in the CNS appear also to contribute to the pathology of HD, as widespread and early activation of microglia has been observed in the brain of HD patients (Sapp et al., 2001; Pavese et al., 2006; Tai et al., 2007). The primary site of brain pathology is the striatum, which displays progressive neuronal death, astrogliosis and changes in dendritic morphology. During

disease progression, more areas become afflicted and also cortex, thalamus, globus pallidus, substantia nigra, nucleus subthalamicus and white matter develop atrophy (De la Monte et al., 1988; Vonsattel and DiFiglia, 1998). The striatum forms part of the basal ganglia, which are important in the indirect control and modulation of movement as well as in cognition. The medium spiny neurons, which constitute about 90% of the striatal neurons, are the most affected cell population in Huntington's disease, whereas the aspiny interneurons survive (Graveland et al., 1985; Vonsattel and DiFiglia, 1998). The extent of neuropathology and clinical symptoms was used to distinguish between 5 grades (0-4) of disease progression. In grade 0, the first clinical symptoms are present, followed by neuropathological abnormalities which only become visible in grade 1. Half of the neurons in the striatum are lost in grade 1, progressing to 95% in grade 4 (Vonsattel et al., 1985).

A characteristic feature of Huntington's disease is the appearance of proteinaceous inclusions or aggregates in cortex and striatum before the onset of clinical symptoms. They are located in the nuclei (termed neuronal intranuclear inclusions, NII) or in the cytoplasm, in particular in the neuronal processes (termed neuropil aggregates), and are positive for N-terminal huntingtin and often for ubiquitin (DiFiglia et al., 1997; Gutekunst et al., 1999; Hoffner et al., 2005). Moreover, some inclusions have been observed in substantia nigra, thalamus, hypothalamic nuclei and some brainstem nuclei (Gutekunst et al., 1999). Electron microscopy reveals granular and filamentous material in the inclusions, which are not surrounded by a membrane (DiFiglia et al., 1997; Gutekunst et al., 1999).

The detection and quantification of neuronal inclusions in post-mortem HD brain is technically challenging, especially in tissue from late stages of HD when neuronal loss in the striatum is severe. Further variation between reports is probably due to the use of different antibodies and methods and the variation between individuals. In adult onset HD post-mortem brains, 2-6% of the neurons in the cortex were observed to have inclusions (grades 2-4) and about 2% in the striatum (grades 3+4). In contrast, many more inclusions (17-52%) were found in the cortex of juvenile onset HD post-mortem brain (grades 3+4),

where the majority of inclusions are nuclear (DiFiglia et al., 1997; Hoffner et al., 2005). Another group reported a much higher frequency of neuropil aggregates for the cortex in adult onset patients, which was 10 times higher than in the striatum (grade 1) (Gutekunst et al., 1999). Therefore the frequency of inclusions does not reflect the selective vulnerability of brain regions in HD with respect to cell death, which is underlined by the high frequency of nuclear inclusions in striatal interneurons, which survive in HD (Kuemmerle et al., 1999).

Nuclear and neuropil aggregates have also been detected in various mouse models for Huntington's disease, which have been developed since the discovery of the huntingtin gene. (For a review on rodent models of HD see Heng et al., 2008.) A widely used HD model are the transgenic R6/2 mice, which express exon-1 of the human huntingtin gene with 150 CAG repeats and display a progressive neurological phenotype with features similar to HD, including abnormal movement, tremor and epileptic seizures as well as abnormal behaviour (Mangiarini et al., 1996; Carter et al., 1999). Motor deficits start at 5 weeks and the mice die prematurely after 12-15 weeks. Nuclear and neuropil aggregates in cortex, striatum and hippocampus are present at birth and increase over time (and thus precede disease onset like in the human disease) (Davies et al., 1997; Li et al., 1999; Stack et al., 2005), while neuronal loss in these mice (ca. 25% reduction in striatal neuron number at 12 weeks) is less pronounced than in the human disease (Stack et al., 2005). Compared to the R6/2 mice, the YAC128 transgenic mice, which express full length human huntingtin with 128 CAG repeats, display a less severe neurological phenotype. They also display progressive motor abnormalities and behavioural deficits, but the onset is later (the motor deficits start at 6 months), the symptoms are milder and they have a normal life span of about 2 years (Hodgson et al., 1999). The neuronal loss is modest (ca. 15% reduction in striatal neuron number at 12 months) like in the R6/2 mice, but huntingtin inclusions were not detected before 18 months and thus form after the disease onset (Slow et al., 2003). In contrast, a similar transgenic mouse model, which expresses full-length human huntingtin with 120 CAG repeats, is free of neurodegeneration and clinical symptoms despite the widespread appearance of protein inclusions (Slow et al., 2005).

### 1.1.3 Huntingtin

Huntingtin is a protein of approximately 348 kDa, depending on the length of the polyglutamine tract. It is ubiquitously expressed, with the highest levels in brain, especially in neurons of dentate gyrus, hippocampus, cerebellum, substantia nigra and the pontine nuclei (Li et al., 1993; Strong et al., 1993; Sharp et al., 1995; Landwehrmeyer et al., 1995). Huntingtin is predominantly a cytosolic protein and is present in the soma as well as in axons, dendrites and synapses, while only little is detected in the nucleus (Sharp et al., 1995; Trottier et al., 1995). The protein is present throughout development and adulthood, but its expression levels peak during the phase of neurogenesis and differentiation (Bhide et al., 1996). Thus, the expression pattern does not match the selective vulnerability in Huntington's disease, nor is the protein expression reduced in Huntington's disease when the neuronal loss in the striatum is taken into account (Li et al., 1993; Aronin et al., 1995).

Huntingtin has a vital function during development, as all three different knock-out mice, which were developed independently after the discovery of the Huntington's disease gene, show embryonic lethality in homozygous mice (Duyao et al., 1995; Nasir et al., 1995; Zeitlin et al., 1995). Heterozygous knock-out mice appear either phenotypically normal (Duyao et al., 1995) or display increased motor activity and cognitive deficits (Nasir et al., 1995).

Huntingtin has no homology to any other known gene (Huntington's Disease Collaborative Research Group, 1993). The sequence is phylogenetically highly conserved, except for the polymorphic CAG repeat and a proline-rich region adjacent to the polyglutamine tract. A map of huntingtin is shown in Fig. 2. The protein consists of 3144 amino acid residues. The polyglutamine tract is located at the N-terminus of the protein and begins at amino acid residue 17. Huntingtin contains multiple HEAT repeats (named after the first 4 proteins in which they were discovered: huntingtin, elongation factor 3, subunit A of protein phosphatase 2 and target of rapamycin 1), which are clustered into 4 major HEAT domains. HEAT repeats are sequences of approximately 40 amino acid residues which form  $\alpha$ -helices and assemble into an elongated super helix with a probable scaffolding function (Andrade and Bork, 1995). They are often found

in large proteins involved in cytosolic and nuclear transport processes, micro-tubule dynamics or chromosome segregation (Andrade and Bork, 1995; Vetter et al., 1999; Neuwald et al., 2000). Many phosphorylation and cleavage sites are located between the first two HEAT domains and present multiple targets for modulation and regulation, suggesting that huntingtin integrates various intracellular pathways (Warby et al., 2009). The HEAT domains are suspected to mediate the numerous interactions of huntingtin with other proteins (Neuwald et al., 2000). More than 30 huntingtin interacting proteins have been identified until today, which play a role in endocytosis, intracellular trafficking, signalling and transcriptional regulation, indicating that huntingtin is involved in multiple cellular functions. (For reviews on huntingtin interacting proteins see Harjes and Wanker, 2003, and Li and Li, 2004.)

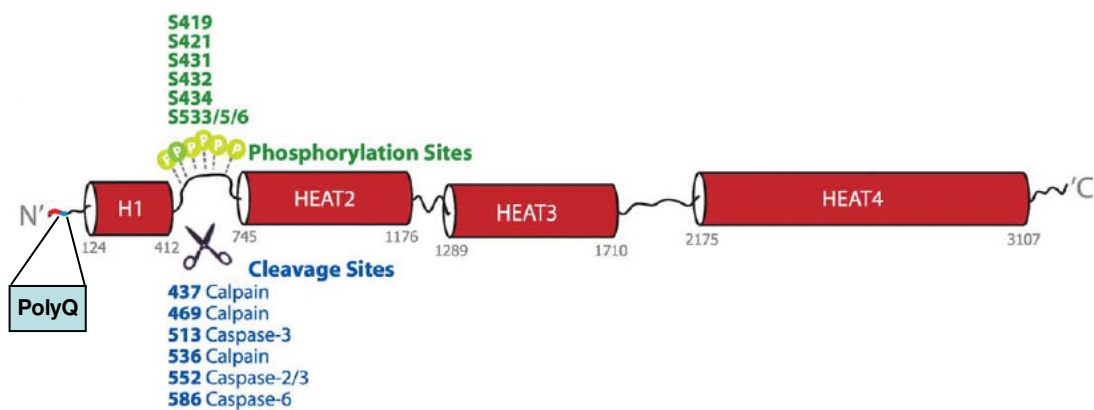


Fig. 2: Huntingtin domain map.

Huntingtin consists of 3144 aa. The polyQ tract is located at the N-terminus and begins at aa17. The four major HEAT domains are displayed as red barrels. Phosphorylation sites are shown in green, proteolytic cleavage sites in blue. (Modified from Warby et al., 2009.)

## 1.2 Pathogenic Mechanisms in Huntington's Disease

The genetic basis of Huntington's disease is remarkably simple, yet the crucial pathogenic mechanism by which the CAG repeat expansion causes the disease is still elusive. A great number of cellular and, in particular, neuronal pathways and functions are abnormal in Huntington's disease, as was revealed by a vast amount of research on post-mortem HD brain or on the various cell culture and

animal models of the disease since the cloning of the disease gene in 1993. However, the challenge is to understand which are the critical pathogenic processes triggering the cascade, or more likely cascades, of events and which are positioned further downstream, where therapeutic intervention has only minor or no beneficial effects. Other changes which have been observed in the disease may reflect the cell's own compensatory or protective mechanisms, and their inhibition could even aggravate the disease.

Recently, the physiological functions of huntingtin have become better understood and have suggested several mechanisms by which the expanded polyglutamine tract can impair the physiological function of huntingtin and thus cause detrimental cellular changes which have been observed in Huntington's disease, such as disturbances in intracellular trafficking (see below). However, the dominant pattern of inheritance clearly argues in favour of a gain of function that is acquired by the disease mutation. This hypothesis is also supported by the fact that the CAG repeat expansion is pathogenic in the other polyglutamine diseases, in which unrelated and functionally diverse proteins carry the same mutation, and even when (in mice) an expanded CAG repeat is inserted in a protein unconnected with disease (Ordway et al., 1997). Also the late onset of the human disease suggests that some time before the clinical onset the mutant protein acquires an additional toxic function, which is not present at birth. Carriers of the mutant gene develop and live normally until the disease onset. The vital function of huntingtin during development, which is revealed by the embryonic lethality of knock-out mice, can therefore not be impaired by the mutation. In accordance, knock-in mice which express mouse huntingtin with an expanded polyglutamine tract (50Q) at wild-type levels develop normally, whereas knock-in mice which express the same mutant protein at reduced levels show perinatal lethality (White et al., 1997). However, other functions of huntingtin than its function in development may be affected in HD.

The degree to which a lack of function contributes to the disease phenotype is a subject of controversy. Hemizygous mice appear either phenotypically normal (Duyao et al., 1995) or display increased motor activity and cognitive deficits (Nasir et al., 1995). In humans, a more severe course of disease in homo-

zygous patients has been reported (Squitieri et al., 2003). Also in transgenic YAC128 mice (expressing full length human huntingtin with 128Q), a higher level of mutant huntingtin or the additional deletion of the mouse huntingtin gene lead to a more severe phenotype (Van Raamsdonk et al., 2005; Graham et al., 2006, a). But whatever the degree of contribution of a loss of function to the disease phenotype, the overexpression of wild-type huntingtin is not able to compensate for the toxicity of mutant huntingtin, as YAC128/18 mice which overexpress mutant (128Q) and wild-type (18Q) human huntingtin show no significant behavioural improvement compared to YAC128 mice (Van Raamsdonk et al., 2006).

### **1.2.1 Loss-of-function Mechanisms**

#### *Antiapoptotic function*

One of the physiological functions that have been attributed to huntingtin is an antiapoptotic function, as wild-type huntingtin protects neurons against apoptotic stimuli like serum withdrawal, death receptors, proapoptotic Bcl-2 homologues and also against toxicity induced mutant huntingtin (Rigamonti et al., 2000; Ho et al., 2001). Two mechanisms for the survival function of huntingtin have been suggested.

First, huntingtin inhibits caspase-9 processing, so that caspase-3 cannot be activated even when cytochrome c is released from the mitochondria during the intrinsic pathway of apoptosis (Rigamonti et al., 2000 and 2001; Leavitt et al., 2001). Also a direct inhibition of caspase-3 by huntingtin has been reported, which was reduced by the polyglutamine expansion (Zhang et al., 2006).

Second, huntingtin inhibits the proapoptotic protein HIP-1 (huntingtin interacting protein 1) by sequestering HIP-1. Free HIP-1, in contrast, binds Hippi (HIP-1 protein interactor), forming a proapoptotic heterodimer that recruits procaspase-8 and thereby triggers the extrinsic pathway of apoptosis. The interaction between huntingtin and HIP-1 is weakened by the expanded polyglutamine tract and thus, in Huntington's disease, more free HIP-1 could be available to form a proapoptotic heterodimer with Hippi (Hackam et al., 2000; Gervais et al., 2002).

### *Transcriptional regulation*

Huntingtin is also suspected to be involved in transcriptional regulation as many polyglutamine-containing proteins have a physiological function as transcription factors or coactivators, e.g. the transcriptional activators CBP (CREB binding protein) and TBP (TATA binding protein), and the polyglutamine domain may play a role in DNA binding or transcriptional activation (Perutz et al., 1994; Gerber et al., 1994). Moreover, a number of huntingtin interacting proteins have a function in transcriptional regulation, such as CBP (CREB binding protein) and p53 (Steffan et al., 2000). (For more interacting proteins see Harjes and Wanker, 2003.)

A mechanism for the involvement of huntingtin in transcription has been demonstrated by its enhancement of the transcription of BDNF (brain-derived neurotrophic factor) (Zuccato et al., 2001). BDNF is a neurotrophic factor produced by the cortical neurons projecting to the striatum and is necessary for the survival of striatal neurons. The transcriptional repressor REST/NRSF (repressor element -1 transcription factor/ neuron restrictive silencer factor) binds to RE-1/NRSE (repressor element-1/ neuron restrictive silencer element) within the BDNF promoter region and silences BDNF transcription. Wild-type huntingtin binds to REST/NRSF, thereby inhibiting its interaction with RE-1/NRSE, but the expanded polyglutamine tract impairs the huntingtin interaction with REST/NRSF, leading to increased levels of REST/NRSF in the nucleus and repression of RE-1/NRSE-controlled genes like the BDNF gene (Zuccato et al., 2003). In accordance with this mechanism, the occupancy of RE-1/NRSE loci by REST/NRSF was higher in HD and led to decreased transcription of BDNF in mice and humans, while inhibition of REST/NRSF binding restored BDNF levels (Zuccato et al., 2007). In post-mortem HD brain, BDNF levels are reduced to 50-80% in the striatum, but not in the cortex (Ferrer et al., 2000).

BDNF signalling triggers CREB-mediated gene expression (Finkbeiner et al., 1997). Reduced BDNF levels could therefore also cause the inhibition of CREB-mediated transcription, which has been observed in several HD models and in post-mortem HD brain (Wyttenbach et al., 2001; Nucifora et al., 2001; Sugars et al., 2004). CREB (cyclic AMP response element binding protein) is a

transcription factor which binds to CRE (cyclic AMP response element) and activates the transcription of CRE-controlled genes, together with the coactivators CBP (CREB binding protein) and TAF<sub>II</sub>130. CREB-mediated transcription is important for neuronal function (Lonze et al., 2002).

In contrast to this specific loss of transcriptional function, extensive and early changes in gene transcription have been observed in cell culture models (Wyttenbach et al., 2001), transgenic mice (Luthi-Carter et al., 2000) and human post-mortem brain (Hodges et al., 2006). The reported transcriptional changes in various mouse models have been shown to be consistent with each other and with those in human post-mortem HD brain when the time scale of disease progression, the CAG repeat length, the length of huntingtin and the expression level were taken into account (Kuhn et al., 2007). However, the underlying mechanisms are unknown and may be a loss or a gain of function.

Apart from the abnormal interaction of mutant huntingtin with specific proteins involved in transcription, overall changes could also be mediated by chromatin modification, such as the acetylation and methylation of histones. There is strong evidence that histone acetylation is reduced in Huntington's disease, while histone methylation is increased, leading to the silencing of gene transcription. In accordance with this hypothesis, histone deacetylase (HDAC) inhibitors restored histone acetylation and had protective effects in mouse models (Ferrante et al., 2003; Gardian et al., 2005; Ryu et al., 2006; Stack et al., 2007; Thomas et al., 2008) and in *Drosophila* models of HD (Steffan et al., 2001; Pallos et al., 2008). However, not only histones are deacetylated by HDACs and therefore HDAC inhibitors may affect the cell in several ways. For example, HDAC6 is associated with microtubules and deacetylates tubulin, regulating aggresome formation and autophagy (Kawaguchi et al., 2003; Iwata et al., 2005) as well as the intracellular transport of BDNF vesicles (Dompierre et al., 2007). Based on these findings, histone deacetylase are considered to be promising targets for therapy.

### *Intracellular trafficking*

Early research on the huntingtin protein suggested that it plays a role in intracellular trafficking. Huntingtin was shown to be associated with vesicle membranes and microtubules (DiFiglia et al., 1995; Sharp et al., 1995; Gutekunst et al., 1995; Hoffner et al., 2002) as well as with clathrin-coated and uncoated endosomes in the endocytic pathway from the plasma membrane and the secretory pathway from the trans-Golgi network (Velier et al., 1998; Kim et al., 1999).

During clathrin-mediated endocytosis, specific receptors and their cargo molecules accumulate in clathrin-coated pits in the plasma membrane, which then bud into new vesicles and are released into the cytoplasm. The process is driven by many accessory factors and is connected with the intracellular actin cytoskeleton. Clathrin forms triskelia which assemble into a coat of pentagons and hexagons, aided by the adaptor protein 2 (AP-2). Huntingtin may have physiological function in endocytosis by forming a complex with HIP-1 (huntingtin interacting protein 1), HIP1R (HIP-1 related protein), clathrin, AP-2 and actin and thereby promoting clathrin assembly (Kalchman et al., 1997; Engqvist-Goldstein et al., 1999; Legendre-Guillemain et al., 2005; Chen et al., 2005). Clathrin-coats are also found on vesicles released from the trans-Golgi network (TGN) and destined for lysosomes, such as vesicles transporting hydrolytic enzymes. This transport pathway requires a complex of optineurin and Rab8 and is impaired by either reduction of wild-type huntingtin or expression of mutant huntingtin, probably by disrupting the localisation of the optineurin/Rab8 complex at the Golgi (deToro et al., 2009).

A function of huntingtin in axonal transport has also been early described (Block-Galarza et al., 1997). During fast axonal transport, vesicles and organelles are transported by motor proteins along microtubules in the axon. The motor protein dynein mediates retrograde transport, while kinesin is responsible for anterograde transport. The vesicle is attached to the motor protein through the dynactin complex. Huntingtin enhances vesicular transport of BDNF along microtubules in a complex with HAP1 (huntingtin associated protein 1) and the p150(Glued) subunit of dynactin (Gauthier et al., 2004).

HAP1 association with dynactin-p150 and kinesin light chain is regulated by phosphorylation of HAP1 (Rong et al., 2006). Moreover, acetylation of  $\alpha$ -tubulin increases the interaction between microtubules and the motor proteins dynein and kinesin-1 and thus enhances BDNF transport (Dompierre et al., 2007). Phosphorylation of huntingtin at S421 was shown to switch the transport direction by promoting recruitment of either kinesin-1 (when phosphorylated) or dynein (when unphosphorylated) (Colin et al., 2008). Either lack of wild-type huntingtin or an elongated polyglutamine tract in huntingtin attenuate the BDNF transport and thus reduce the neurotrophic support for the neurons and induce toxicity (Gauthier et al., 2004). The same mechanism was suggested to reduce the intracellular levels of the NGF receptor TrkA (tropomyosin-related kinase A receptor tyrosine kinase), the internalisation and trafficking of which is necessary for neurite outgrowth (Rong et al., 2006). Two mechanisms were shown to restore BDNF transport: the increased acetylation of microtubules after treatment with HDAC inhibitors and the constitutive phosphorylation of mutant huntingtin at S421 (Dompierre et al., 2007; Zala et al., 2008). (For a review on the role of huntingtin in intracellular vesicle trafficking see Caviston and Holzbaaur, 2009.)

A connection has been suggested between the vesicle transport complex containing huntingtin and the transcriptional repressor REST/NRSF. It was shown that huntingtin, HAP-1 and the p150(Glued) subunit of dynactin are bound through RILP (REST/NRSF-interacting LIM domain protein) to REST/NRSF and that this complex controls the localisation of REST/NRSF in neurons (Shimojo et al., 2008).

Other scientists suggest a gain-of-function mechanism for the impairment of axonal transport of vesicles and organelles, such as mitochondria, either by the sequestration of motor proteins and wild-type huntingtin in aggregates (Lee et al., 2004; Trushina et al., 2004) or by physical blockage of axonal transport by cytoplasmic aggregates (Chang et al., 2006).

## 1.2.2 Gain-of-function Mechanisms

### *Protein aggregation*

Correct protein folding is essential for cells, which have developed a complex system of molecular chaperones to promote protein folding and prevent aggregation and proteases to degrade misfolded proteins. If these systems fail, the misfolded proteins aggregate and accumulate in inclusion bodies. Intra-cellular or extracellular accumulation of aggregated proteins is a characteristic feature of several neurodegenerative diseases, including Alzheimer's disease, Parkinson's disease, amyotrophic lateral sclerosis and the polyglutamine diseases. The aggregates usually consist of fibres containing misfolded protein with a beta-sheet conformation, termed amyloid (Ross and Poirier, 2004). Accumulation of aggregated proteins in inclusion bodies is not a passive process, but an active response of the cell to misfolded proteins. These inclusion bodies, which also form when misfolded proteins are overexpressed in cells, have been termed aggresomes (Johnston et al., 1998). They form near the microtubule organising centre (MTOC) and are surrounded by vimentin, an intermediate filament protein. Aggresome formation has been postulated to be a cellular response when proteasome capacity is exceeded, and it may act together with the autophagic system to facilitate the disposal of insoluble proteins (Taylor et al., 2003). During this process, small aggregates form within the cell periphery and are transported by dynein motors along the microtubules to the aggresome at the MTOC (Garcia-Mata et al., 1999). In addition, HDAC6 (histone deacetylase 6) was identified as a component of this transport system, binding to dynein motors and polyubiquitinated proteins. In HDAC6-deficient cells, aggresome formation is inhibited and sensitivity to stress induced by misfolded proteins is increased (Kawaguchi et al., 2003).

Also the protein aggregates which form in HD are suspected to be aggresomes, as many cytosolic huntingtin aggregates in cultured cells are located in vicinity to the MTOC and some were moreover surrounded by vimentin (Waelter et al., 2001). Other experiments on cultured cells showed that an intact microtubule skeleton is required for the formation of large juxtannuclear huntingtin aggregates (Muchowski et al., 2002).

The x-ray structure of a synthetic polyglutamine peptide indicated that it forms  $\beta$ -sheets which are held together by hydrogen bonds (Perutz et al., 1994). Later this x-ray structure was interpreted as fibrillar nanotubes because the data match a cylindrical  $\beta$ -sheet with 20 residues per helical turn and a diameter of 31 Å. Hydrogen bonds form between the amides of the main chain and the side chains, and side chains point alternately into and out of the cylinder. The typical pathogenic threshold of approximately 40 polyglutamine residues would then correspond to 2 helical turns stabilising the structure (Perutz et al., 2002). Other scientists propose a model of stacked  $\beta$ -sheets to explain the x-ray data (Sikorski and Atkins, 2005).

In HD, electron micrographs of huntingtin inclusions in human post-mortem brain (Gutekunst et al., 1999) and brain from R6 transgenic mice (Davies et al., 1997; Scherzinger et al., 1997) reveal filamentous as well as granular material. It was demonstrated at the same time in vitro that N-terminal huntingtin fragments containing a polyglutamine tract in the pathogenic range are able to form insoluble protein aggregates of high molecular weight with a fibrillar structure (Scherzinger et al., 1997). They have a diameter of 10-12 nm and vary in length from 100 nm to several micrometers (Scherzinger et al., 1997). The rate of self-assembly in vitro depends not only on the polyglutamine length, but also on concentration and time. Moreover, the aggregation process can be seeded by pre-formed fibrils (Scherzinger et al., 1999).

Many cell culture models expressing full length or N-terminal fragments of huntingtin with varying polyglutamine tracts have demonstrated that huntingtin with an expanded repeat forms aggregates and that the extent of aggregation increases when the length of the huntingtin fragment decreases and the length of the polyglutamine tract increases. All mutant huntingtin constructs lead to the formation of aggregates in the cytoplasm, but only shorter N-terminal fragments produce nuclear aggregates. Increased aggregation correlates with increased susceptibility to apoptotic stimuli (Martindale et al., 1998; Lunkes and Mandel, 1998; Li and Li, 1998; Hackam et al., 1998 and 1999; Cooper et al., 1998).

The toxicity of huntingtin aggregates is probably the most controversial subject in the field of HD research. Despite an enormous amount of data, no consensus has been reached whether the aggregates are toxic, protective or only by-products of the disease process. The various models do not have to be mutually exclusive, as the aggregate formation could reflect a cellular defence mechanism against an overload of misfolded proteins, which has nevertheless negative side effects for the cell.

### *Sequestration*

Many proteins have been reported to colocalise with huntingtin aggregates based on immunocytochemical studies in cell culture or mouse models of HD. Based on these reports, it has been proposed that huntingtin aggregates are toxic by the sequestration of vital cellular components. The reduction of specific proteins would then cause either cell dysfunction or death.

Proteins that colocalise with inclusion include ubiquitin, heat shock proteins such as Hsp40 and Hsp70 and proteasome components (DiFiglia et al., 1997; Wyttenbach et al., 2000; Jana et al., 2001; Waelter et al., 2001). Other proteins detected in huntingtin aggregates were proteins involved in transcriptional regulation, such as CBP (CREB binding protein) and p53 (Steffan et al., 2000). Many more proteins colocalising with huntingtin aggregates have been published, but the findings were inconsistent. Sequestration of CBP and TAF<sub>II</sub>130 in the huntingtin inclusions was suggested to cause downregulation of CRE-controlled genes (Jiang et al., 2003 and 2006), but other reports show that TBP, CBP and Sp1 are neither downregulated nor taken up into aggregates (Yu et al., 2002). According to one report, chaperones are not sequestered into aggregates, but only transiently associated (Kim et al., 2002). Several groups attempted to purify aggregates and to identify their components (Suhr et al., 2001; Hazeki et al., 2002). These publications are discussed in chapter 4.

### *Heat shock proteins*

Heat shock proteins aid the correct folding of proteins as chaperones and protect the cell from misfolded proteins. Therefore it was suspected that chaperones may affect the aggregation process of mutant huntingtin and

reduce toxicity in HD models. Many studies confirm this assumption, as the expression of various heat shock proteins and chaperones reduced inclusion formation and toxicity in cell culture models of Huntington's disease. These include proteins such as the bacterial chaperone GroEL and the yeast heat shock protein Hsp104 (Carmichael et al., 2000), the mammalian heat shock proteins Hsp40, Hsp70 and Hsp90 (Sittler et al., 2001) and the chaperonin TRiC, which acts during de novo biogenesis of proteins (Tam et al., 2006; Kitamura et al., 2006; Behrends et al., 2006). The observation that the over-expression of heat shock proteins reduces protein aggregation is not surprising, but does not clarify their role in HD pathology. Crossing of R6/2 mice with mice overexpressing HSP70 had only a modest effect on the R6/2 phenotype (Hansson et al., 2003), but HD mice haploinsufficient for the co-chaperone and ubiquitin-ligase CHIP (C-terminal Hsp70 interacting protein) had a quicker disease process (Miller et al., 2005).

#### *Proteolytic cleavage*

The fact that aggregates in post-mortem brain consists of a wide range of N-terminal fragments of mutant huntingtin suggests that proteolytic cleavage of mutant huntingtin precedes the aggregate formation (Hoffner et al., 2005). Moreover, shorter fragments of mutant huntingtin form aggregates faster than longer fragments and are more toxic to cells in culture (Martindale et al., 1998; Lunkes and Mandel, 1998). The same effect is observed in animal models, where shorter fragments of mutant huntingtin trigger an earlier onset and a faster progression of disease (Heng et al., 2008). Therefore, it is a plausible hypothesis that proteolytic cleavage of mutant huntingtin is relevant in HD and that it precedes as well as enhances aggregate formation. However, it is difficult to understand how the proteolytic enzymes are initially activated and what the physiological function of proteolytic cleavage of huntingtin is, as there is evidence for the presence of N-terminal huntingtin fragments in cortex, striatum and cerebellum also in normal post-mortem brain (Kim et al., 2001).

Huntingtin possesses several regions which are susceptible to proteolytic cleavage; one of them is the region between residues 460 and 600, which contains multiple cleavage sites for caspases and calpains (Schilling et al.,

2006). Caspase-3 consensus sites are located at residues D513 and D530. Inhibition of caspase-3-mediated cleavage of huntingtin by addition of caspase inhibitors or the creation of non-cleavable mutants is protective in cell culture, as indicated by the reduced toxicity of mutant huntingtin and the smaller number of inclusions (Wellington et al., 2000). Moreover, a consensus site for caspase-2 was identified at D552, the mutation of which is protective in striatal neurons from transgenic mice. Activated caspase-2 was detected in the medium spiny neurons of the striatum and in cortical projection neurons in post-mortem HD brain (Hermel et al., 2004). Caspase-6 cleaves huntingtin at D586 (Wellington et al., 2000). Transgenic HD mice which express a non-cleavable mutant of caspase-6 do not develop striatal degeneration and are moreover resistant to NMDA and quinolinic acid, whereas mice expressing a non-cleavable mutant of caspase-3 are not, suggesting that cleavage at the caspase-6 site is required for neuronal dysfunction and degeneration in HD (Graham et al., 2006, b).

Calpains also have been reported to cleave huntingtin, for example under excitotoxic conditions after treatment with glutamate or 3-nitropropionic acid, when intracellular  $Ca^{2+}$  is increased (Goffredo et al., 2002; Bizat et al., 2003). There are two calpain cleavage sites in huntingtin, and mutation of them reduces toxicity in a cell culture model of Huntington's disease (Gafni et al., 2004). Moreover, raised levels of activated calpains were detected in post-mortem HD brain and brain of transgenic mice (Gafni et al., 2004).

Proteolytic cleavage of huntingtin appears to be modulated by phosphorylation, for which it has at least 8 sites (Humbert et al., 2002; Luo et al., 2005; Schilling et al., 2006). Phosphorylation at S536 reduces calpain-mediated cleavage and toxicity of mutant huntingtin (Schilling et al., 2006), while phosphorylation at S434 reduces cleavage at D513 by caspase-3, which also has a protective effect (Luo et al., 2005). Huntingtin is phosphorylated at serine 421 by the pro-survival signalling kinases Akt and SGK (see below), leading to reduced cleavage by caspase-6 and reduced nuclear localisation of huntingtin (Warby et al., 2009). Phosphorylation at this site is lowest in striatum and even further reduced by the polyglutamine expansion (Warby et al., 2005).

### *Ubiquitin-proteasome system*

The ubiquitin-proteasome system (UPS) is the major proteolytic system in the cell for the degradation of cytosolic and nuclear proteins. Besides its importance in the removal of misfolded proteins and general protein turnover, it regulates the stability of cytoplasmic and nuclear proteins and is therefore essential for correct cell function. The role of the UPS in Huntington's disease is not clear. Initially it was suggested that proteasome function is inhibited by the expression of mutant huntingtin (Bence et al., 2001), but new evidence from R6/2 mice does not confirm the widespread inhibition of UPS-dependent degradation (Bett et al., 2009).

It has been shown that a sequence within the huntingtin protein targets it to the proteasome for degradation and that mutation of this site increases the steady-state level of the protein (Chandra et al., 2008), but whether mutant huntingtin can be degraded by the proteasome is a controversial subject. While some studies suggest that eukaryotic proteasomes cannot digest polyglutamine sequences (Venkatraman et al., 2004), others claim that the proteasome is able to digest polyglutamine peptides (Pratt et al., 2008). Yet other studies report that wild-type and mutant huntingtin are degraded by the proteasome and that the rate of degradation is inversely proportional the length of the polyglutamine tract (Jana et al., 2001).

Several mechanisms were suggested for the impairment of the proteasome by mutant huntingtin. If the proteasome cannot digest polyglutamine sequences, the released polyglutamine tract could interfere with proteasome function in polyglutamine diseases (Venkatraman et al., 2004). However, other reports indicate that aggregates do not directly block the proteasome (Bennet et al., 2005) and that huntingtin fibrils and not inclusion bodies interfere with proteasome function (Diaz-Hernandez et al., 2006), while inclusion bodies may be protective (Mitra et al., 2008).

### *Autophagy*

Autophagy is a process that is involved in the degradation of long-lived cytoplasmic proteins and cell organelles and plays moreover a role in the

defence against invading microorganisms. During autophagy, the organelle or macromolecule destined for degradation is surrounded by a double membrane, forming an autophagosome or autophagic vacuole, which subsequently fuses with lysosomes. There is a basal level of autophagy for the degradation of cytoplasmic components, but it also can be induced by certain stimuli, such as a deficit of nutrients.

Autophagy and endosomal-lysosomal activity were observed to be stimulated by mutant huntingtin in striatal neurons (Kegel et al., 2000). In addition, polyglutamine-containing aggregates were shown to be degraded by autophagy. Mutant huntingtin accumulated when the autophagy-lysosome system was inhibited, whereas the induction of autophagy enhanced the clearance of mutant huntingtin and the number of inclusions (Ravikumar et al., 2002; Qin et al., 2003). The mammalian target of rapamycin (mTOR) is a key regulator of autophagic activity. Inhibition of mTOR by rapamycin induces autophagy and reduces toxicity of mutant huntingtin in fly and mouse models of HD (Ravikumar et al., 2004). Inducing autophagy with other substances, acting dependently or independently of mTOR, were also shown to have a protective effect in HD cell culture and *Drosophila* models (Sarkar et al., 2007 and 2009; Floto et al., 2007).

It has been suggested that the autophagic degradation of aggresomes is coordinated by recruiting autophagosomes and lysosomes to the pericentriolar inclusion bodies by a process that requires an intact microtubule cytoskeleton and the deacetylase HDAC6, indicating retrograde transport along microtubules (Iwata et al., 2005). Also the fusion of autophagosomes and lysosomes was shown to depend on microtubules (Webb et al., 2004).

### *Intracellular signalling*

Several other cellular pathways have been implicated in Huntington's disease, but it is not known whether they represent loss- or gain-of-function mechanisms or whether they are located up- or downstream in the pathogenic process. For example, abnormalities in intracellular signalling pathways have been observed in Huntington's disease. IGF-1 (insulin-like growth factor 1) protects

striatal neurons expressing mutant huntingtin from cell death (Humbert et al., 2002). The IGF-1 signalling pathway includes the activation of Akt/PKB (protein kinase B) which phosphorylates huntingtin at serine 421 and leads to protection from cell death and reduced aggregate formation. The phosphorylation of huntingtin at S421 by Akt is partly responsible for the survival effect of IGF-1 (Humbert et al., 2002). Levels of active and inactive Akt were lower in a rat model of HD at a time of neuronal dysfunction before neurodegeneration, while in late-stage post-mortem HD brains, a caspase-3-cleaved Akt fragment was detected (Colin et al., 2005). SGK (serum- and glucocorticoid-induced kinase) is another kinase in the IGF-1 signalling pathway. Like Akt, it is able to phosphorylate huntingtin at S421 and to protect against cell death induced by mutant huntingtin, but in contrast to Akt, it is upregulated in Huntington's disease, probably as part of a stress response pathway (Rangone et al., 2004). Phosphorylation of huntingtin at S421 was reduced in mouse and human HD brain, particularly in the striatum and cortex (Warby et al., 2005).

### *Excitotoxicity*

Early evidence for a role of excitotoxicity in HD was the fact that the disease could be modelled with the NMDA-R agonist quinolinic acid (QA), which induces specific neurodegeneration of the medium spiny neurons of the striatum and HD-like symptoms in rats (Schwarcz et al., 1983).

R6/1 and R6/2 transgenic mice acquire partial or complete resistance to excitotoxins during the disease course, including the NMDA-R agonist quinolinic acid (QA) and the mitochondrial toxin malonate, but not AMPA. The  $\text{Ca}^{2+}$  influx upon stimulation was unchanged, but the basal level of intracellular  $\text{Ca}^{2+}$  was higher, possibly representing a protective mechanism against  $\text{Ca}^{2+}$  overload (Hansson et al., 2001, a+b). In contrast, the excitotoxic cell death was increased in a YAC HD model upon treatment with QA (Zeron et al., 2002), while in yet another model the susceptibility remained unchanged (Petersen et al., 2002). In YAC128 mice, the sensitivity to NMDA and QA was increased before onset, but by the symptomatic stage the mice had developed resistance (Graham et al., 2009). A possible mechanism for the observed resistance to excitotoxins in HD models may be the reduction of BDNF in mice, as cross-

breeding of R6/1 mice with BDNF knock-out mice rendered the mice less sensitive to QA (Torres-Peraza et al., 2008).

Alternatively, the resistance against excitotoxins may be linked to the transcriptional changes in the kynurenine pathway. 3-hydroxykynurenine (3-HK) is the precursor of QA, an endogenous metabolite which was elevated in several mouse models of HD (Guidetti et al., 2006). These metabolites are generated during tryptophan degradation by microglia and macrophages. In a yeast model of HD, mutant huntingtin induced the transcription of the kynurenine pathway, which was attenuated by an HDAC inhibitor (Giorgini et al., 2008). Closer analysis of post-mortem HD brains over time showed that QA was increased early during the disease process and reduced later, which could explain the changes in sensitivity to excitotoxins in HD models.

### *Mitochondria*

Mitochondria in transgenic mice neurons or in lymphoblasts from HD patients have a lower membrane potential and depolarise at a lower  $\text{Ca}^{2+}$  load. In addition, mutant huntingtin was detected on mitochondrial membranes, though it is unknown whether this had any negative effect (Panov et al., 2002). A potential mechanism for mitochondrial dysfunction has been suggested, involving PGC-1 $\alpha$  (PPAR $\gamma$ -coactivator-1 $\alpha$ ), a transcriptional regulator and potent stimulator of mitochondrial biogenesis and function. In Huntington's disease, mouse and human striatum had a reduced expression of PGC-1 $\alpha$  target genes, providing a link between transcriptional regulation and mitochondrial dysfunction (Weydt et al., 2006). Mutant huntingtin inhibits PGC-1 $\alpha$  transcription and thus disturbs mitochondrial function, while overexpression of PGC-1 $\alpha$  is protective in cell culture and mouse models of HD (Cui et al., 2006). PGC-1 $\alpha$  is moreover important for the expression of ROS-detoxifying enzymes, and PGC-1 $\alpha$  knock-out mice are more sensitive to oxidative stress (St-Pierre et al., 2006).

### 1.3 Endosomal Recycling

The cell has a highly complex vesicular sorting and transport system, the function of which is to deliver membrane components, proteins and solute molecules to their correct position. The best understood process is receptor-mediated endocytosis where membrane proteins with their ligands concentrate in clathrin-coated pits and are endocytosed into clathrin-coated vesicles. (There exist also non-clathrin-coated-pit internalization pathways, which will not be described here.) The clathrin-coated vesicles shed their coats and fuse with short-lived sorting endosomes, from where the membrane proteins are either directly returned to the plasma membrane, passed on to late endosomes for later degradation in lysosomes or transported to the endocytic recycling compartment (ERC). The ERC is a long-lived tubular structure, which is associated with microtubules and is in most cells concentrated at the microtubule organizing centre (MTOC). However, recycling endosomes (RE) can also be located in the cell periphery, for example in the dendrites of neurons. Proteins in the ERC are either recycled back to the plasma membrane or transported to the trans-Golgi network (TGN). The ERC appears also to have storage function and to respond quickly to stimuli by transporting certain receptors to the plasma membrane. The whole endocytic recycling system is highly dynamic, as new transport vesicles permanently fuse with the compartments or leave them. In addition, compartments often change over time, a process which is termed 'maturation'. Therefore, there are probably no true resident molecules and the various compartments are often more easily defined by their cargo than by resident molecules. However, several proteins are known to be enriched in a certain organelle, such as Rab5 and EEA1 (early endosomal antigen 1), which are found in sorting endosomes, and Rab11 and EHD1/Rme-1 (Eps15-homology domain protein), which are concentrated in the ERC. (For a review on endosomal recycling see Maxfield and McGraw, 2004.) A simplified diagram of endosomal recycling is shown in Fig. 3.

In neurons, the endosomal recycling is even more complex because the distinct distribution of axonal versus somatodendritic membrane proteins has to be maintained and the long distances between cell body and synapses require

special recycling pathways and compartments. For example, recycling endosomes not only regulate synaptic strength by providing AMPA receptors for insertion into the postsynaptic membrane, but they probably supply also the membrane for the formation of dendritic spines (Park et al., 2004 and 2006). (For a review on endosomal recycling in neurons see Schmidt and Haucke, 2007.)

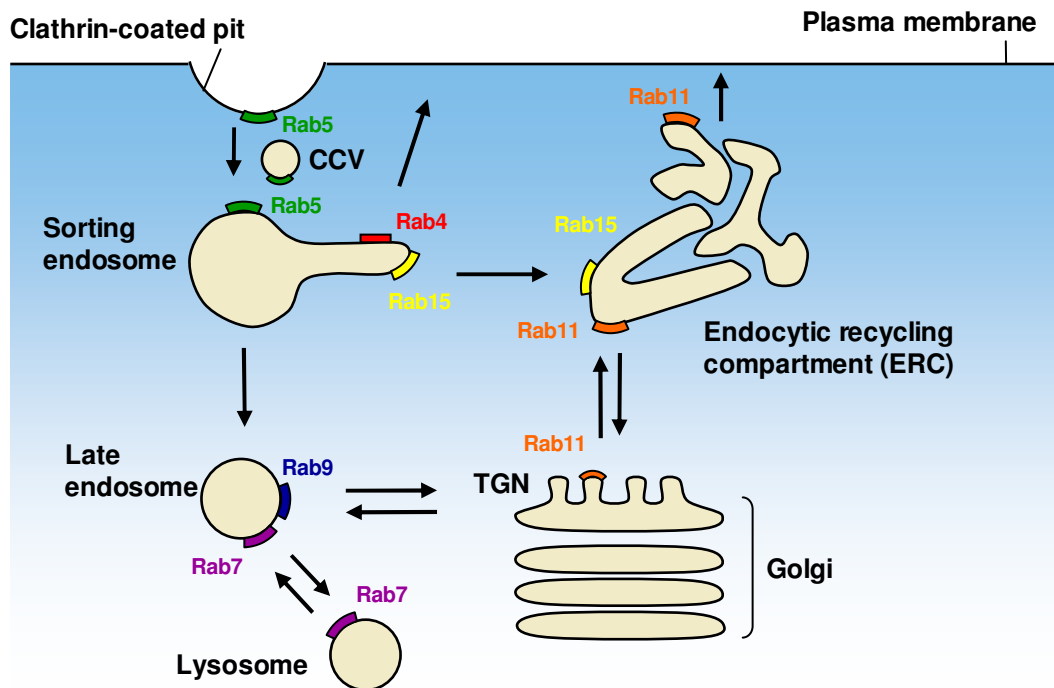


**Fig. 3: Endosomal recycling.**

During endocytosis, cargo is taken up from clathrin-coated pits into clathrin-coated vesicles (CCV) and delivered to sorting endosomes. Cargo receptors either return directly to the plasma membrane or indirectly through the ERC. Ligands and receptors which are destined for degradation are transported from sorting endosomes to late endosomes and ultimately to lysosomes, where they are degraded by hydrolytic enzymes. Sorting and retrieval pathways also exist between the ERC, the TGN (trans-Golgi network), late endosomes and lysosomes. Selected Rab GTPases which mediate vesicular trafficking between compartments are shown in colour. (Modified from Maxfield & McGraw, 2004, Stenmark, 2009, and Zerial & McBride, 2001.)

Rab proteins are small GTPases which have a crucial function in intracellular membrane trafficking. With at least 60 Rab GTPases in humans, they constitute the largest group within the Ras GTPase superfamily. They are localised at the cytosolic face of vesicle membranes in specific domains and recruit a set of

specific effector proteins to these membrane domains in order to carry out a certain function. The GTPase function enables Rab proteins to switch between an active GTP-bound form and an inactive GDP-bound form (Fig. 4). Guanine nucleotide exchange factors (GEFs) trigger the binding of GTP, while GTPase-activating proteins (GAPs) accelerate the hydrolysis of bound GTP. Combined with the GTP/GDP cycle is the cycle between membrane attachment and cytosolic localisation. Rab GTPases can attach to membranes through a prenyl anchor, which is masked by the GDP dissociation inhibitor (GDI), when the Rab protein is located in the cytosol. The Rab-GDI complex can be dissociated by the GDI displacement factor (GDF), which allows Rab insertion into membranes and Rab activation by specific GEFs. GTP-bound Rab proteins recruit specific Rab effector proteins, which then carry out their specific function. The cycle is ended when the Rab proteins are inactivated by specific GAPs and extracted from the membrane by GDI.

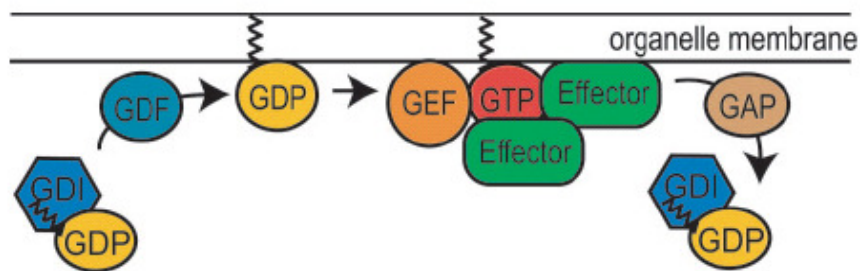


Fig. 4: Activation and inactivation of Rab GTPases.

Inactive (GDP-bound) prenylated Rab GTPases are bound to GDI (Rab GDP dissociation inhibitor), which keeps the Rab in a soluble cytosolic form. GDF (GDI displacement factor) dissociates the GDI-Rab complex and allows membrane attachment of the Rab through the prenyl anchor. Specific GEFs (guanine nucleotide exchange factor) exchange GDP for GTP and thereby activate the Rab GTPase and allow binding of specific effector proteins. Finally, specific GAPs (GTPase-activating protein) inactivate the Rab by accelerating the hydrolysis of the bound GTP into GDP. The inactive Rab can then be dissociated from the membrane by GDI (Grosshans et al., 2006).

The interaction between Rab GTPases and their effectors is very specific and is mediated through switch regions in the Rab proteins which undergo a conformational change between GTP- and GDP-bound states.

As a result, the Rab proteins and their effectors define specific membrane domains, which are the basis for specificity in intracellular trafficking. The group of known Rab effector proteins is growing rapidly and revealing a great diversity of effector functions, including sorting of the correct vesicle cargo, attachment to intracellular motors, recognition of the target membrane, vesicle tethering and membrane fusion. (For reviews on Rab proteins see Zerial and McBride, 2001, Grosshans et al., 2006, and Stenmark, 2009.)

The Rab GTPase which is of interest in this thesis is Rab11. It is localised in the pericentriolar ERC and plays a key role in the exit of cargo from the ERC to the plasma membrane (Ullrich et al., 1996; Ren et al., 1998; Chen et al., 1998; Trischler et al., 1999). Also a role in the transport from the ERC to the trans-Golgi network (TGN) (Wilcke et al., 2000) and from the TGN to the plasma membrane (Chen et al., 1998) has been reported.

Mammalian cells possess three related proteins which belong to the Rab11 family: Rab11a, Rab11b and Rab25. Rab11 effector proteins include the rab11BP (Rab11 binding protein), Rab11-FIP1, -2 and -3 (Rab11 Family Interacting Protein 1-3), pp75/Rip11 and myosin Vb (Zeng et al., 1999; Hales et al., 2001 and 2002). The ternary complex consisting of Rab11a, Rab11-FIP2 and the motor protein myosin Vb was shown to have a function in the recycling of the muscarinic acetylcholine receptor m4 and the chemokine receptor CXCR2 (Volpicelli et al., 2002; Fan et al., 2004).

A well established method to investigate endosomal recycling is to monitor the recycling of labelled transferrin in the cell. Transferrin and its receptor are responsible for the very efficient uptake of iron from the blood into all cells. Transferrin (Tf) is a single chain glycoprotein of less than 80,000 Da, which has two non-identical iron binding sites. Several transferrin isoforms exist, of which most abundant and well described is serum-transferrin. It binds to the transferrin receptor (Tf-R), which is a transmembrane glycoprotein consisting of 2 identical disulfide-bonded subunits of approximately 90,000 Da. The binding affinity is higher for diferric transferrin (transferrin loaded with 2 iron atoms) than for apo-transferrin (unloaded transferrin). Each receptor subunit binds 1 transferrin molecule; thus 2 transferrin and 4 iron molecules are transported with 1

internalised receptor. During recycling (Fig. 5), the transferrin receptor in the plasma membrane binds diferric transferrin in the extracellular space and is then internalised by receptor-mediated endocytosis through clathrin-coated pits into endosomes. With the increasingly acidic environment in the endosome, the iron is released from the transferrin and transported into the cytosol by the DMT1 (divalent metal transporter 1). Transferrin receptor and apo-transferrin are recycled back to the cell surface, either directly from the sorting endosome or indirectly through the ERC. The direct recycling pathway is faster than the indirect one, and the molecular differences which determine whether recycling occurs through the direct or indirect pathway are not known (Maxfield and McGraw, 2004). At the plasma membrane the apo-transferrin is released into the extracellular space. (For a review on iron metabolism and transferrin recycling see Aisen et al., 2001.)

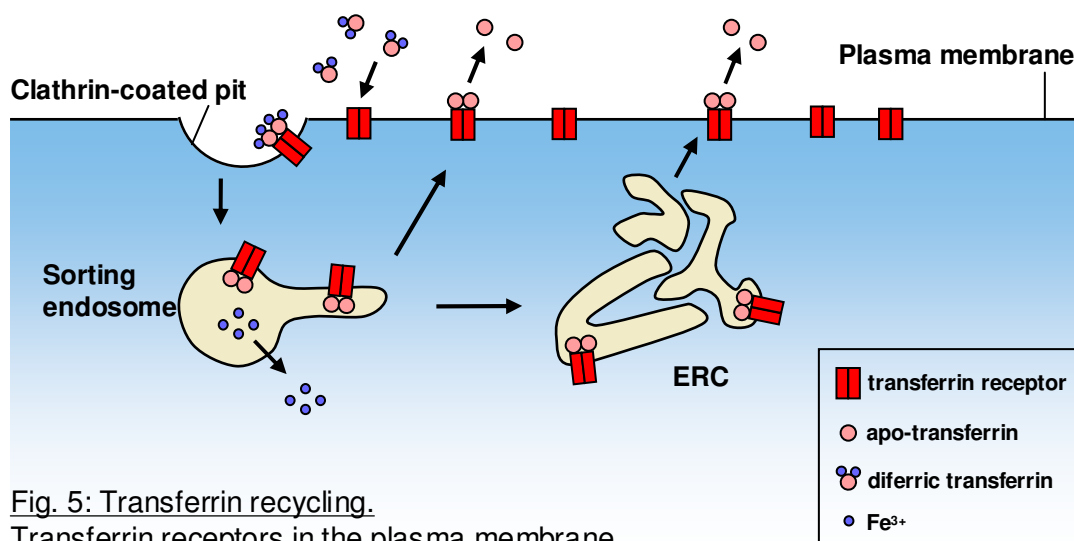


**Fig. 5: Transferrin recycling.**

Transferrin receptors in the plasma membrane bind diferric transferrin in the ec space and are then internalised by receptor-mediated endocytosis through clathrin-coated pits into endosomes. The iron is released and transported into the cytosol, while transferrin receptors and apo-transferrin are recycled back to the cell surface either directly from the sorting endosome or through the ERC. At the plasma membrane the apo-transferrin is released into the ec space. (Modified from Maxfield & McGraw, 2004).

## 1.4 Aims

This thesis aimed to investigate the pathogenic mechanism of Huntington's disease and, in particular, to clarify the role of protein aggregation in a cell culture model of this disease.

The first project was based on the results of a proteomics study on PC12 cells expressing huntingtin exon-1 with varying CAG repeat length that had been carried out in Prof. Pierluigi Nicotera's group. One of the proteins that were downregulated during the time of aggregate formation was Rab11, a protein involved in the function of the recycling endosome. I therefore intended to explore whether the endosomal recycling system is affected in this cell culture model of Huntington's disease.

The second project focused on the purification of huntingtin aggregates from PC12 cells. One hypothesis on how aggregates in Huntington's disease could mediate toxicity suggests the sequestration of vital cellular components into aggregates, based on several publications demonstrating colocalisation of cellular proteins with the huntingtin inclusions in various models of HD. However, the nature of these proteins was controversial and no proof was given whether sufficient amounts of proteins other than huntingtin were sequestered into inclusions to affect the cell. Therefore, I aimed to purify the huntingtin aggregates from PC12 cells and analyse their components.

## **2 Material and Methods**

### **2.1 Material**

#### **2.1.1 Antibodies**

The following primary antibodies were used for Western blotting: rabbit anti GFP (Molecular Probes A6455), rabbit anti GFP IgG-fraction (Molecular Probes A11122), mouse anti PolyQ (Chemicon MAB1574; clone 5TF1-1C2), HRP-linked goat anti biotin (Cell Signaling 7075), rabbit anti Rab11a (Zymed 71-5300), rabbit anti Rab11a/b (Abcam AB3612) and mouse anti GAPDH (Abcam AB8245). For immunocytochemistry, the following primary antibodies were used: rabbit anti Rab11a (Zymed 71-5300), mouse anti  $\beta$ -tubulin (Sigma), mouse anti  $\beta$ -III-tubulin (Promega) and mouse anti Glu- $\alpha$ -tubulin (Synaptic Systems).

HRP-conjugated secondary antibodies produced in goat against rabbit and mouse for Western blotting were purchased from Chemicon and BioRad. For fluorescence microscopy, the following secondary antibodies were obtained from Molecular Probes: goat anti mouse-Alexa Fluor 546 (A11030), goat anti mouse-Alexa Fluor 647 (A21236), goat anti rabbit-Alexa Fluor 546 (A11035) and goat anti rabbit-Alexa Fluor 647 (A21245).

#### **2.1.2 Transferrin**

The transferrin conjugates Transferrin-AlexaFluor 568 (T23365), Transferrin-AlexaFluor 633 (T23362) and Transferrin-biotin XX conjugate (T23363) were obtained from Molecular Probes.

#### **2.1.3 Chemicals**

For SDS-PAGE and Western blotting, polyacrylamide as 30% stock solution was purchased from BioRad and Geneflow. 'Plus one'-grade SDS, Tris, glycine and DTT were obtained from Amersham Biosciences.

All other chemicals were bought from Sigma or Fisher, unless otherwise mentioned in the method section.

## 2.2 Methods

### 2.2.1 Cell Culture

The PC12 clones 23.20 (23Q), 72.16 (74Q), and 74.10 (74Q) were kindly given to us by Dr. D. Rubinsztein, in whose laboratory they were generated (Wytttenbach et al., 2001). The cells were cultured in DMEM with high glucose (Sigma), supplemented with 2 mM L-glutamine or 2 mM L-alanyl-L-glutamine (Invitrogen), 10% horse serum (Sigma), 5% Tet system approved fetal bovine serum (BD Biosciences/Clontech), 75 µg/ml hygromycin and 100 µg/ml G418 (Invitrogen), at 37 °C with 5% CO<sub>2</sub> for maintenance.

The cells were subcultured 2-3 times per week. To this purpose, the cells were detached with trypsin-EDTA in PBS (0.005% trypsin, Invitrogen) at 37 °C, harvested with medium and pelleted for 4 minutes at 1000 rpm. To disperse the clumps and improve even cell growth, the cells were passed 10 times through a G18 syringe needle. They were not grown over 75% confluence. Transgene expression is under the control of the Tet-On system and was induced by addition of 1 µg/ml doxycycline (Sigma) to the medium one day after seeding the cells. The medium was changed every 2 days during induction, when also fresh doxycycline was added. According to Wytttenbach et al. (2001), genomic DNA from individuals with 21 or 72 CAG repeats was used as a template for amplifying a fragment of exon-1 (codons 8-57 in the case of 21 CAG repeats) of the HD gene. PCR products were ligated into the *Bgl*II and *Eco*RI restriction sites of the vector EGFP-C1 (Clontech). The resulting plasmids were digested with *Eco*47III and *Eco*RI to release exon-1 tagged to EGFP, which was religated into the *Eco*RI and blunt-ended *Sac*II sites of the vector pTRE (Clontech).

Untransfected PC12 cells were used for the siRNA experiments. There were purchased from ECACC (#88022401) and cultured in RPMI 1640 medium, supplemented with 2 mM L-alanyl-L-glutamine (Invitrogen) and 10% fetal bovine serum (Sera laboratories). These cells grow partly adherent, partly in large clumps in suspension when cultured in uncoated flasks. Their preferred substrate is collagen IV, on which they adhere tightly and often form small processes. Before and during experiments, they were therefore always grown on collagen IV-coated plasticware (BD Biosciences).

### **2.2.2 Collagen IV Coating**

Collagen IV coating also allowed growing PC12 cells on glass coverslips which is necessary for confocal microscopy. The procedure was optimised over a length of time. Collagen type I, which is mentioned in most publications for PC12 culture, did not prove to be a good substrate, because it led to very poor adhesion and survival of the PC12 cells. PC12 cells strongly prefer collagen type IV as a substrate, which is produced from Engelbreth-Holm-Swarm lathrytic murine sarcoma and was first purchased from Sigma, later from BD Biosciences. The best results were achieved by the following procedure: The mouse collagen IV from BD, supplied in a solution of 0.05 M HCl in ultra pure water, was thawed slowly on ice and diluted in 0.05 M HCl in ultra pure water to a final concentration of 100 µg/ml. A droplet was placed in the centre of a thoroughly cleaned and sterile coverslip, air-dried within 2 to 3 hours, washed in ultra pure water, and air-dried again before use.

### **2.2.3 SDS-PAGE**

Cells were lysed for 30-60 minutes on ice in 1% Triton lysis buffer (10 mM Tris-HCl pH 8.0, 10 mM KCl, 1.5 mM MgCl<sub>2</sub>, 0.5 mM DTT and 1% Triton X-100) or RIPA lysis buffer (10 mM Tris-HCl pH 7.2, 150 mM NaCl, 5 mM EDTA, 0.1% SDS, 1% deoxycholate, 1% Triton x-100), both containing 1 x protease inhibitors (Complete™, Roche). The protein concentration of the lysate was determined with the DC Protein Assay (BioRad). Usually, 10 or 30 µg of protein were mixed with 10 µl of 2 x sample buffer (65 mM Tris-HCl pH 6.8, 30% glycerol, 4% SDS, 10% DTT, 0.04 % bromophenol blue) and incubated for 5 minutes at 99°C in an Eppendorf Thermomixer. Samples were loaded onto 10-15% acrylamide gels (8 x 7 cm) with a 4% stacking gel (cast with the BioRad minigel system) and run at 100-200 V for 45 minutes to 2 hours with 1x SDS running buffer (25 mM Tris, 190 mM glycine, 0.1% SDS). 5 µl prestained broad range molecular weight marker (BioRad, 161-0373) served as a standard.

### **2.2.4 Western Blotting**

Following SDS-PAGE, the proteins were blotted onto a nitrocellulose membrane (Hybond™ ECL™, Amersham Pharmacia) for 1 hour at 30 V in a NuPage transfer cell in 1x NuPage transfer buffer (25 mM Bicine, 25 mM Bis-Tris, 1 mM

EDTA, 50  $\mu$ M chlorobutanol, 20% v/v methanol, pH 7.2). Alternatively, the proteins were blotted with the BioRad system for 1 hour at 100 V or over night at 30 V in 1 x transfer buffer (25 mM Tris, 192 mM glycine, 20% v/v methanol). Subsequently, the membrane was stained with Ponceau Red (0.25% Ponceau S, 1% glacial acetic acid in ultra pure water) to check whether the proteins had been transferred to the membrane and whether the gels had run correctly. The membrane was destained in TBST (10 mM Tris-HCl pH 8.0, 150 mM NaCl, 0.1% Tween 20) and blocked overnight at 4 °C in TBSMT (TBST plus 3% skimmed milk powder Marvel<sup>TM</sup>). Blots were incubated for 1-2 hours at RT with primary or secondary antibody diluted in TBSMT. After incubation with antibody, blots were washed 3 x 10 min in TBST, plus an additional rinse in PBS before developing. Blots were developed with Super Signal (Pierce) and the chemiluminescent signal was detected on film (Kodak BioMax Light Film). The developed films were scanned with a densitometer at a resolution of 100  $\mu$ m. For quantitative analysis, the signal intensity of each band was quantified using the software ImageJ.

### **2.2.5 Filter Retardation Assay**

Cells were lysed in 1% triton lysis buffer for 30 minutes on ice and treated with benzonase (50 U for 1 well in 6-well plate) for 30 minutes at 37°C at 300 rpm. The protein concentration was determined with the DC protein assay (BioRad). Subsequently, 50  $\mu$ l of each sample were transferred to a new tube, mixed with a buffer (10% SDS, 250 mM DTT) to reach a final concentration of 2% SDS and 50 mM DTT and incubated for 5 minutes at 98°C. A sample volume containing 40  $\mu$ g protein was transferred again to a new tube and filled up to 200  $\mu$ l with a 2% SDS solution. The samples were filtered through a 0.2  $\mu$ m cellulose acetate membrane (Schleicher & Schuell) in a dot blot manifold, and each well was washed twice with 200  $\mu$ l of a 0.1% SDS solution, while the membrane was still in the manifold. The filter was dried for 10 minutes at 37°C, and processed like a normal Western blot.

### **2.2.6 MTS Viability Assay**

The MTS assesses cell viability based on the metabolic activity of the mitochondria. MTS (3-(4,5-dimethylthiazol-2-yl)-5-(3-carboxymethoxyphenyl)-2-(4-sulphophenyl)-2H-tetrazolium, Sigma) is a tetrazolium salt which is reduced by mitochondrial dehydrogenases to formazan. The formation of formazan can be quantified by reading the absorbance at 490 nm.

The assay was carried out according to the supplier's instructions. At the start of the assay, the MTS working solution was added to the cells in a ratio 1:5 (MTS solution to medium) and the cells were incubated at 37°C for 3 hours. The reaction was quantified in a plate reader by reading the absorbance at 490 nm before and after the 3 hour incubation period. The difference in absorbance between both time points was calculated and the resulting dehydrogenase activity was presented as percentage of uninduced control cells. Average and standard deviation were calculated from 4 wells per condition.

### **2.2.7 Immunocytochemistry**

PC12 cells were grown on collagen-IV coated coverslips, washed once in warm PBS and fixed in 4% PFA in PBS for 20-30 min at RT. In later experiments, the PFA was added directly to the warm medium in a final concentration of 2% as a milder method of fixation. After the fixation, the cells were washed 3 times in PBS and permeabilised for 5 min in 0.1% Triton X-100 in PBS for 5 min at RT. After 3 more washes, the cells were blocked over night at 4°C in PBS containing 1% BSA and 2% NGS. On the next day, the samples were incubated for 2 h at RT first with the primary antibody and then with the secondary antibody, both diluted in PBS containing 0.5% BSA. Between the 2 incubation times and afterwards, the cells were washed 3 times in PBS containing 0.5% BSA and 0.1% Tween 20. After 2 more washes in PBS alone, the coverslips were dipped briefly in ultrapure water, drained on paper and mounted on a slide in Aqua Polymount (Polysciences). After drying at RT, the samples were sealed with nail varnish and stored at 4°C. Images were taken with the Zeiss laser scanning microscope LSM510 and a 63x objective (oil).

### 2.2.8 Transferrin Recycling

For quantitative measurements of transferrin recycling, biotinylated transferrin was used, which can be detected by an HRP-conjugated biotin antibody. The Western blot signal from several experiments was then quantified by scanning the films at a resolution of 100  $\mu\text{m}$  and measuring the signal intensity of each band using the Image J software, followed by analysis in Excel.

To measure the uptake of transferrin into the cell, the cells were washed twice with warm serum-free medium (SFM) and incubated for 1 h at 37°C to clear them of transferrin. Subsequently, the cells were loaded with 2  $\mu\text{g}/\text{ml}$  transferrin-biotin in SFM at RT for 5, 10, 20 or 30 minutes. At a respective time point, the cell culture plate was placed directly on ice, the cells were washed twice with cold PBS and lysed in RIPA buffer (10 mM Tris-HCl pH 7.2, 150 mM NaCl, 5 mM EDTA, 0.1% SDS, 1% deoxycholate, 1% Triton x-100, plus 1 x protease inhibitors, Complete<sup>TM</sup>, Roche). Proteins were resolved by SDS-PAGE, blotted and probed with an HRP-conjugated biotin antibody.

To measure the extrusion of transferrin from the cell, the cells were as before washed twice with pre-warmed serum-free medium and incubated for 1 h at 37°C. Subsequently, the cells were loaded with biotinylated transferrin at a concentration of 10  $\mu\text{g}/\text{ml}$  in SFM for 1 h at 37°C. After loading, the cells were quickly washed twice in pre-warmed SFM and then chased for 0, 15, 30 or 60 min in pre-warmed full medium. At a respective time point, the cells were harvested and processed as described for the uptake experiment.

To analyse the transferrin recycling by confocal microscopy, the cells were grown on collagen-IV-coated coverslips and loaded with transferrin-Alexa-633 at a concentration of 10  $\mu\text{g}/\text{ml}$  in SFM for 1 h at 37°C. As described above, the cells were chased for 0, 15, 30 or 60 min in pre-warmed full medium. At a respective time point, the cells were fixed in 4% PFA, washed and mounted in Aqua Polymount on a slide. Images were taken with the Zeiss laser scanning microscope LSM510 and a 63x objective (oil).

### **2.2.9 Live Cell Imaging**

Live cell imaging was used to monitor the uptake of transferrin into the ERC at single cell level. 23Q and 74Q cells, uninduced or induced with doxycycline for 4 d, were grown in collagen-IV-coated 4-well chamber slides, which can be mounted on the stage of the confocal microscope. Before the experiment, the cells were washed with pre-warmed serum-free medium (SFM) and incubated for 30 min at 37°C to clear the cells of transferrin. The cells were then incubated in 600 µl SFM (RT) containing 25 mM HEPES, pH 7.4, and transferred onto the microscope stage of a Zeiss laser scanning microscope LSM510. After 15 min to allow equilibration of the temperature and adjusting the microscope settings, 100 µl medium were taken out of the chamber, mixed with a working solution of 0.5 mg/ml transferrin-Alexa-633 in PBS and added very carefully back into the chamber, resulting in a final concentration of 5 µg/ml transferrin. The time lapse was immediately started and run for 1 h at RT. Z-Stacks of 8-9 images were taken at each time point, starting at an interval of 30 sec and finishing with an interval of 5 min. A 63x oil objective was used, lasers 488 and 633, and images were taken at a resolution of 512 x 512. For analysis, a subset of 5 images of one stack (comprising the centre of the cell) was combined in a projection using the Zeiss software, a ROI (region of interest) was drawn around the ERC and the intensity values of channel 2 (transferrin) at each time point were exported into Excel and analysed.

### **2.2.10 Rab11 overexpression**

Four plasmids for Rab11 were kindly given to us by Dr. Jim Norman, overexpressing wild-type Rab11 or three Rab11 dominant-negative mutants, Rab11-Q70L, Rab11-S24N and Rab11-N124I. The Rab11 constructs were tagged with a modified HA epitope, which can only be detected by a special HA antibody, which is compatible with immunocytochemistry but not with Western blotting. Cells were transiently transfected with Lipofectamine 2000 (Invitrogen) in a 24-well plate, using 0.8 µg DNA and 2.0 µl Lipofectamine per well and following the method described in the instruction manual. Assessed by immunocytochemistry, the transfection efficiency reached approximately 25%.

### **2.2.11 Rab11 siRNA**

Rab11a and Rab11b were downregulated by siRNA. The siRNAs for rat Rab11a/b (3 siRNAs per isoform) were commercially available at Ambion. A siRNA for GAPDH and a scrambled siRNA, both supplied by Ambion, served as positive and negative control. Initial tests for transfection methods were made also with a fluorescently tagged siRNA from Quiagen, siRNA-AlexaFluor 568, the uptake of which into cells could be monitored by fluorescence microscopy. First, transfection was attempted with Lipofectamine 2000 as described above. Later, the Amaxa system (Amaxa Biosystems) was used to transfect the cells with siRNA. This method is based on a combination of electroporation with a transfection agent, in this case part of the 'cell line nucleofector kit V' from Amaxa. During the procedure, PC12 control cells were harvested as usual, resuspended in medium, dispersed thoroughly by passing the suspension through an 18G syringe needle and counted. Aliquots containing  $3.5 \times 10^6$  cells were transferred to tubes with a conical bottom and centrifuged again, but at only 90 g for 5 min at RT (essential), and all medium was carefully removed. The resulting cell pellet was resuspended gently in 100  $\mu$ l solution V (kit), 1.5  $\mu$ g siRNA was added and the suspension mixed well by pipetting up and down. The solution was transferred immediately to the electroporation cuvette (kit) and the nucleoporation performed in the Amaxa machine with programme P-25. The cells were immediately transferred into 600  $\mu$ l pre-warmed medium and divided into 2-3 wells of a 6-well plate with 2 ml pre-warmed medium per well. The medium was changed after 24 h and the cells harvested or subjected to further experiments after 48 or 72 h.

### **2.2.12 Density Gradient Centrifugation**

A continuous sucrose gradient between 40% and 70% (w/v), containing sucrose in PBS plus 1 x protease inhibitors (Complete<sup>TM</sup>, Roche), was prepared with a gradient mixer in a 13 ml polyallomer centrifugation tube (Beckman). Cell pellets of  $\sim 1 \times 10^7$  cells of each clone were lysed in 1% Triton lysis buffer (10 mM Tris-HCl pH 8.0, 10 mM KCl, 1.5 mM MgCl<sub>2</sub>, 0.5 mM DTT and 1% Triton X-100) plus 1 x protease inhibitors for 30 min on ice and carefully layered on top of the sucrose gradient. The sample was centrifuged for 90 min at 20,000 rpm (50,000 g) at 4°C in a swing out rotor (SW40Ti) in a Beckman L8-M centrifuge.

After the centrifugation, 12 x 1.1 ml fractions were collected from top to bottom. The pellet was washed and resuspended in 1.1 ml PBS with 1 x protease inhibitors. 10 µl of each fraction was subjected to Western blotting against GFP.

Nycodenz (N,N'-bis(2,3 dihydroxypropyl)-5-N-(2,3 dihydroxypropyl)acetamido-2,4,6-tri-iodo-isophthalamide, Sigma) is an iodinated compound used in gradient centrifugation because of its high density. Nycodenz solutions of various concentrations were made up in PBS plus 1 x protease inhibitors (Complete<sup>TM</sup>, Roche). The discontinuous Nycodenz gradient of the experiment selected for the results chapter was prepared by carefully layering the solutions between 45% and 20% (w/v) on top of each other in a 13 ml polyallomer centrifugation tube (Beckman). 23Q and 74Q cells, induced for 4 days with doxycycline, were lysed in RIPA buffer (10 mM Tris-HCl pH 7.2, 150 mM NaCl, 5 mM EDTA, 0.1% SDS, 1% deoxycholate, 1% Triton x-100, plus 1 x protease inhibitors) ( $3 \times 10^7$  cells per clone) and centrifuged for 15 minutes at 16,000 g. The pellets were washed in PBS and centrifuged again before they were finally resuspended in PBS and loaded onto the gradients. The density gradient centrifugation was carried out at 100,000 g for 20 hours. Fractions were collected with a needle from the bottom of the tube, starting with the heaviest solution. The fractions of the 23Q and 74Q gradient were analysed by SDS-PAGE and Western blotting against GFP.

### **2.2.13 Solubilisation of Aggregates**

A method described by Hazeki and co-workers (2000) was used to solubilise GFP-HttEx1 aggregates. The aggregate-containing pellets were resuspended in 100% formic acid and incubated for 30 min at 37 °C in an Eppendorf Thermomixer. Subsequently, the formic acid was evaporated in a speed vac (Concentrator SpeedVac DNA120 Savant) and the solubilised sample resuspended in SDS sample buffer for SDS-PAGE or in rehydration buffer for 2-dimensional SDS-PAGE (see below). In some cases the sample turned yellow, indicating a low pH, and was readjusted with a few µl Tris-HCl buffer pH 8.0.

### 2.2.14 2-Dimensional Electrophoresis

Samples containing 100-300 µg protein for a 13 cm IPG strip (precipitated protein from cell lysate or aggregates after evaporation of the formic acid) were resuspended in 250 µl rehydration buffer (7 M urea, 2 M thiourea, 2% Chaps, 1% Triton X-100, 65 mM DTT, 0.5% ampholytes and bromophenol blue) and shaken at RT (800 rpm, Eppendorf Thermomixer) for at least 5 hours. To avoid loading unsolved material, samples were centrifuged for 5 min at 16,000 g immediately before loading. The first dimension was set up on the IPGphor system (Amersham Pharmacia) following the instructions and run at 20 °C with 50 µA per strip. After a 12 hour rehydration period at low voltage (30 V), the proteins were focused for 1 h at 500 V, 1 h at 1000 V and 2 h at 8000 V, resulting in a total of 17860 Vhr (volt hours) over 16 h. Subsequently, the strips were washed with ultrapure water and equilibrated for 2 x 15 min in equilibration buffer (50 mM Tris-HCl pH 8.8, 6 M urea, 2% SDS, 35% glycerol and bromophenol blue). The first equilibration solution additionally contained 65 mM DTT to reduce disulfide bridges, the second solution 135 mM iodoacetamide to block the reduced cysteine residues.

For the second dimension, the gel strip was placed on a 10% polyacrylamide gel (16 x 18 x 0.1 cm). 1 ml warm agarose solution (0.5% low melting point agarose in 1x SDS running buffer) was used to seal the strip tightly to the gel surface. A small piece of filter paper containing 10 µl of molecular weight marker (Invitrogen Mark12™ MW Standard 1 x) was placed beside the blunt (basic) end of the gel strip. Two gels were run in the Pharmacia system with 1x SDS running buffer (see above) at 18 °C, limited to 200 V and 20 mA for 15 min and to 400 V and 40 mA for 4 h.

Protein gels were usually stained with a standard silver stain procedure in the Hoefer Processor Plus (Amersham Pharmacia) after fixation overnight in 40% methanol and 10% glacial acetic acid. The advantage of this method is its high sensitivity, but it is incompatible with mass spectrometry. Therefore, Sypro Ruby (Molecular Probes) was used according to instructions to stain 2D gels that were intended for mass spectrometry. Sypro-Ruby-stained gels were scanned at a resolution of 100 µm with the ProXpress Scanner (Genomic solutions)

according to the instruction manual. The resulting images were analysed with the programme ProGenesis (Genomic solutions). Silver-stained gels were scanned with a densitometer at a resolution of 100  $\mu\text{m}$ .

### **2.2.15 Immunomagnetic Separation**

The magnetic beads used for the purification of aggregates were Dynabeads (DynaL Biotec) which are superparamagnetic polystyrene beads with a diameter of 2.8  $\mu\text{m}$  +/- 0.2  $\mu\text{m}$ , in this case coated with covalently bound sheep anti rabbit IgG. With a density of 1.3  $\text{g}/\text{cm}^3$ , they settle in suspension and need therefore to be resuspended before use and to be agitated during incubation times.

Dynabeads were isolated by placing a 1.5 ml tube containing the suspension in a special magnet. After 2-3 minutes, the beads collected at the side of the tube and the solution could be removed with a pipette. The Dynabeads were first coated with the primary antibody, in this case rabbit IgG anti GFP, at a concentration of 1  $\mu\text{g}$  IgG per  $1 \times 10^7$  beads in PBS plus 0.1% BSA over night at 4°C. After 2 washing steps in PBS/BSA,  $1 \times 10^7$  coated beads were incubated with resuspended pellets from 23Q and 74Q cells ( $1 \times 10^6$  cells per clone, induced for 4 days) for 1 hour at 4°C. The beads were extracted in the magnet and washed twice in PBS/BSA; the bound proteins were eluted from the beads with hot SDS sample buffer for 5 min at 99°C. The eluates were subjected to further analysis by SDS-PAGE and Western blotting.

## 3 Results

### 3.1 PC12 Cell Culture Model of Huntington's Disease

The cell culture model of Huntington's disease used in this thesis consists of several stable PC12 cell lines expressing a GFP-tagged huntingtin exon-1 fragment with varying CAG repeat length under the control of an inducible promoter (Tet-On). These cell lines have been generated in Dr. D. Rubinsztein's laboratory and described with respect to transgene expression, aggregate formation and cell death (Wyttenbach et al., 2001). In this thesis, I use three stable PC12 cell lines, clones 23.20, 72.16 and 74.10. Clone 23.20, also referred to as 23Q cells or 23Q clone, expresses a fusion protein consisting of a huntingtin exon-1 fragment with a polyglutamine tract of 23 glutamine residues and EGFP at the N-terminus (GFP-HttEx1-23Q, wild-type). The clones 72.16 and 74.10 express the same fusion protein, however with a prolonged polyglutamine tract of 74 glutamine residues (GFP-HttEx1-74Q, mutant). Most experiments were performed on clone 72.16 and, in case of significant results, double-checked with clone 74.10. As no significant differences between the two clones were seen and to avoid confusion, both clones are usually referred to as 74Q cells or 74Q clone, and the clone name is only noted in the figure legend.

Normal PC12 cells can be differentiated with NGF (nerve growth factor) to adopt a more neuronal character, but attempts to differentiate the PC12 clones with NGF on collagen or laminine did not give satisfactory results (data not shown). NGF concentrations from 100 ng/ml to 250 ng/ml combined with low-serum conditions between 1% and 5% horse serum were tested. However, serum conditions that were low enough to lead to a complete cell cycle arrest and a high percentage of cells with processes also induced cell death, whereas higher serum levels did not stop cell proliferation. All experiments were therefore performed on cycling PC12 cells.

Expression of the transgene is induced with addition of doxycycline to the culture medium. In the Tet-On system, tetracycline or doxycycline bind to the reverse Tet repressor (rTetR) which subsequently binds to the Tet responsive

element (TRE) and activates transcription of the transgene. As described by Wyttenbach et al., 2001, the induction is dose-dependent and maximal expression of the transgenes is achieved with 1  $\mu\text{g/ml}$  doxycycline, which was therefore used in all experiments.

Imaging the PC12 cells by confocal microscopy showed that, upon induction with doxycycline, GFP-HttEx1-23Q is homogeneously distributed throughout the cell (predominantly in the cytoplasm and at lower levels in the nucleus) and was never observed to form aggregates (Fig. 6D). The expression level of GFP-HttEx1-23Q varies from cell to cell. In contrast to GFP-HttEx1-23Q, the mutant GFP-HttEx1-74Q is homogeneously distributed only during the first 24 hours of induction (Fig. 6B). Afterwards it starts to aggregate and reaches a maximal level of aggregation after 4 days (Fig. 6C), when approximately 40% of the cells contain aggregates. The aggregates are extremely variable in size and can be located in the nucleus as well as in the cytosol. Also after 4 days of induction, there are still cells present which express high levels of GFP-HttEx1-74Q but have not formed aggregates. In addition, many cells with aggregates also contain soluble GFP-HttEx1-74Q, but its concentration is usually lower than in cells without aggregates.

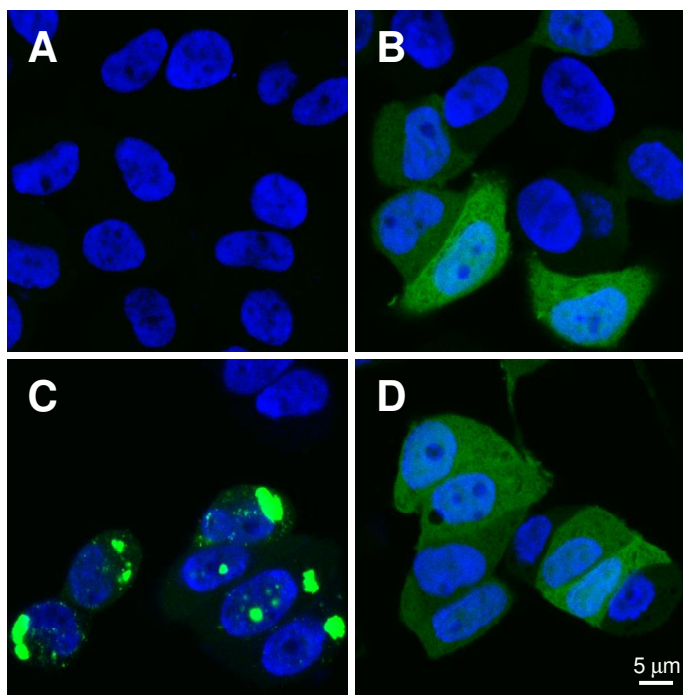


Fig. 6: Expression of GFP-HttEx1 in PC12 cells  
74Q cells (clone 72.16) were left uninduced (A), induced for 1 d (B) or induced for 4 d (C) with 1  $\mu\text{g/ml}$  doxycycline (dox). 23Q cells are shown only after 4 d of induction with 1  $\mu\text{g/ml}$  dox (D). The cells were grown on collagen-IV-coated coverslips and imaged by confocal microscopy. The nuclei (Hoechst) are shown in blue, GFP-HttEx1 in green.

Western blots of PC12 cells cultured over 5 days with or without 1  $\mu\text{g/ml}$  doxycycline show expression of the transgene after 10 hours of induction, which increases over time (Fig. 7). The blots detect a very low background expression in the absence of doxycycline, which increases slightly in the 74Q cells over time in culture, revealing leakiness of the inducible promoter, as was reported before (Wytenbach et al., 2001). However, the background expression is too low to be detected by confocal microscopy (Fig. 6A). The expression of GFP-HttEx1-23Q increases continuously after induction, while the GFP-HttEx1-74Q expression drops at 3 days of induction before it rises again. This decrease coincides with a strong increase in aggregate formation, which is visible in the filter retardation assay in Fig. 9. The GFP-HttEx1-23Q protein has a calculated mass of 36.6 kDa, but migrates at approximately 44 kDa in a SDS-polyacrylamide gel. Similarly, the GFP-HttEx1-74Q protein has a calculated mass of 43.2 kDa, but migrates at approximately 56 kDa. This deviation between predicted and actual migration during electrophoresis might be due to an effect of the polyglutamine tract or the polyproline tract or both on the migration behaviour of both proteins and has been observed before (Aronin et al., 1995).

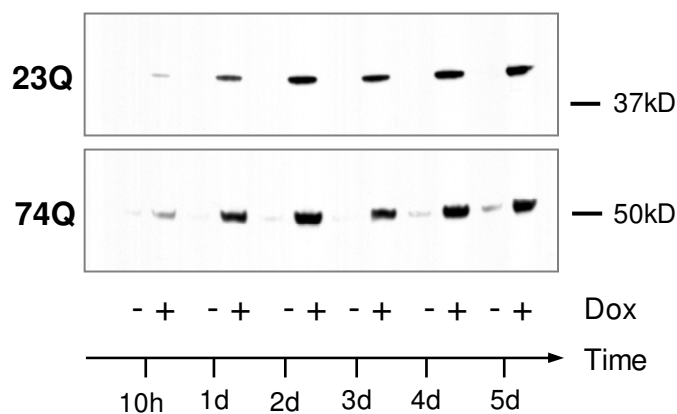


Fig. 7: Time course of induction of GFP-HttEx1 in PC12 cells  
23Q cells and 74Q cells (clone 72.16) were cultured over 5 d, with or without 1  $\mu\text{g/ml}$  dox. Expression of the fusion proteins GFP-HttEx1-23Q and -74Q was detected by Western blotting against GFP.

### 3.1.1 Aggregate Formation

When the proteins in the whole cell lysate of 74Q cells containing aggregates, i.e. after 4 days of induction with doxycycline, are separated by SDS-PAGE, the insoluble aggregates are retained in the stacking gel (Fig. 8). After transfer onto a nitrocellulose membrane, the antibody specific for GFP recognises this band in addition to the band of the soluble GFP-HttEx1-74Q in the resolving gel. A

polyQ-specific antibody (clone 5FT1-1C2), in contrast, detects only the soluble form, suggesting that the polyQ epitope is not accessible in the insoluble form.

The formation of aggregates was quantified by a filter retardation assay. For this purpose, cell lysate was treated with 2% SDS and 50 mM DTT and incubated for 5 minutes at 98°C before it was filtered through a 0.2 µm cellulose acetate membrane in a dot blot manifold. Subsequently, the membrane was dried and processed like a Western blot with an antibody against GFP. Aggregated proteins are trapped on the cellulose acetate membrane during this procedure and can be quantified by the luminescence intensity of the dot blot. The filter retardation assay (Fig. 9) shows an increasing amount of aggregated GFP-HttEx1-74Q over time with the strongest signal at 4 days of transgene induction with doxycycline.

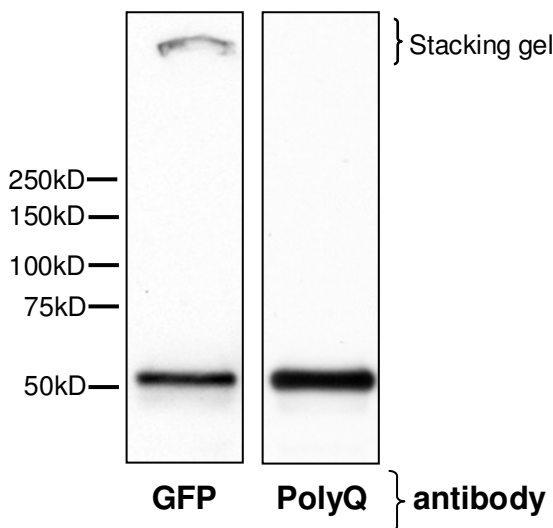


**Fig. 8: Retention of insoluble GFP-HttEx1-74Q aggregates in the stacking gel**

After 4 d of induction with 1 µg/ml dox, 74Q cells (clone 72.16) were lysed in 1% triton lysis buffer. Lysate containing 20 µg protein was submitted to SDS-PAGE and Western blotting. The blot was first probed with an antibody against GFP, then stripped and probed with an antibody against PolyQ.

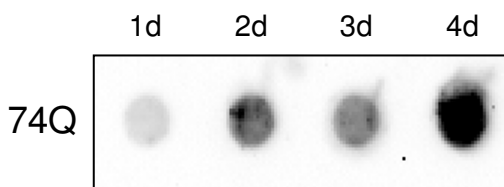


**Fig. 9: Filter retardation assay**

74Q cells (clone 72.16) were induced for 1, 2, 3 or 4 d with 1 µg/ml dox. The cell lysates were solubilised and filtered through a 0.2 µm membrane, on which aggregated proteins were trapped and probed with an antibody against GFP.

### 3.1.2 Cell Viability and Apoptosis

Staining the cell cultures with the nuclear dye Hoechst shows a negligible incidence of apoptosis based on the presence of pycnotic nuclei (< 0.1%; data not shown). The incidence of apoptosis does not increase within 4 days of expression of either transgene. This result was confirmed by Western blot analysis of 74Q cells which showed neither cleavage of the caspase substrates PARP and fodrin nor activation of caspase-3 after 4 days of induction (Fig. 10).

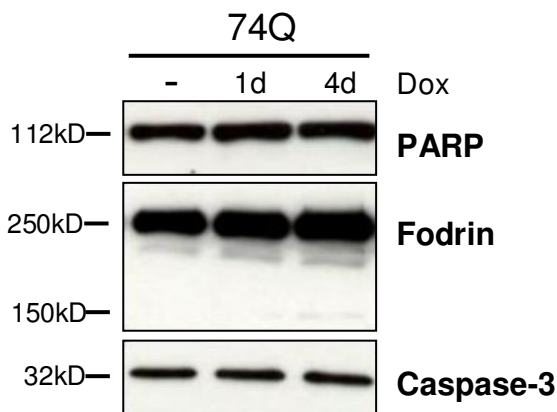


**Fig. 10: Apoptosis after transgene induction**

74Q cells (clone 72.16) were left uninduced or induced for 1 or 4 d with 1  $\mu$ g/ml dox before they were lysed in RIPA buffer.

The lysates were subjected to SDS-PAGE and Western blotting against PARP, fodrin and caspase-3 to check for apoptosis.

In addition, the viability of the PC12 clones after transgene induction was tested with the MTS assay. This assay is based on the reduction of the tetrazolium salt MTS by mitochondrial dehydrogenases to formazan, which can be quantified by reading its absorbance at 490 nm. It is a measure for the metabolic activity in a population of cells and is therefore often equated with the cell number. Cells of both clones were cultured in a 48-well plate and either left uninduced or induced for 1, 3 or 4 days with 1  $\mu$ g/ml doxycycline. The difference in absorbance at 490 nm within an interval of 3 hours was calculated and the dehydrogenase activity expressed as percentage of the uninduced control (Fig. 11). The results reveal a slightly increased metabolic activity per well after expression of either wild-type or mutant GFP-HttEx1, which confirms that the viability of the PC12 cells is not impaired by the induction and expression of either transgene.

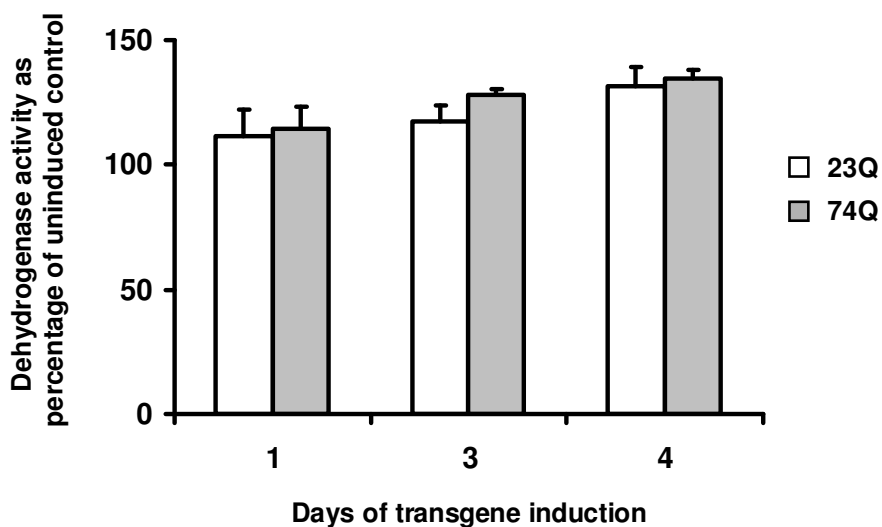


Fig. 11: Cell viability after transgene induction

The cell viability was assessed by the MTS assay, which is based on the reduction of MTS by mitochondrial dehydrogenases to formazan, the absorbance of which can be measured at 490 nm. 23Q cells and 74Q cells (clone 72.16) were cultured in a 48-well plate and either left uninduced or induced for 1, 3 or 4 d with 1  $\mu\text{g/ml}$  dox before the assay. The result is presented as the dehydrogenase activity in percent of the uninduced control (average + SD; n=4).

## 3.2 Effect of GFP-HttEx1 Aggregates on Endosomal Recycling

### 3.2.1 Endosomal Recycling, ERC and Rab11

Eukaryotic cells have a very complex transport, sorting and recycling system to deliver membrane components, proteins and solute molecules to their correct position, which is described in more detail in the introduction (chapter 1.3).

The focus of this project was the endosomal recycling that begins with clathrin-mediated endocytic delivery to the sorting endosome from where cargo can either be transported to lysosomes, back to the plasma membrane or to the recycling endosome. The recycling endosome is a long-lived tubular structure often concentrated at the centrioles near the nucleus and is therefore named pericentriolar endosomal recycling compartment (ERC). Cargo can be trafficked between the ERC and the plasma membrane or the Golgi apparatus. The small GTPase Rab11 has a vital function in regulating traffic through the ERC, where it is predominantly located.

A proteomics study on the PC12 cells had been carried out by Dr. Paul Richards and Anna Simpson at the beginning of this project with the aim to identify proteome changes linked to the expression of soluble GFP-HttEx1-74Q or to the presence of GFP-HttEx1-74Q aggregates (4 days induction). Among the identified proteins was Rab11b, which was downregulated in 74Q cells after 4 days of induction, but not in 23Q cells (Fig. 12A). This result was confirmed by Western blot analysis with an antibody against Rab11 (isoforms a+b) (Fig. 12B).

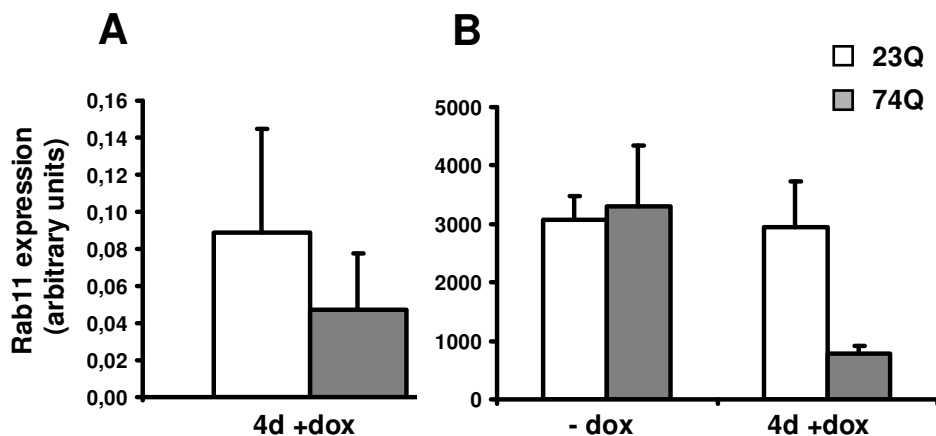


Fig. 12: Rab11 expression in a cell culture model of HD

23Q cells and 74Q cells (clone 72.16) were either left uninduced or induced for 4 d with 1  $\mu$ g/ml dox. Cells were lysed in 1% triton lysis buffer, the lysates were centrifuged for 5 min at 16,000 g and a proteomics screen was carried out on the supernatants by Anna Simpson and Dr. Paul Richards, who provided the data for this figure. A) Results from the quantitative 2D gel analysis for Rab11b (average + SD; n=6). B) The supernatants were then analysed by Western blot analysis against Rab11 (isoforms a/b) (average + SD; n=6).

Rab11 expression in 23Q and 74Q cells was also examined by immunocytochemistry. The antibody used in this experiment was specific for Rab11a, which is the predominant isoform in these cells. (No antibody specific for the isoform Rab11b was available, and the antibody against Rab11 isoforms a and b was not suitable for immunocytochemistry.) Uninduced cells and cells induced for 4 days with 1  $\mu$ g/ml doxycycline were analysed by confocal microscopy. The images in Fig. 13 display a Rab11 pattern as described in the literature (Ullrich et al., 1996), with faintly stained vesicles throughout the cytoplasm and a strong increase in the concentration of Rab11 and in the density of labelled vesicles towards the ERC. Induced 74Q cells containing aggregates appear to

have a less pronounced staining of the ERC (marked by arrows in Fig. 13B), but the signal intensity at the ERC also varies in 23Q and 74Q control cells without expression of the transgene (Fig. 13A).

Rab11 has been suggested to regulate transport through the ERC (Ullrich et al., 1996; Ren et al., 1998; Wilcke et al., 2000). Therefore, I will explore in this chapter whether the endosomal recycling system is affected by expression of either wild-type (23Q) or mutant GFP-HttEx1 (74Q) or by the presence of GFP-HttEx1-74Q aggregates.

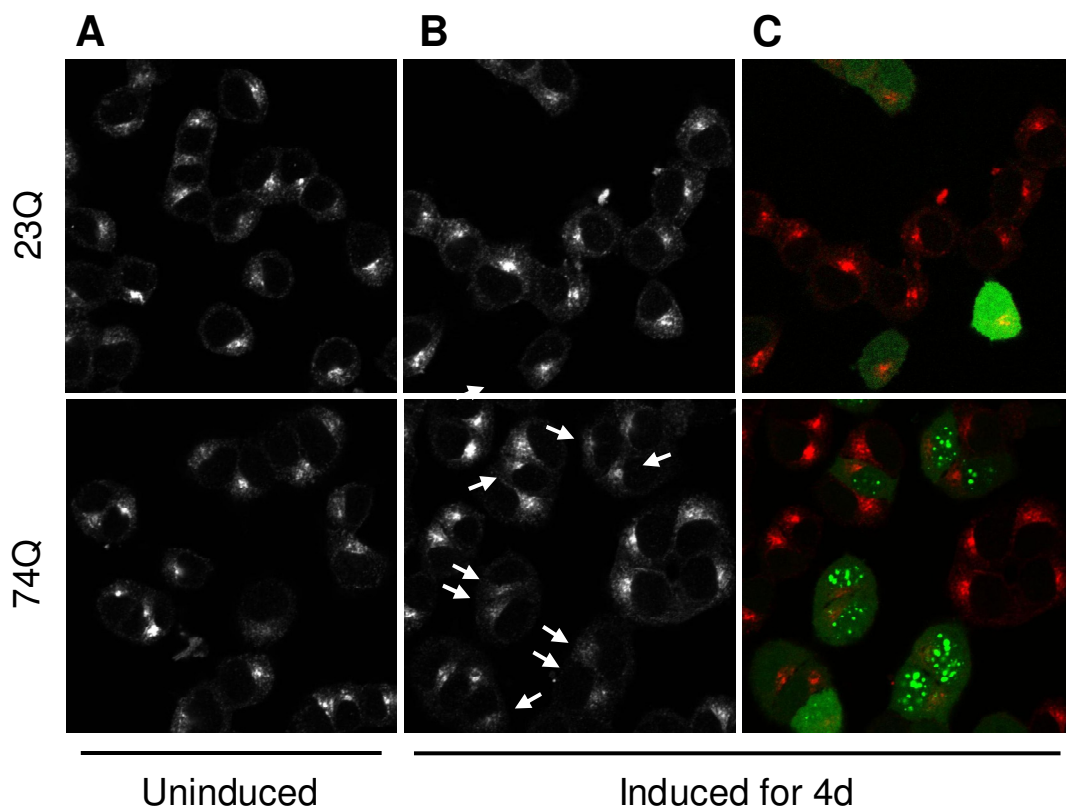


**Fig. 13: Rab11 expression in a cell culture model of HD**

23Q cells and 74Q cells (clone 72.16) were grown on collagen-IV-coated coverslips and left uninduced or induced for 4 d with 1  $\mu\text{g/ml}$  dox. The cells were fixed in PFA and immuno-stained with an antibody specific for Rab11a. The samples were analysed by confocal microscopy.

A) Uninduced 23Q and 74Q cells. Rab11a is shown in white

B) 23Q and 74Q cells, induced for 4 d. Rab11a is shown in white. Cells with aggregates and reduced levels of Rab11a are marked by arrows.

C) Same images as in B). Rab11a is shown in red, GFP-HttEx1 in green.

A well established method to investigate endosomal recycling is to monitor the recycling of transferrin, which delivers iron into the cell (chapter 1.3). A standard protocol from the literature (Lapierre et al., 2001) was used to test the uptake of Alexa-568-labelled transferrin into PC12 cells. Uninduced 23Q and 74Q cells were washed twice with warm serum-free (and thus transferrin-free) medium and incubated for 1 hour at 37°C to clear the cells of unlabelled transferrin. Subsequently, the cells were incubated with serum-free medium containing 10 µg/ml transferrin-Alexa-568 for 1 hour at 37°C to load the cells with labelled transferrin before fixation in 4% PFA. The cells were additionally immuno-stained with an antibody against Rab11a and imaged by confocal microscopy.

The labelled transferrin (Fig. 14A) is present in vesicles throughout the cytoplasm, but the concentration of transferrin and the density of labelled vesicles are the highest in a perinuclear region, indicative of the ERC. Co-staining with Rab11a (Fig. 14B) reveals a partial overlap of labelled transferrin and Rab11 at the ERC, whereas the vesicles in the cell periphery, which are (based on the literature) primary endosomes and sorting endosomes, only contain transferrin. The Rab11 signal in the cell periphery is extremely faint compared to the intense staining at the ERC. Uninduced 23Q and 74Q cells were undistinguishable with regard to the pattern of transferrin and of Rab11a.

The immuno-staining of the endogenous Rab11 was confirmed by transfection of cells with an HA-tagged Rab11, which was detected by an antibody specific for the HA-tag. The images in Fig. 14C display a pattern of the overexpressed Rab11 which is similar to that of the endogenous Rab11. The transfected cells (the transfection efficiency was about 25%) show a cytoplasmic staining with a dramatic increase in signal intensity towards a perinuclear position.

This experimental system of transferrin recycling can be used in multiple ways to look at sections of the recycling pathway more closely.

The uptake of transferrin can be monitored over time after addition of labelled transferrin to the medium. To study the extrusion pathway, a pulse-chase experiment can be conducted. In this type of experiment, the cells are loaded first with labelled transferrin (pulse) and are then transferred into normal

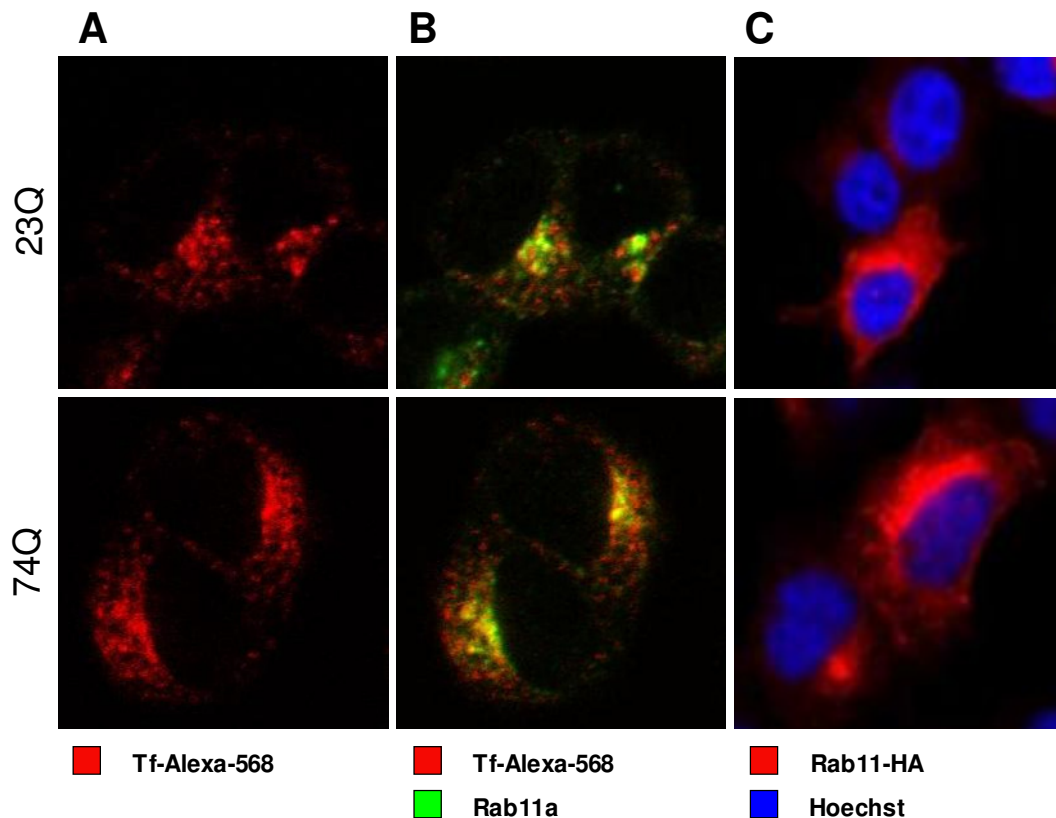


**Fig. 14: The ERC, transferrin and Rab11**

A) + B) 23Q cells and 74Q cells (72.16) were loaded with 10  $\mu\text{g/ml}$  Tf-Alexa-568, briefly washed in PBS and fixed in PFA. The cells were subsequently immuno-stained with an antibody against Rab11a and imaged by confocal microscopy. Panel A shows the Tf-Alexa-568 signal alone in red; panel B shows the same images, but with the Tf-Alexa-568 signal displayed in red and the Rab11a signal in green.

C) 23Q cells and 74Q (72.16) cells were transfected with an HA-tagged Rab11 construct. After 24 h, the cells were fixed in PFA and immuno-stained with an antibody specific for the HA-tag. The samples were analysed by confocal microscopy. The nuclei are displayed in blue (Hoechst), Rab11-HA in red.

medium containing unlabelled transferrin (chase). While the unlabelled transferrin is taken up, the labelled transferrin is extruded from the cell. The recycling can be examined by confocal microscopy on either living or fixed cells when fluorescently labelled transferrin is used. Imaging techniques have the advantage that single cells can be analysed (e.g. cells with or without aggregates), and not only the whole cell population. Alternatively, biochemical methods can be used with biotinylated transferrin. For this purpose, cells are placed on ice at certain time points to arrest the recycling process, washed and

lysed. Subsequently, the lysates are analysed by SDS-PAGE and Western blotting against biotin, which is suitable for the quantification of transferrin recycling in a cell population.

### **3.2.2 Uptake of Transferrin**

To investigate whether endosomal recycling is affected by the expression of wild-type (23Q) or mutant GFP-HttEx1 (74Q), I first examined the biochemistry of transferrin uptake into PC12 cells.

23Q and 74Q cells were either left uninduced or were induced for 1 or 4 days with 1 µg/ml doxycycline. 23Q and 74Q cells were cultured in different wells of the same 6-well plate for each time point to allow direct comparison between the clones and conditions. The cells were washed with warm serum-free medium and incubated for 1 hour at 37°C to clear them of unlabelled transferrin. Subsequently, the cells were loaded with 2 µg/ml transferrin-biotin in serum-free medium for 5, 10, 20 or 30 minutes at RT, because the process was too rapid at 37°C to be monitored effectively (data not shown). At a respective time point, the cell culture plate was immediately placed on ice, and the cells were washed twice with cold PBS and lysed in RIPA buffer. Proteins were resolved by SDS-PAGE, blotted and probed with an HRP-conjugated antibody specific for biotin. Control lysates of 23Q and 74Q cells without transferrin-biotin were run in the outer lanes of all gels.

The Western blots (Fig. 15A) show two bands of biotinylated proteins. The lower band (ca. 80 kDa) represents the transferrin-biotin with which the cells in lanes 2-7 were loaded. The upper band (130 kDa) can be attributed to the mitochondrial pyruvate carboxylase, which is an endogenous biotinylated protein. The bands were quantified using the software ImageJ and the data were analysed using Excel. The transferrin-biotin band intensities were normalised to the carboxylase band intensities in each lane and plotted as uptake of transferrin-biotin over time. Data of one representative experiment are presented in the graph in Fig. 15B. The transferrin-biotin signal is already strong after 5 minutes and reaches a maximum at 20 minutes. 74Q cells display, induced or uninduced, a higher rate of transferrin uptake than 23Q cells.

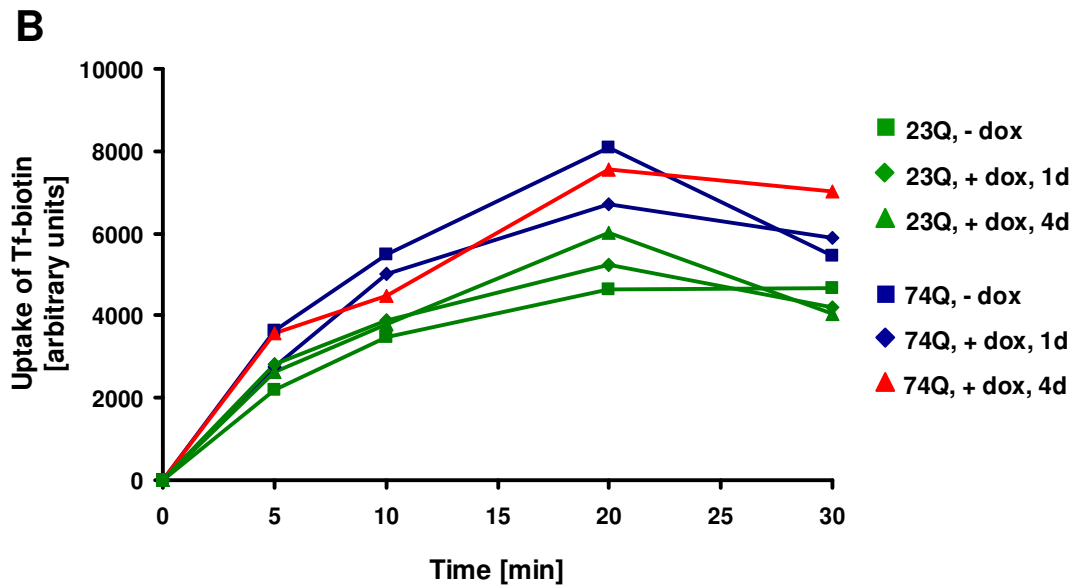
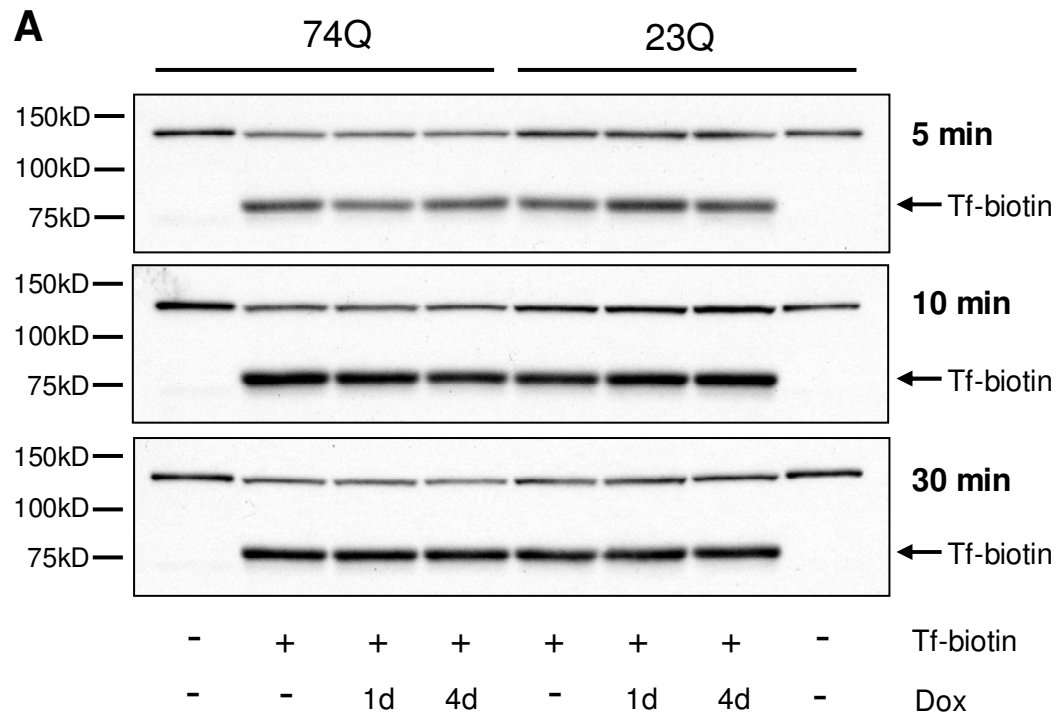


**Fig. 15: Uptake of transferrin into cells, Western blotting**

23Q cells and 74Q cells (clone 72.16) were either left uninduced or induced for 1 or 4 d with 1  $\mu\text{g/ml}$  dox. At the start of the experiment, the cells were loaded for 5, 10, 20 or 30 min with 2  $\mu\text{g/ml}$  Tf-biotin (ca. 80 kDa), before they were placed on ice, lysed in RIPA buffer and submitted to SDS-PAGE and Western blotting against biotin. Control lysates of 23Q and 74Q cells without Tf-biotin were run in the outer lanes. The Western blots for 5, 10 and 30 min uptake of Tf-biotin are shown in A). The band intensities of Tf-biotin from one representative experiment (n=1) were quantified and plotted in a graph as uptake of Tf-biotin over time in B).

This was observed in both 74Q clones, clone 72.16 and clone 74.10 (only the results for clone 72.16 are shown in Fig. 15). As the transgene expression is not completely switched off in the absence of doxycycline (see Fig. 7), this higher basal uptake of transferrin could be caused by the background expression of mutant GFP-HttEx1. However, cells with a very low expression level in the absence of doxycycline display a similar rate of transferrin uptake as cells with high expression levels after 1 or 4 days of induction with doxycycline. Therefore, it is more likely that the higher rate of transferrin uptake in the 74Q clones is independent of transgene induction.

Altogether, the results suggest that the uptake of transferrin in this cell culture model is neither affected by the expression of wild-type or mutant GFP-HttEx1 nor in the presence of aggregates.

Live cell imaging was used to monitor the uptake of transferrin at the single cell level. 23Q and 74Q cells, either uninduced or induced with doxycycline for 4 days, were grown in chamber slides which can be mounted on the microscope stage. Before the experiment, the cells were washed with serum-free medium and incubated for 30 minutes at 37°C to clear them of transferrin. The cells were then incubated in serum-free, HEPES-buffered medium at RT and mounted on the microscope stage. The time lapse was started immediately after transferrin-Alexa-633 was added to the cells in a final concentration of 5 µg/ml. Two channels were recorded in a multitrack scan, one detecting GFP-HttEx1, the other transferrin-Alexa-633. Images were taken initially every 30 seconds, then every minute and every 5 minutes for up to 1 hour. A z-stack of 8-9 images was scanned at each time point. Afterwards, a subset of 5 images of one stack, comprising the centre of the cell, was combined in a projection. Single images at 6 time points of one time lapse with induced 23Q cells (A) and one time lapse with induced 74Q cells (B) were selected for Fig. 16.

Both imaged fields present a mixed population of cells with respect to the expression of GFP-HttEx1. The 23Q cells can be divided into two groups: with or without GFP-HttEx1-23Q. In contrast, the 74Q cells can be divided into three groups: without expression, with soluble GFP-HttEx1-74Q or with aggregated GFP-HttEx1-74Q.

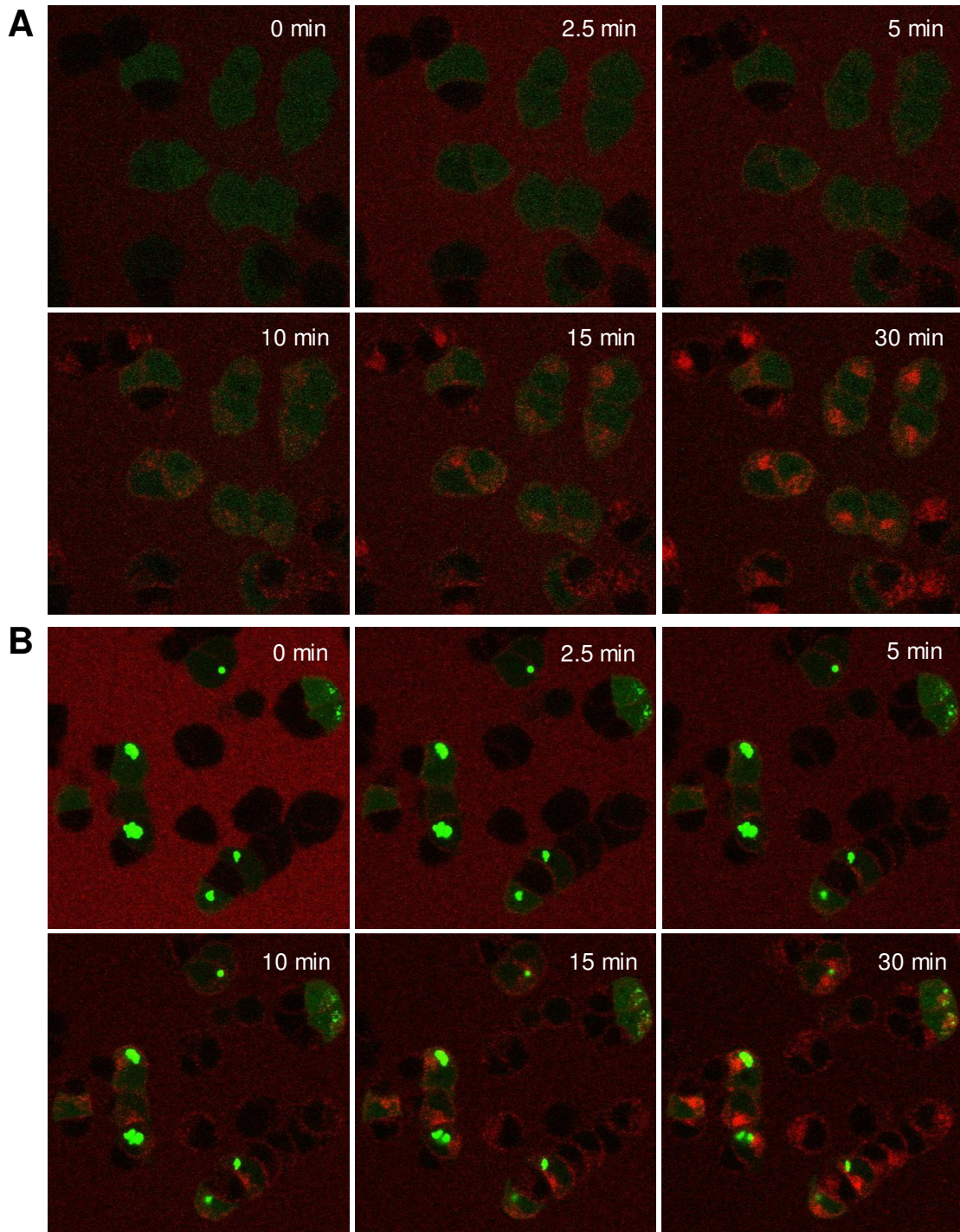


**Fig. 16: Uptake of transferrin into cells, live cell imaging**

23Q cells and 74Q cells (clone 72.16) were grown in collagen-IV-coated chamber slides and induced for 4 d with dox, before they were incubated with serum-free, HEPES-buffered medium and mounted on the microscope stage. The time lapse was started when Tf-Alexa-633 was added to the cells in a final concentration of 5  $\mu\text{g/ml}$ . Single images at 6 time points from 23Q cells (A) and 74Q cells (B) were selected for this figure. Tf-Alexa-633 is shown in red, GFP-HttEx1 in green.

Immediately after addition, transferrin-Alexa-633 is detected only in the medium surrounding the cells, but is subsequently taken up by all cells and accumulates in the pericentriolar ERC (Fig. 16A and B). No difference with respect to uptake of transferrin is visible between the five subgroups of cells summarised above (no quantitative analysis of the images was performed at this point). The images confirm the results of the Western blot analysis, i.e. that the internalisation of transferrin is neither impaired by the expression of wild-type or mutant GFP-HttEx1 nor in the presence of aggregates.

### **3.2.3 Extrusion of Transferrin**

Next, I examined whether the expression of wild-type or mutant GFP-HttEx1 affects the extrusion pathway of transferrin in PC12 cells.

A pulse-chase experiment with transferrin-biotin was carried out to quantify the extrusion in 23Q and 74Q cells, which were either left uninduced or induced for 1 or 4 days with 1  $\mu\text{g/ml}$  doxycycline. The cells were, as before, washed with warm serum-free medium and incubated for 1 hour at 37°C to clear them of unlabelled transferrin. Subsequently, the cells were loaded with 10  $\mu\text{g/ml}$  transferrin-biotin in serum-free medium for 1 hour at 37°C. After loading, the cells were quickly washed twice in warm serum-free medium and then chased for 0, 15, 30 or 60 minutes at 37°C in full medium (i.e. medium containing unlabelled transferrin). At a respective time point, the cell culture plate was immediately placed on ice and the cells were washed twice in cold PBS and lysed in RIPA buffer. The samples were analysed by SDS-PAGE and Western blotting against biotin. Control lysates of 23Q and 74Q cells without transferrin-biotin were run in the outer lanes of all gels.

The Western blots (Fig. 17A) show, as in the uptake experiment, the band of transferrin-biotin at approximately 80 kDa (in lanes 2-7) and the band of the mitochondrial pyruvate carboxylase at 130 kDa. Because of longer exposure time of the film in this experiment, there is a third band visible just below the transferrin-biotin, which is an unknown endogenously biotinylated protein. The bands were quantified using the software ImageJ and the data were analysed using Excel. The transferrin band intensities were normalised to the carboxylase

band intensities in each lane. The loading of transferrin at time point 0 was equal in all 6 lanes and was therefore set as 100% as saturation point, while the transferrin values at 15, 30 and 60 minutes were calculated as percentage of that value. Data from 4 independent experiments were plotted in the graph in Fig. 17B as percentage of retained transferrin-biotin (average +/- standard deviation) over time. In addition, the values at the 60 minutes time point are shown in a separate chart in Fig. 17C.

The graph in Fig. 17B demonstrates that the transferrin-biotin is rapidly expelled by the PC12 cells, which retain 29-48% of the initial amount after 15 minutes and 12-22% after 30 minutes chase. In the second half of the experiment, the rate of extrusion is much lower so that the cells still retain 6-19% transferrin-biotin after 60 minutes chase. 23Q cells display similar rates of transferrin extrusion in all 3 conditions (i.e. -dox, 1d +dox, 4d +dox) and the amount of transferrin-biotin after 60 minutes chase does not differ significantly between uninduced 23Q cells (13.8 +/- 6.3%; n=4) and 23Q cells induced for 1 day (9.8 +/- 2.9%; n=4) (t-test; p=0.30) or 23Q cells induced for 4 days (10.6 +/- 5.5%; n=4) (t-test; p=0.48), which demonstrates that the clearance of transferrin in 23Q cells is independent of transgene induction. Also 74Q cells which were left uninduced or induced for 1 day have similar rates of transferrin extrusion. Here, uninduced 74Q cells retain 5.8 +/- 3.7% (n=4) of the transferrin-biotin after 60 minutes chase and the 74Q cells induced for 1 day retain 7.2 +/- 2.8% (n=4), which is not significantly different (t-test; p=0.55).

Comparison between 23Q and 74Q cells which were uninduced or induced for only 1 day shows that 74Q cells extrude transferrin faster than the 23Q cells, resulting in less transferrin-biotin after 60 minutes chase in 74Q cells (6.5 +/- 3.1%; n=8) than in 23Q cells (11.8 +/- 5.0%, n=8) (t-test; p=0.023). Faster extrusion of transferrin was observed in both 74Q clones (data are only shown for clone 72.16), which together with the previous observation of faster transferrin uptake in the 74Q clones (see 3.2.2) suggests that these two clones recycle transferrin more quickly than the 23Q clone.

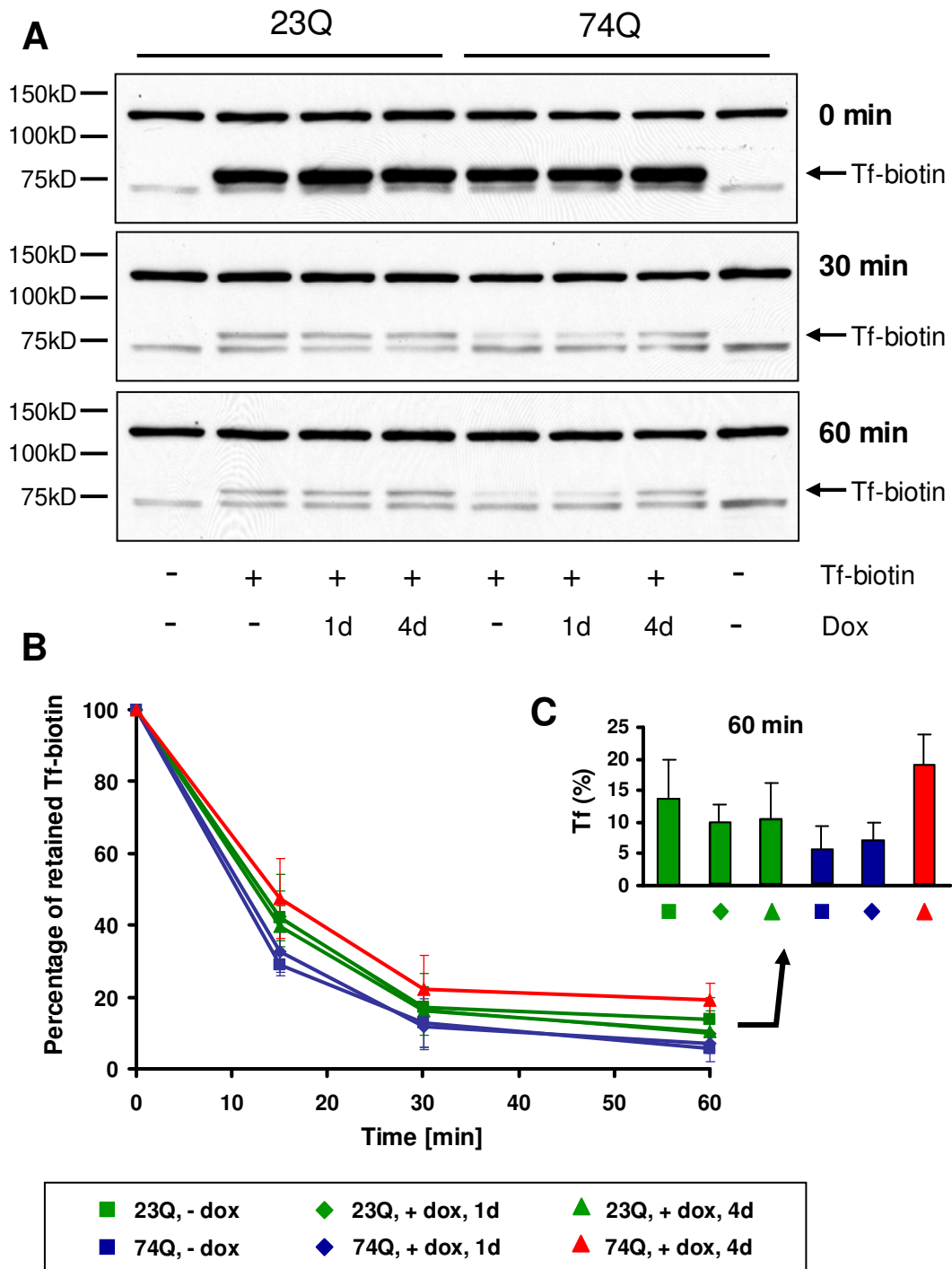


**Fig. 17: Extrusion of transferrin from cells, Western blotting**

23Q cells and 74Q cells (clone 72.16) were either left uninduced or induced for 1 or 4 d with 1  $\mu\text{g/ml}$  dox. The cells were loaded for 1 h at 37°C with 10  $\mu\text{g/ml}$  Tf-biotin (ca. 80 kDa) and then washed and chased for 0, 15, 30 or 60 min in full medium. At a respective time point, the cells were placed on ice, lysed in RIPA buffer and submitted to SDS-PAGE and Western blotting against biotin. Control lysates without transferrin-biotin were run in the outer lanes. The Western blots for 0, 30 and 60 min chase of Tf-biotin are shown in A). The band intensities of Tf-biotin were quantified and plotted in a graph as percentage of retained Tf-biotin (average  $\pm$  SD) (n=4) over time in B) and at the 60 min time point in C).

In contrast to the 23Q cells, the 74Q cells differ with regard to transferrin extrusion dependent on the expression of GFP-HttEx1-74Q. The extrusion rate in 74Q cells containing aggregates (induced for 4 days) is decreased compared to 74Q cells without aggregates (uninduced or induced for 1 day), leading to a significantly larger amount of retained transferrin-biotin after 60 minutes chase in cells induced for 4 days ( $19.1 \pm 4.7\%$ ;  $n=4$ ) than in 74Q cells induced for 1 day ( $7.2 \pm 2.8\%$ ;  $n=4$ ) (t-test;  $p=0.0048$ ) or in uninduced 74Q cells ( $5.8 \pm 3.7\%$ ;  $n=4$ ) (t-test;  $p=0.0042$ ). This was again observed in both 74Q clones, but data are only shown for clone 72.16. As this effect on the extrusion of transferrin occurred only in the presence of microscopically visible GFP-HttEx1 aggregates and not when all GFP-HttEx1-74Q was soluble (i.e. after 1 day of induction), these data indicate that the impairment of transferrin clearance specifically correlates with GFP-HttEx1 aggregates.

A similar pulse-chase experiment was repeated with cells that were grown on collagen-IV-coated coverslips to allow visualisation of the intracellular transferrin by confocal microscopy and analysis on the single cell level. The experiment was carried out with 23Q and 74Q, either left uninduced or induced for 1 or 4 days with  $1 \mu\text{g/ml}$  doxycycline. The cells were, as before, washed with warm serum-free medium and incubated for 1 hour at  $37^\circ\text{C}$  to clear them of unlabelled transferrin. Subsequently, the cells were loaded with  $10 \mu\text{g/ml}$  transferrin-Alexa-633 in serum-free medium for 1 hour at  $37^\circ\text{C}$ . After loading, the cells were quickly washed twice in warm serum-free medium and then chased for 0, 15, 30 or 60 minutes at  $37^\circ\text{C}$  in full medium (containing unlabelled transferrin). At a respective time point, the cells were fixed in 4% PFA and mounted on slides. Images were taken with a confocal microscope, recording GFP-HttEx1 and transferrin-Alexa-633.

The pattern of transferrin-Alexa-633 during the chase was equivalent in all cells, therefore only a selection of images comparing 74Q cells with and without aggregates is presented in Fig. 18. At time point 0, the internalised transferrin-Alexa-633 has the same pattern as before, i.e. vesicles are stained throughout the cytoplasm with the highest concentration at the ERC.

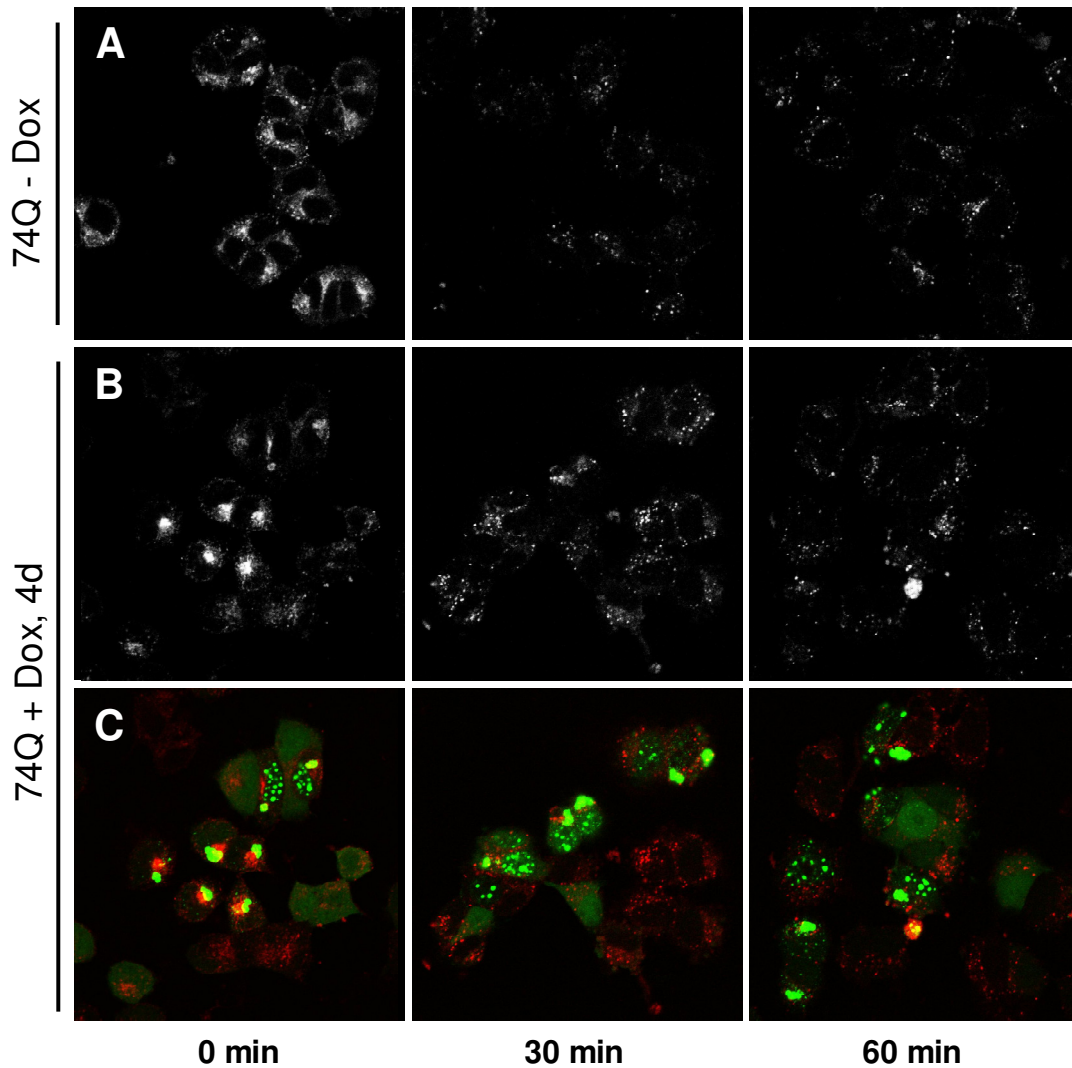


Fig. 18: Extrusion of transferrin from cells, confocal microscopy

74Q cells (clone 72.16) were grown on collagen-IV-coated coverslips and left uninduced or induced for 4 d with 1  $\mu\text{g/ml}$  dox. At the start of the experiment, the cells were loaded for 1 h at 37°C with 10  $\mu\text{g/ml}$  Tf-Alexa-633, before they were washed and chased for 0, 30 or 60 min in full medium. At a respective time point, the cells were fixed in PFA and imaged by confocal microscopy.

A) Uninduced 74Q cells. Tf-Alexa-633 is shown in white.

B) 74Q cells, induced for 4 d. Tf-Alexa-633 is shown in white.

C) Same images as in B). Tf-Alexa-633 is shown in red, GFP-HttEx1 in green.

In cells containing aggregates, especially cytoplasmic ones, this signal at the ERC is stronger than in cells without aggregates, indicating an accumulation of transferrin in the ERC during the loading with labelled transferrin. During the chase with unlabelled transferrin, the concentration of transferrin-Alexa-633 at the ERC disappears, leaving only isolated stained vesicles throughout the cytoplasm. The pattern and signal intensity of transferrin during the chase do

not differ visibly between the 3 time points (15, 30 and 60 minutes) or between cells with or without aggregates or with soluble GFP-HttEx1-74Q.

### **3.2.4 Flux of Transferrin through the ERC**

Given the impaired transferrin clearance and the accumulation of transferrin in the ERC of cells containing aggregates, I decided to analyse the time lapse data (chapter 3.2.2) more closely with respect to the flux of transferrin through the ERC.

The software of the Zeiss microscope LSM 510 was used to quantify the uptake of transferrin into the ERC. For this purpose, a subset of 5 images of one z-stack, comprising the centre of the cell, was combined in a projection and a region of interest (ROI) was drawn around the ERC of each cell based on the image at the end of the time lapse, when the concentration of transferrin-Alexa-633 in the ERC was maximal. This step is illustrated in Fig. 19A, where single images (zoomed) at 5 time points from 2 time lapse experiments are displayed with white circles marking the ROIs. More than 25 ROIs in 2 time lapse runs were selected per clone and the fluorescence intensity of transferrin-Alexa-633 within this ROI at each time point was subsequently analysed using Excel. The individual cell traces were grouped into the 5 subgroups that have already been mentioned above: 23Q cells without or with soluble GFP-HttEx1-23Q; 74Q cells without, with soluble or with aggregated GFP-HttEx1-74Q. The average amount of transferrin in the ERC for each group (+/- standard error) over time is shown in 2 graphs in Fig. 19B (23Q) and Fig. 19C (74Q). The traces of 23Q and 74Q cells cannot be combined in one graph because the absolute fluorescence intensity values at the start of the time lapse differ.

The traces from cells with or without soluble GFP-HttEx1 are almost identical in both graphs, indicating that the flux of transferrin through the ERC is not affected by the presence of soluble wild-type or mutant GFP-HttEx1. In contrast, the trace from cells containing aggregates is clearly different. The initial uptake of transferrin during the first minutes is similar to that of the controls, but then the accumulation of transferrin in the ERC is much more pronounced, resulting in a significantly higher amount of transferrin in the ERC of cells containing aggregates at the end of the time lapse (t-test;  $p=0.001$ ; fluorescence intensity

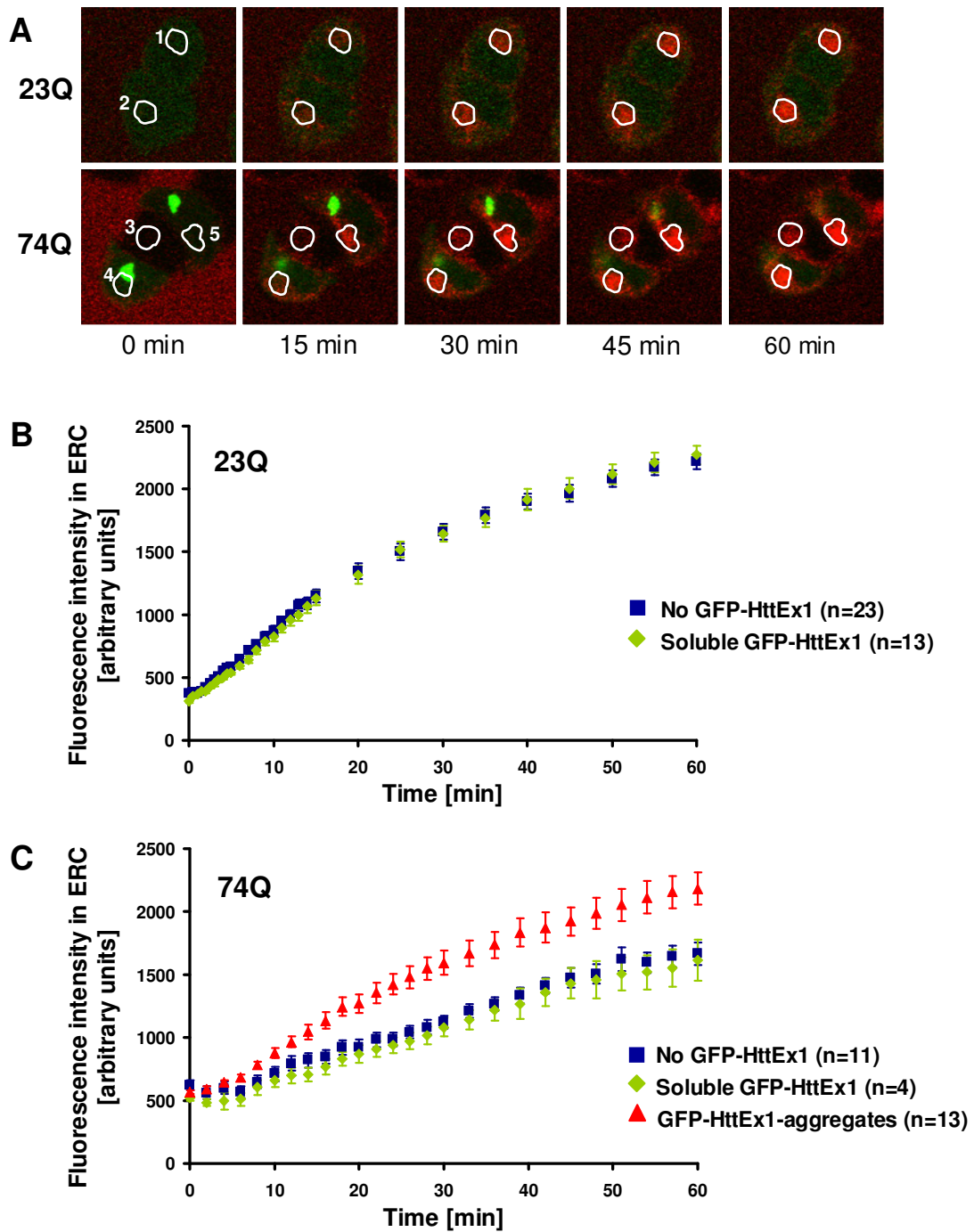


**Fig. 19: Uptake of transferrin into the ERC, live cell imaging**  
 23Q cells and 74Q cells (clone 72.16), induced for 4 d with dox, were incubated with serum-free, HEPES-buffered medium and mounted on the microscope stage. The time lapse was started when Tf-Alexa-633 was added to the cells in a final concentration of 5  $\mu\text{g}/\text{ml}$  and run for 1 h. Single images (zoomed) at 5 time points from 2 time lapse experiments (23Q and 74Q) are displayed in A) to illustrate the selection of the ERC as region of interest (ROI), marked by white circles. Tf-Alexa-633 is shown in red, GFP-HttEx1 in green. The uptake of transferrin into the ERC over time (average  $\pm$  SE) was plotted for 23Q cells in B) and for 74Q cells in C).

values, arbitrary units, at the end of the time lapse were compared between cells with aggregates, n=13, and cells without aggregates, n=15). With no impairment in uptake, these data reflect an aggregate-specific decrease in export of transferrin from the ERC.

### **3.2.5 siRNA Silencing of Rab11a and Rab11b**

The function of Rab11 in the export of transferrin from the ERC in this cell culture model was examined by knockdown experiments. Small interfering RNAs (siRNAs) specific for Rab11a and Rab11b were used to downregulate the expression of both genes. In this method, cells are transfected with synthetic siRNAs to activate a conserved cellular pathway of RNA interference that leads to the post-transcriptional silencing of the respective genes.

Three different siRNAs for Rab11a and for Rab11b were purchased to be tested for their knockdown efficiency. In addition, a siRNA conjugated with Alexa-488, a validated siRNA for GAPDH and a scrambled siRNA were used as controls to establish the best method for transfection and gene silencing. The experiments were carried out on normal PC12 cells because of difficulties in transfecting the HD cell lines.

The transfection of PC12 cells with siRNA was initially attempted by using the transfection reagent Lipofectamine. PC12 cells were transfected with 50 nM siRNA conjugated with Alexa-488, fixed 16 hours later in PFA and stained additionally with Hoechst. Confocal microscopy revealed that the Alexa-labelled siRNA was taken up into most cells (Fig. 20A).

The transfection was repeated with siRNA specific for GAPDH and a scrambled siRNA as negative control in a concentration of 50 and 100 nM. The cells were harvested 2 days after transfection and lysed in RIPA buffer. SDS-PAGE and Western blot analysis showed that no downregulation of GAPDH was achieved by this transfection method (Fig. 20B).

The next transfection of PC12 cells with siRNA was carried out with the Amaxa system, which is based on electroporation combined with a transfection agent. The company recommends for PC12 cells the “cell line nucleofactor kit V” as

transfection reagent and the programmes U-29 or P-25 (encoded by Amaxa) for electroporation. Like before, the method was tested on PC12 cells with siRNA specific for GAPDH and a scrambled siRNA as negative control (1.5 µg per cuvette). As visible in Fig. 20C, GAPDH was downregulated 48 hours after transfection by the specific siRNA compared to the negative control. The Amaxa method is harsher than the transfection with Lipofectamine and many cells are killed during the electroporation. One day after plating, the medium in the cell culture plates was therefore changed again to remove floating cells. The cells that have attached to the collagen IV are vital and of normal morphology, except a few large syncytia.

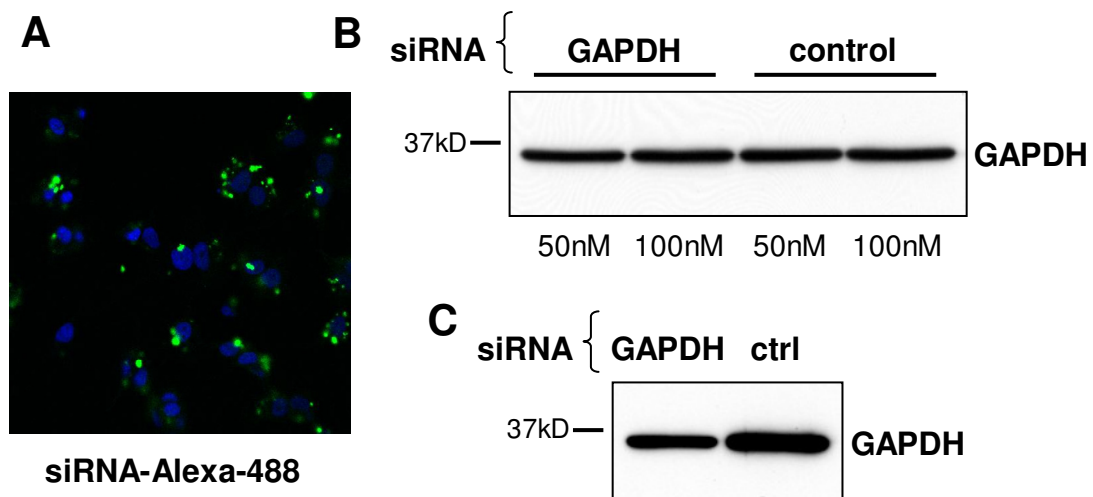


**Fig. 20: siRNA silencing, technique**

A) PC12 cells were transfected with Alexa488-conjugated siRNA with Lipofectamine, fixed 16 h later in PFA and imaged with confocal microscopy. The nuclear dye Hoechst is shown in blue, siRNA-Alexa-488 in green.

B) PC12 cells were transfected with siRNA specific for GAPDH and a scrambled siRNA (50 and 100 nM) with Lipofectamine. The cells were lysed after 48 h and submitted to SDS-PAGE and Western blotting against GAPDH.

C) PC12 cells were transfected with siRNA specific for GAPDH and a scrambled siRNA with the Amaxa system. The cells were lysed after 48 h and submitted to SDS-PAGE and Western blotting against GAPDH.

The transfection of PC12 cells with the Amaxa method was repeated twice with three different siRNAs against Rab11a (Rab11a-1, Rab11a-2 and Rab11a-3). All three siRNAs achieved downregulation of Rab11a, as is visible in the Western blots against Rab11a in Fig. 21A. The quantification of the Western

blots showed that the siRNAs Rab11a-1 and Rab11a-3 reduced the expression very effectively, i.e. by approximately 90% (Fig. 21B). The siRNA Rab11a-3 was chosen to silence Rab11a in the following experiments.

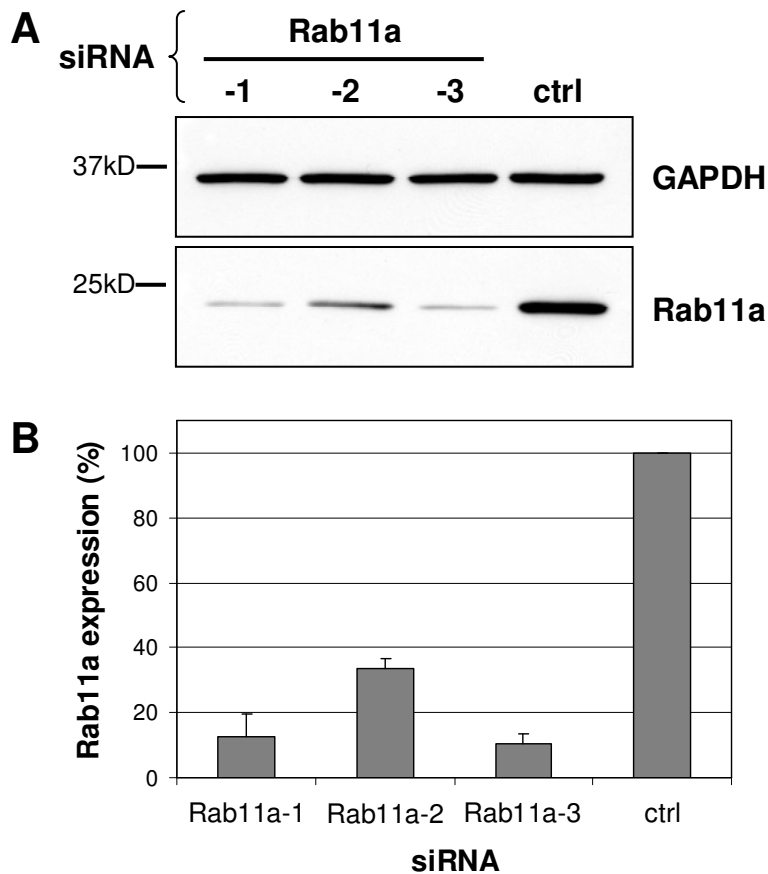


Fig. 21: siRNA silencing of Rab11a

A) PC12 cells were transfected with 3 different siRNAs specific for Rab11a (Rab11a-1, -2, and -3) and a scrambled siRNA as control, using the Amaxa system. The cells were lysed 48 h later and analysed by SDS-PAGE and Western blotting against GAPDH (as loading control) and Rab11a.

B) The Rab11a band intensities were quantified and plotted as Rab11a-expression in percent of the control (n=2).

The three siRNAs for Rab11b were tested next, while the siRNA Rab11a-3 and a scrambled siRNA served as positive and negative control. Unfortunately, there was no specific Rab11b antibody commercially available and attempts to produce one for our group failed. Therefore, the amount of Rab11b can only be derived from comparing Western blots against Rab11a with Western blots against Rab11a and b. The Western blots of the first experiment, when Rab11a

and Rab11b were silenced separately (Fig. 22), indicate that Rab11a is the predominant isoform (approx. 75% of the total Rab11), with the effect that any possible reduction of Rab11b is masked by the presence of Rab11a.

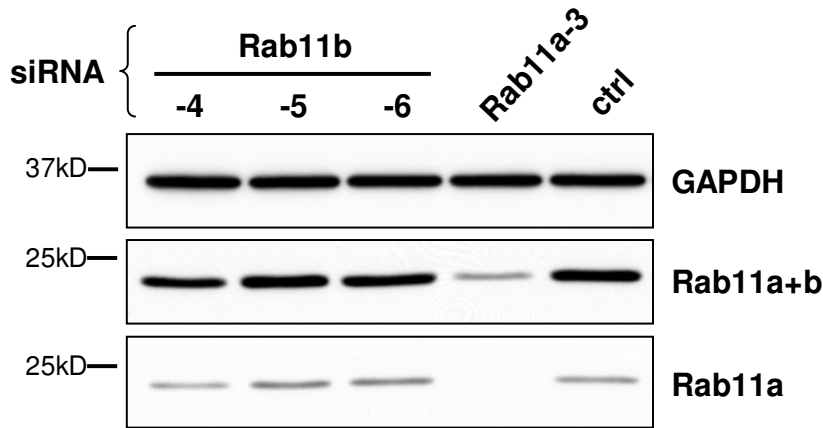


**Fig. 22: siRNA silencing of Rab11b, single knockdown**

PC12 cells were transfected with three different siRNAs specific for Rab11b (Rab11b-4, -5, and -6) and a scrambled siRNA as control, using the Amaxa system. The cells were lysed 48 h after transfection and analysed by SDS-PAGE and Western blotting against GAPDH (as loading control), Rab11a+b, and Rab11a alone.

Based on the above results, Rab11 isoform b was silenced together with isoform a in a double-knockdown experiment in order to detect the efficiency of the three siRNAs against Rab11b. All cells were harvested 48 h after transfection and Western blots were performed with antibodies against GAPDH, Rab11a and b, and Rab11a alone. The Western blots are displayed in Fig. 23A.

In lanes 1-3, the silencing effect of Rab11b siRNAs (Rab11b-4, Rab11b-5 and Rab11b-6) combined with the siRNA Rab11a-3 was tested. In lane 4, cells transfected with the siRNA Rab11a-3 alone were analysed to get an estimate for the total amount of Rab11b. In lane 5, cells transfected with the siRNA Rab11a-3 together with the same amount of scrambled siRNA (ctrl) were analysed to test whether the double amount of transfected siRNA affects the silencing efficiency of the siRNA specific for Rab11a. In lane 6, cells were transfected solely with scrambled siRNA as negative control.

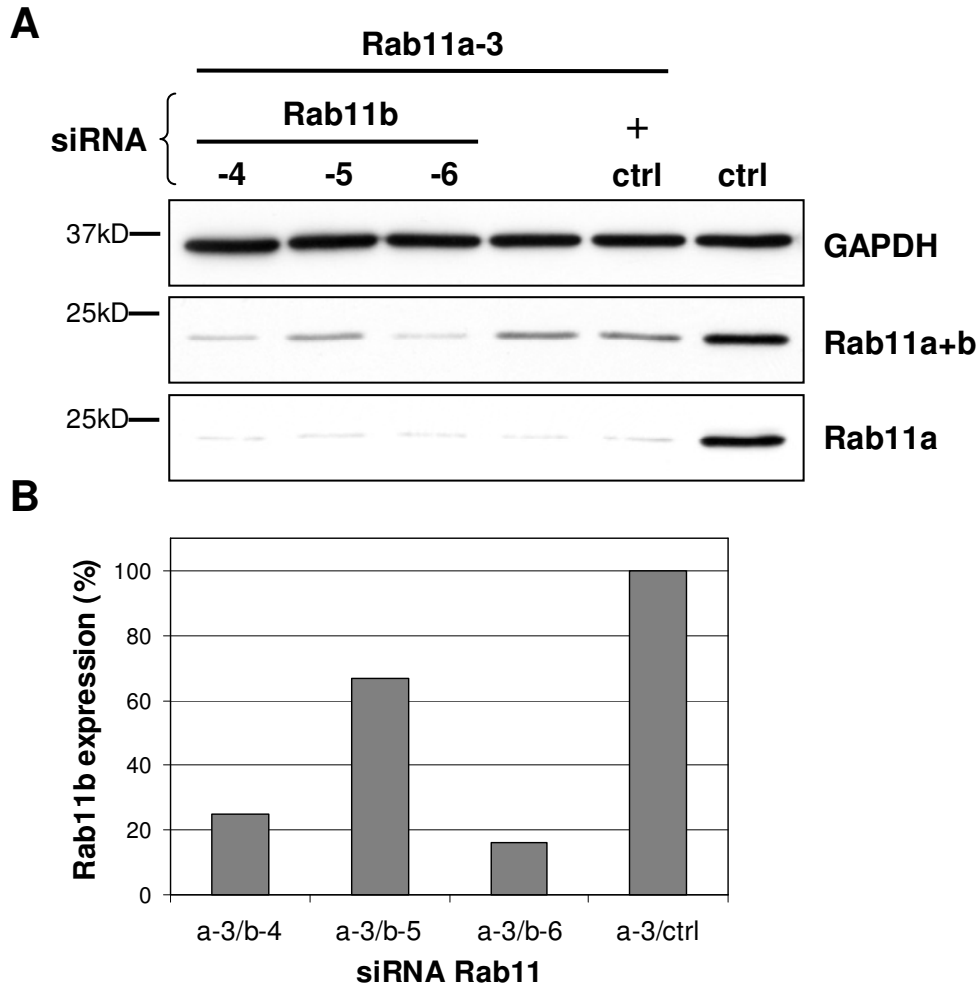


Fig. 23: siRNA silencing of Rab11b, double knockdown

A) A double knockdown of Rab11a and Rab11b was performed using the Amaxa system. Three different siRNAs for Rab11b (Rab11b-4, -5, and -6) were combined with the siRNA Rab11a-3 (lanes 1-3). The controls were Rab11a-3 alone (lane 4), Rab11a-3 plus scrambled siRNA (lane 5) and scrambled siRNA alone (lane 6). The cells were lysed 48 h after transfection and analysed by SDS-PAGE and Western blotting against GAPDH (as loading control), Rab11a+b and Rab11a alone.

B) The amount of Rab11b was derived from the Western blot against Rab11a+b after the double knockdown and plotted as Rab11b-expression in percent of the control in which only Rab11a was silenced (n=1).

The knockdown of Rab11a by the siRNA Rab11a-3 was equally efficient in samples 1-5, as is visible in the Western blot against Rab11a alone (Fig. 23A, bottom panel). The additional RNA in the samples treated with two different siRNAs (lanes 1-3 and 5) had no effect on the downregulation of Rab11a compared to the application of Rab11a-3 alone (lane 4).

With Rab11a being nearly absent in samples 1-5, the differences in band intensity detected by the antibody against Rab11a and b (Fig. 23A, middle panel) can therefore be attributed in these samples to different amounts of the Rab11b. Accordingly, the band intensities were quantified and plotted in Fig. 23B as Rab11b expression in percent of the control (sample 5), in which only Rab11a was silenced. The quantification of Rab11b shows that the siRNA Rab11b-6 (sample 3) achieves the most effective downregulation, reducing the amount of Rab11b to approximately 16% of the control (sample 5). The siRNA Rab11b-6 was therefore chosen for further experiments.

### **3.2.6 Effect of Rab11 Silencing on Transferrin Recycling**

When an efficient downregulation of Rab11a and b by siRNA was established, I investigated whether the silencing of Rab11 had any effect on the recycling of transferrin. Rab11a and b expression was therefore silenced by siRNA in a single or double knockdown, followed by a pulse-chase experiment with biotinylated transferrin to measure the clearance of transferrin from the cells. For this purpose, PC12 cells were transfected with the siRNA Rab11a-3 alone, the siRNA Rab11b-6 alone, the siRNAs Rab11a-3 and b-6 together, or a scrambled siRNA (ctrl). 48 hours after transfection, the cells were incubated in serum-free medium for 1 hour at 37°C to clear them of unlabelled transferrin and then loaded with 10 µg/ml biotinylated transferrin in serum-free medium for 1 hour at 37°C. After loading, the cells were washed quickly and chased for 0, 30 or 60 minutes at 37°C in full medium until lysis. The Western blot analysis of the lysates with antibodies against biotin, Rab11a and b, and GAPDH is shown in Fig. 24A. The Western blot against GAPDH confirms that all wells were loaded with an equal amount of protein, while the Western blot against Rab11a and b confirms the effective silencing of Rab11a or Rab11b or both.

The Western blot against biotin reflects the amount of biotinylated transferrin which decreases rapidly during the chase. The transferrin-biotin bands of the samples with reduced Rab11b (single or double knockdown) at 30 and 60 minutes chase are significantly stronger than those of the samples with reduced Rab11a (single knockdown) or the control. The increased intensity of the

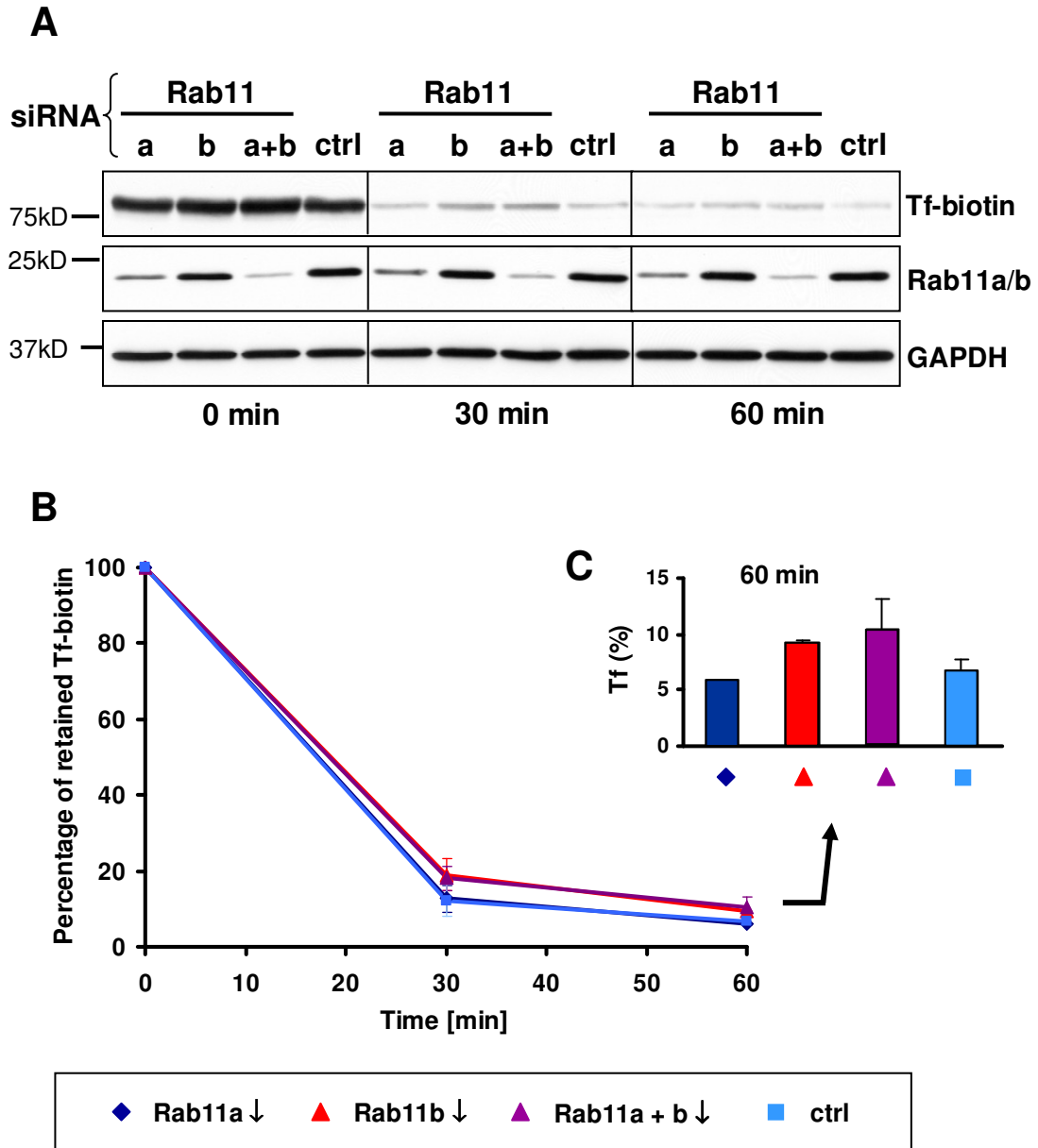


**Fig. 24: Effect of Rab11 silencing on transferrin recycling**  
Rab11a and b were silenced by siRNA in a single or double knockdown in PC12 cells, using the Amaxa system. A scrambled siRNA served as control. 48 h after transfection, the extrusion of Tf-biotin from the cells was measured in a pulse-chase experiment. The cells were loaded for 1 h at 37°C with 10 µg/ml Tf-biotin, before they were washed and then chased for 0, 30 or 60 min in full medium. At a respective time point, the cells were placed on ice, lysed in RIPA buffer and submitted to SDS-PAGE and Western blotting against biotin, Rab11a+b and GAPDH, as shown in A). The Tf-biotin signal was quantified and plotted as percentage of retained Tf-biotin (average +/- SD) (n=2) over time in B) and at the 60 min time point in C).

transferrin-biotin band in the samples with reduced Rab11b indicates a retention of transferrin in the cell, as it was seen before in cells containing GFP-HttEx1-74Q aggregates. The band intensities of transferrin-biotin from 2 independent experiments were quantified and plotted as percentage of retained transferrin-biotin (average +/- standard deviation) over time in a graph in Fig. 24B, setting the amount of transferrin-biotin at the start of the chase (0 minutes) as 100%. In addition, the values at the 60 minutes time point are shown in a separate chart in Fig. 24C.

The graph in Fig. 24B includes traces for all 4 conditions, i.e. Rab11a single knockdown, Rab11b single knockdown, Rab11a and b double knockdown, and the negative control. The traces of the Rab11b single and double knockdown are almost identical and display a lower rate of transferrin extrusion than the traces of the Rab11a single knockdown and the negative control, which are likewise almost identical. The lower rate of transferrin clearance in cells with reduced Rab11b (single and double knockdown) leads to a significantly larger amount of retained transferrin-biotin after 60 minutes chase in these cells (9.9 +/- 1.7%; n=4) than in cells with reduced Rab11a (single knockdown) and control cells (6.3 +/- 0.8%; n=4) (t-test; p=0.007). This result indicates that the silencing of Rab11b, and not of Rab11a, impairs the extrusion of transferrin from the cell.

### **3.2.7 Immunocytochemistry of Microtubules**

The position of the ERC at the microtubule organising centre (MTOC) and evidence from the literature suggest that the ERC is associated with microtubules. For example, it has been described in the literature that the concentration of particularly stable microtubules containing Glu- $\alpha$ -tubulin (detyrosinated  $\alpha$ -tubulin with a glutamine residue at the C-terminus) correlates with the distribution of the ERC. Antibodies against Glu- $\alpha$ -tubulin or kinesin (a motor protein for plus-end-directed transport on microtubules) slowed the recycling of transferrin from the ERC to the plasma membrane (Lin et al., 2002). To test whether the microtubule network was disturbed in this cell culture model of HD, uninduced and induced 74Q cells were immuno-stained with 3 different

antibodies for tubulins: mouse anti  $\beta$ -tubulin, anti  $\beta$ -III-tubulin and anti Glu- $\alpha$ -tubulin. Alexa-647-conjugated goat anti mouse antibody was used as secondary antibody, and the samples were analysed by confocal microscopy, recording GFP-HttEx1 and the microtubules immuno-stained with Alexa-647, as is presented in Fig. 25.

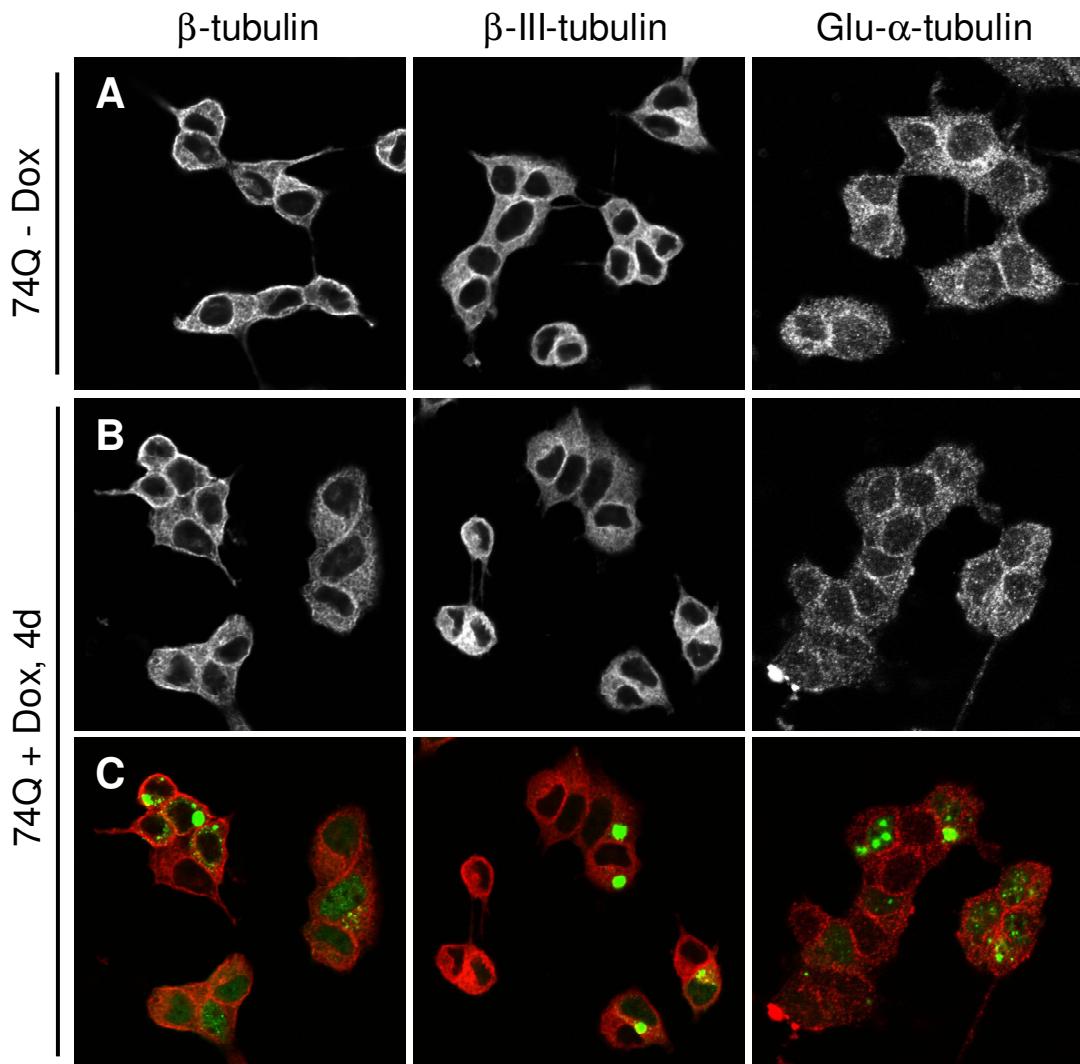


Fig. 25: Immunocytochemistry of microtubules in a cell culture model of HD 74Q cells (clone 72.16) were grown on collagen-IV-coated coverslips and left uninduced or induced for 4 d with 1  $\mu$ g/ml dox. The cells were fixed in PFA and immuno-stained with antibodies specific for  $\beta$ -tubulin (1. column),  $\beta$ -III-tubulin (2. column) or Glu- $\alpha$ -tubulin (3. column).  
A) Uninduced 74Q cells. Tubulin is shown in white.  
B) 74Q cells, induced for 4 d. Tubulin is shown in white.  
C) Same images as in B). Tubulin is shown in red, GFP-HttEx1 in green.

Immunocytochemistry with the antibodies against  $\beta$ -tubulin and  $\beta$ -III-tubulin marked a network of filaments throughout the cytoplasm, as expected for microtubules, whereas staining with the antibody against Glu- $\alpha$ -tubulin revealed a punctuate staining throughout the cytoplasm, indicative of tubulin monomers. With the exception of a slightly weaker  $\beta$ -tubulin signal directly at the position of large cytoplasmic GRP-HttEx1-74Q aggregates, the microtubule network appears to be undisturbed by the expression of mutant GFP-HttEx1.

### **3.3 Purification of GFP-HttEx1-74Q Aggregates**

Several strategies were attempted to purify the aggregates based on their physico-chemical properties. The aggregates measure several microns in diameter and are detergent-resistant, suggesting purification methods based on mass, size or density like density gradient centrifugation. In addition, the GFP-tag provides a good target for antibodies in affinity purification methods.

#### **3.3.1 Gradient Centrifugation**

Initially a density gradient centrifugation with sucrose was chosen. Whole cell lysates of clones 23Q and 74Q after 4 days of induction (consisting of  $1 \times 10^7$  cells per clone in 1% triton lysis buffer) were loaded onto continuous sucrose gradients from 40-70% (w/v) and centrifuged at 50,000 g for 90 minutes. After the centrifugation, a greenish band (GFP) had formed below the top and an almost clear pellet at the bottom of both gradients. Fractions were collected starting from the top of the gradient and subjected to SDS-PAGE and Western blotting against GFP. Fig. 26A shows the Western blots for the gradients with 23Q cell lysate (top) and 74Q cell lysate (bottom), detecting GFP-HttEx1-23Q respectively GFP-HttEx1-74Q, both starting with the lightest fraction in lane 1. Almost all soluble protein, wild-type as well as mutant GFP-HttEx1, is detected in the light fractions 1-3, a small amount of GFP-HttEx1-23Q also in fraction 4. Moreover, there is a weak GFP signal in fraction 12. The presence of soluble GFP-HttEx1-23Q in the heaviest fraction suggests a contamination of the last fraction with material floating at the surface and therefore containing soluble GFP-HttEx1, which happened during the process of fraction collection.

The 74Q sample shows in addition a faint signal in the stacking gel, which may have been caused by collecting also a small amount of material from the pellet.

The pellets were resuspended in PBS and transferred to a new tube. A small volume was taken off for Western blot analysis, which is shown in Fig. 26B (lane 1) for the 74Q sample. The GFP-HttEx1-74Q protein is mostly retained in the stacking gel, indicative of insoluble material, while only a small portion has entered the resolving gel because it was solubilised during the incubation at 99°C in SDS sample buffer before SDS-PAGE. According to the Western blot results of fractions and pellet, the aggregates accumulated in the pellet during this density gradient centrifugation and their density is therefore higher than that of a 70% sucrose solution, which is 1.34 g/cm<sup>3</sup>.

According to a publication by Hazeki et al. (2000), Htt-Ex1 aggregates can be dissolved in 100% formic acid. To test the method in this cell culture model, the resuspended pellet resulting from the 74Q clone was divided into 4 equal parts and centrifuged at 16,000 g in a desktop centrifuge for 15 minutes. Two of the resulting pellets were incubated either in 100% formic acid or in 10% SDS for 1 hour at 37°C. The sample treated with formic acid was additionally dried in a speed vac before both samples were incubated at 99°C in SDS sample buffer and subjected to SDS-PAGE and Western blotting against GFP (Fig. 26B, lanes 2 and 3). The pellet treated with formic acid revealed a strong band at the size of GFP-HttEx1-74Q in the resolving gel plus two faint bands above, which may correspond to ubiquitinated forms of the protein. Only a very weak signal was detected in the stacking gel, suggesting that the HttEx1 aggregates were almost completely dissolved. In contrast, only a very small portion of the GFP-HttEx1-74Q entered the resolving gel after SDS treatment and most protein was retained in the stacking gel, confirming that the fibrils are SDS-resistant.

The pellets from both sucrose density gradients were moreover analysed by 2D electrophoresis to determine how many cellular components besides the aggregates were contained in the pellets. Half of each pellet (23Q and 74Q) was solubilised in 100% formic acid, dried and rehydrated in rehydration buffer.

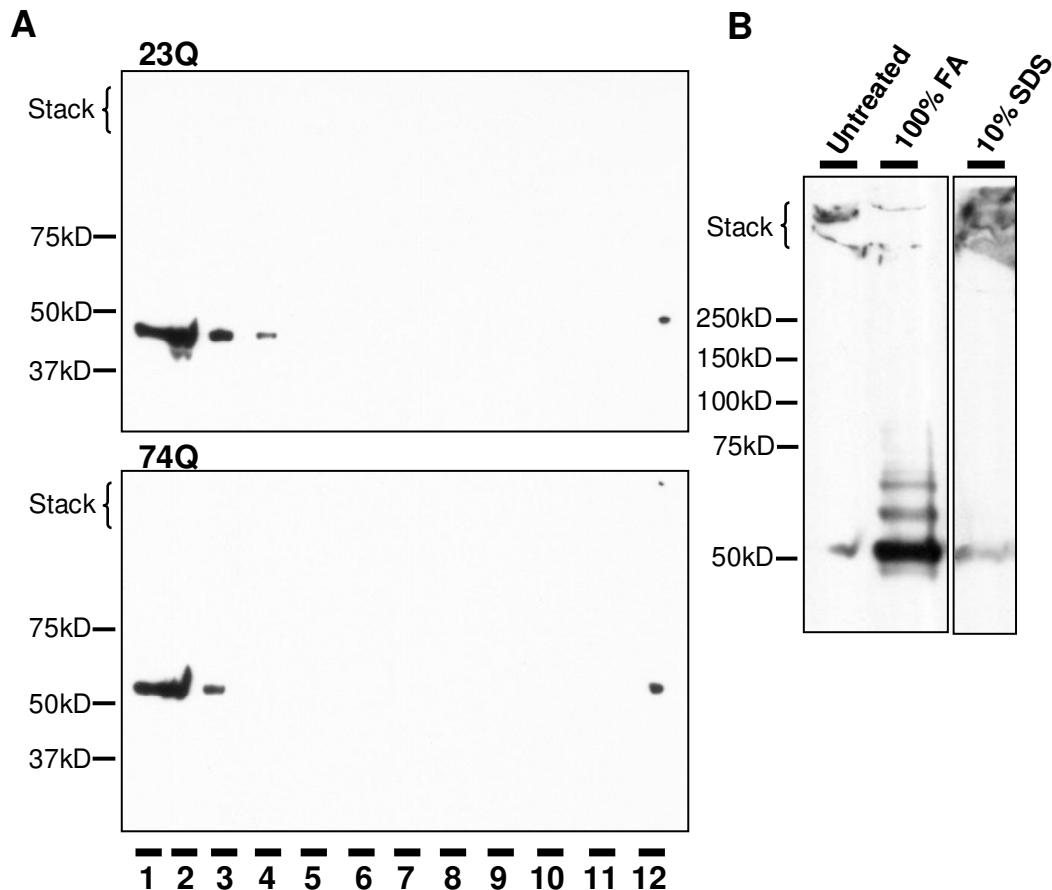


**Fig. 26: Density gradient centrifugation with sucrose**

A) Whole cell lysates of 23Q cells and 74Q cells (clone 72.16) after 4 d induction with 1  $\mu\text{g}/\text{ml}$  dox were loaded onto continuous gradients from 40-70% sucrose (w/v). The gradients were centrifuged for 90 min at 50,000 g. 12 fractions were collected and analysed by Western blotting against GFP. The lightest fraction is shown in lane 1, the heaviest in lane 12.

B) Equal portions (25%) of the sucrose gradient pellet from the 74Q sample were incubated in either 10% SDS or 100% formic acid for 1 h at 37°C. 2% (v/v) of each sample were analysed by Western blotting against GFP.

Approximately 120  $\mu\text{g}$  total protein of each sample were focused on IPG strips with a linear pI-gradient from 3 to 10 and separated by SDS-PAGE. The 2D gels were stained with the fluorescent dye Sypro Ruby, imaged and analysed with the software Progenesis (Genomic Solutions).

Both gels have a highly similar pattern (Fig. 27). Only one spot was detected in the 74Q sample which has no match in the 23Q sample. According to its size, it could be GFP-HttEx1-74Q, solubilised from the aggregates, but the protein could not be identified by mass spectrometry (MALDI, Micromass), possibly because the GFP portion, the polyglutamine tract and the proline-rich region

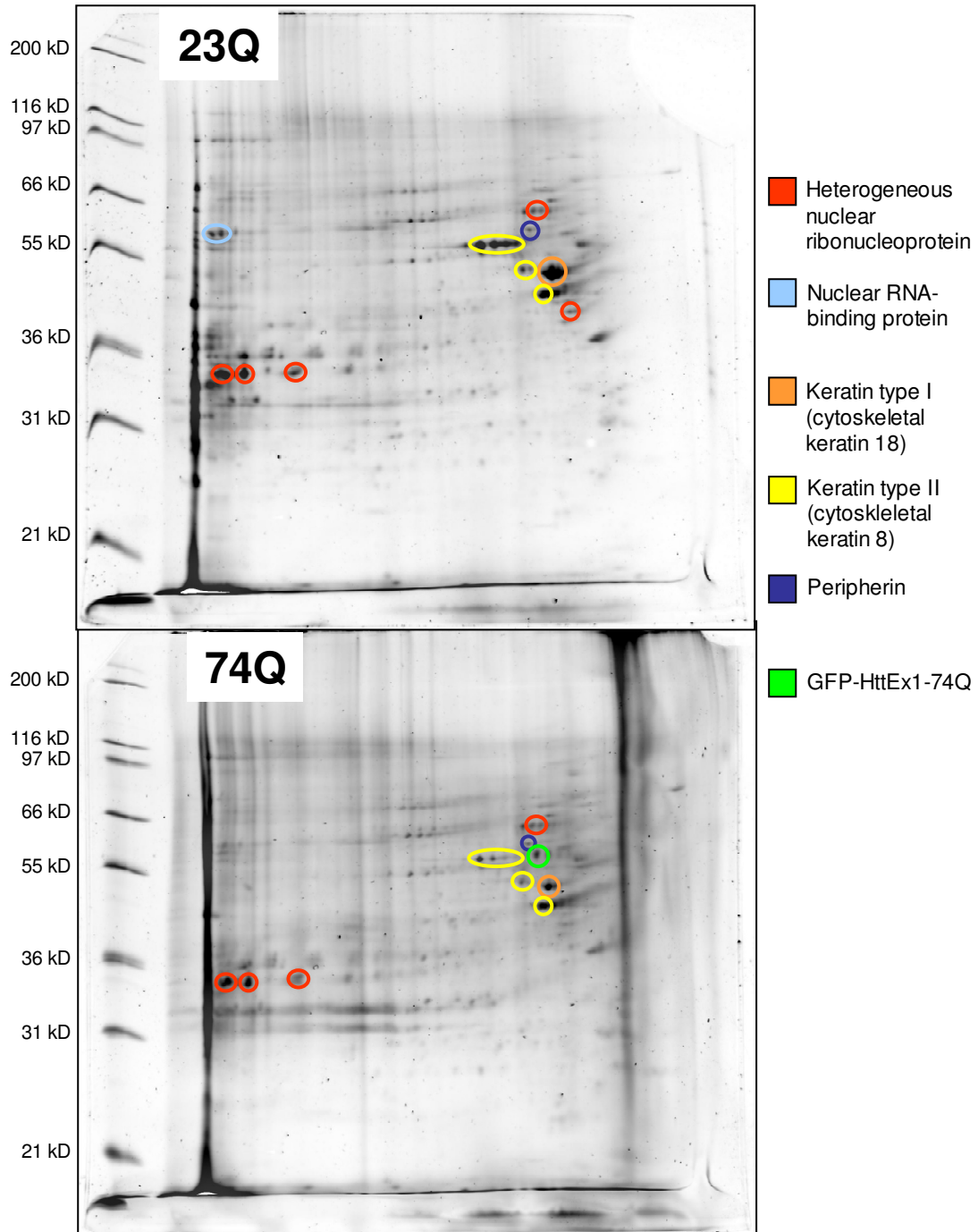


**Fig. 27: Density gradient centrifugation with sucrose, 2D gels**  
 Whole cell lysates of 23Q cells and 74Q cells (clone 72.16) after 4 d induction with 1  $\mu\text{g/ml}$  dox were subjected to density gradient centrifugation (40-70% sucrose). The pellet of each gradient was solubilised in 100% formic acid and separated by 2D electrophoresis. After staining the gels with Sypro Ruby, protein spots were analysed by mass spectrometry (MALDI). Preliminary identification of several spots is shown in the legend.

interfere with the trypsin digestion. A number of other protein spots were also picked and analysed by mass spectrometry. The preliminarily identified proteins include several heterogeneous nuclear ribonucleoproteins, nuclear RNA-binding proteins, keratins type I and II, and peripherin, a neuronal intermediate filament. All these proteins are not aggregate components because they were also found in the pellet of the control. Instead, they appear to be components of the cytoskeleton and the nucleus.

The previous sucrose density gradient centrifugation showed that the sucrose gradient could not separate GFP-HttEx1 aggregates from nuclear components because its maximum density was insufficient, therefore a medium of higher density was tested instead. Nycodenz is an iodinated compound used in gradient centrifugation because of its high density, non-ionic property, medium viscosity and low osmolarity. A number of experiments with varying Nycodenz gradients, centrifugation speed, duration and sample preparation were carried out, one of which is described here in more detail.

23Q and 74Q cells, induced for 4 days with doxycycline, were lysed in RIPA buffer ( $3 \times 10^7$  cells per clone) and centrifuged for 15 minutes at 16,000 g. The pellets were washed in PBS and centrifuged again before they were finally resuspended in PBS and loaded onto discontinuous Nycodenz gradients between 45% and 20% (w/v). The density gradient centrifugation was carried out at 100,000 g for 20 hours. No pellet formed during the centrifugation in either sample, but two bands of white material collected at the interphases of 30/35% Nycodenz and 35/40% Nycodenz, which could be chromatin or denatured DNA. Fractions were collected with a needle from the bottom of the tube, starting with the heaviest solution. The fractions of the 23Q and 74Q gradient were analysed by SDS-PAGE and Western blotting against GFP, starting with the lightest fraction in lane 1 (Fig. 28).

No signal of soluble GFP-HttEx1-23Q (top blot) or soluble GFP-HttEx1-74Q (bottom blot) was detected in the Western blots because only the insoluble pellets were loaded onto the gradients. The signal of aggregated GFP-HttEx1-74Q in the stacking gel, however, is present in fractions 8-13, with decreasing intensity towards the heavier fractions. These positive fractions comprise a

range of Nycodenz solutions from 30% to 45% (w/v). The first positive fraction (8) contains the interphase between the layers of 30% and 35% Nycodenz, while the last positive fraction (13) contains the interphase between the layers of 40% and 45% Nycodenz. It follows that the aggregates cover a range of buoyant densities, higher than that of 30% Nycodenz (1.16 g/ml) and lower than that of 45% Nycodenz (1.24 g/ml). In addition, silverstaining of the fractions containing aggregates showed that there are many other proteins with similar densities collected in the same fractions (data not shown).

Hence, the strategy to purify GFP-HttEx1-74Q aggregates from PC12 cells by density gradient centrifugation failed because of two problems: First, the aggregates are heterogeneous with respect to buoyant density and therefore do not collect at one position in the gradient. Second, their range of buoyant densities overlaps with many other proteins which makes the separation of the aggregates from other proteins based on density unfeasible.

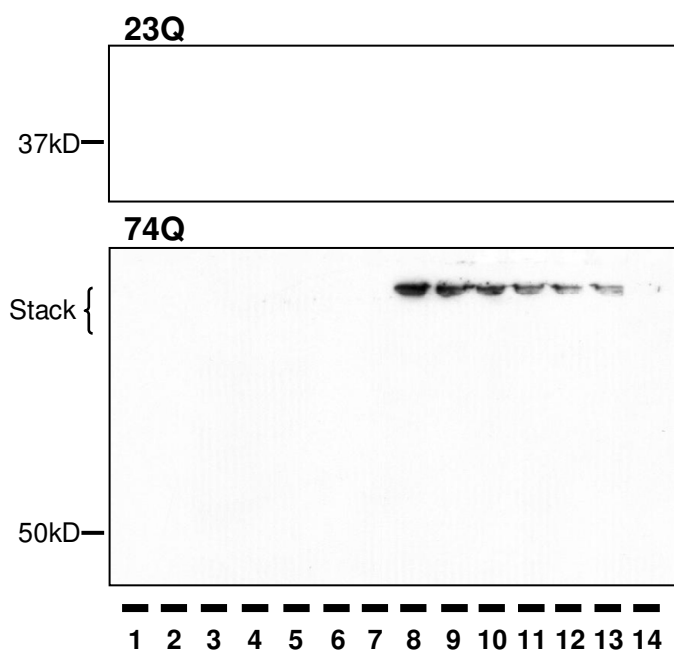


**Fig. 28: Density gradient centrifugation with Nycodenz**  
23Q cells and 74Q cells (clone 72.16) were induced for 4 d with 1  $\mu$ g/ml dox and lysed in RIPA buffer. Insoluble pellets from these lysates were resuspended in PBS and loaded onto discontinuous gradients from 20-45% Nycodenz (w/v). The gradients were centrifuged for 20 h at 100,000 g. 14 fractions were collected and analysed by Western blotting against GFP. The lightest fraction is shown in lane 1, the heaviest in lane 14.

### 3.3.2 Immunomagnetic Separation

The previous experiments demonstrated that gradient centrifugation is not suitable to separate the GFP-HttEx1-74Q aggregates from other dense cellular components. Immunomagnetic separation, in contrast, is based on isolating the target by specific binding to antibody-coated magnetic beads which are pulled out of a suspension by magnetic force. This method therefore does not require centrifugation steps in the procedure.

The magnetic beads used for the purification of aggregates were dynabeads (Dynal Biotec) which are superparamagnetic polystyrene beads with a diameter of  $2.8 \mu\text{m} \pm 0.2 \mu\text{m}$ , in this case coated with covalently bound sheep anti rabbit IgG. With a density of  $1.3 \text{ g/cm}^3$  they settle in suspension and need therefore to be resuspended before use and to be agitated during incubation times.

Dynabeads are isolated by placing a 1.5 ml tube containing the suspension in a special magnet. After 2-3 minutes, the beads collect at the side of the tube and the solution can be removed with a pipette.

A model of the procedure is shown in Fig. 29. The dynabeads are first coated with the primary antibody, in this case rabbit IgG anti GFP. After several washing steps, the beads are then incubated with the suspension containing the target, i.e. the PC12 cell lysate containing the GFP-HttEx1-74Q aggregates. Subsequently, the beads are extracted from the suspension by magnetic force, washed several times, and the target is eluted.

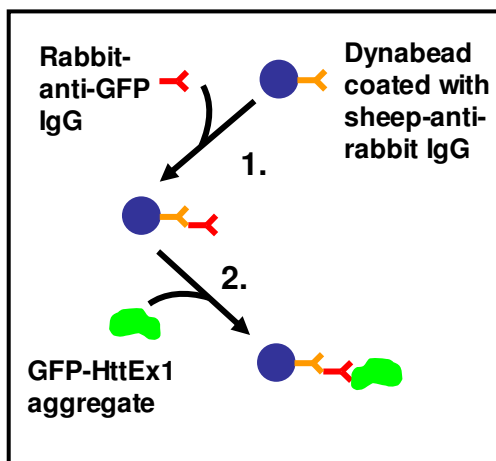


**Fig. 29: Immunomagnetic separation.** Dynabeads are magnetic beads covalently coated with sheep-anti-rabbit IgG. They are additionally coated with rabbit anti GFP IgG (1.) and washed several times, before they are incubated with the suspension containing the target (2.), in this case the GFP-HttEx1-74Q aggregates. Subsequently, the beads are extracted from the suspension by magnetic force, washed several times, and the target is eluted.

First, the coating and elution conditions for the dynabeads were optimised. To determine the best method for coating, the beads were coated with increasing concentrations of rabbit IgG anti GFP. In each sample  $4 \times 10^6$  beads were mixed with the respective amount of antibody in 40  $\mu$ l PBS with 0.1% BSA and incubated over night at 4°C on a roller. Subsequently, the beads were extracted and washed twice, incubated for 5 minutes at 99°C in SDS sample buffer and extracted again. The sample buffer containing the released IgG was analysed by SDS-PAGE and Western blotting with HRP-conjugated goat anti rabbit antibody. The signal intensity was quantified, representing the amount of bound IgG in each sample, which is displayed in a graph in Fig. 30A. An amount of 1  $\mu$ g IgG per  $1 \times 10^7$  beads reached almost maximal coating, which could not be substantially improved by increasing the IgG concentration and was therefore used in the following experiments.

Different elution protocols were tested and evaluated on the basis of the elution efficiency of the non-covalently bound rabbit IgG. In each sample  $1 \times 10^6$  coated beads were incubated with certain elution buffers at different temperatures for different lengths of time and subsequently extracted from the eluate. Both beads and eluate were mixed with sample buffer, heated for 5 minutes at 99°C and analysed by SDS-PAGE and Western blotting against the rabbit IgG. The resulting elution efficiency, expressed as percentage of eluted antibody compared to the total antibody (i.e. bound and eluted), is shown in Fig. 30B. Only one method, the elution in SDS sample buffer for 5 minutes at 99°C proved to be effective, releasing 100% of the IgG from the beads. However, the SDS sample buffer is incompatible with 2D gel electrophoresis and the high temperature damages the dynabeads. Elution with SDS sample buffer at RT or heating to 99°C in PBST released less than 5% of the bound IgG. Equally ineffective were incubation in 2 M NaCl, 8 M urea, 1% Triton X-100 or 100 mM DTT for 10 minutes at RT. Incubation in acidic glycine buffer (0.5 M glycine, 0.15 M NaCl, pH 2.3) for 30 minutes at RT achieved an elution efficiency of 35%; the rehydration buffer used for 2D gel electrophoresis (see methods) was less efficient with 21%.

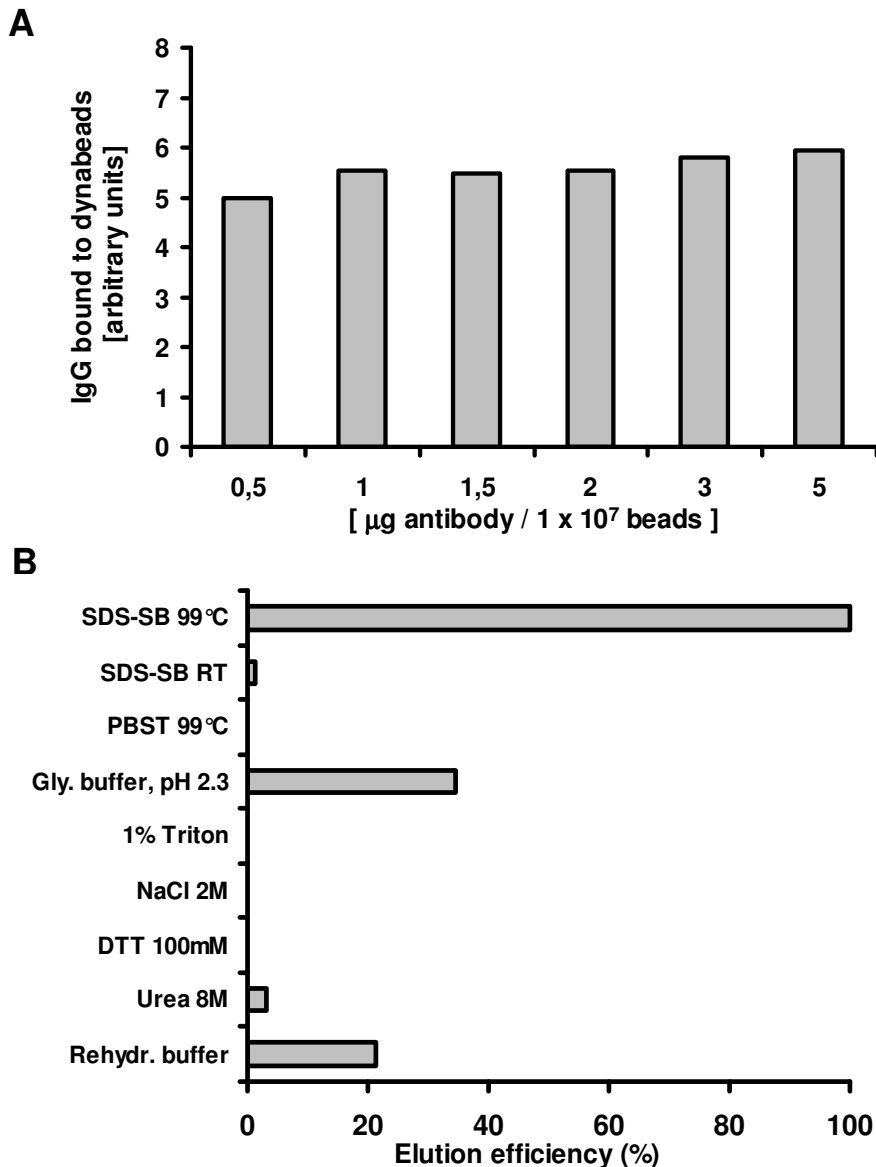


**Fig. 30: Immunomagnetic separation with Dynabeads, coating and elution.**  
 A) Dynabeads were coated with increasing concentrations of rabbit anti GFP IgG over night at 4°C. Subsequently, the beads were extracted and washed, incubated for 5 minutes at 99°C in SDS sample buffer and run on a gel. The Western blot was probed with HRP-conjugated goat anti rabbit antibody and the band intensity of the IgG in each sample was quantified (n=1).  
 B) Coated beads were incubated with various elution buffers at different temperatures and then extracted from the eluate. Beads and eluate were mixed with sample buffer, heated for 5 minutes at 99°C and subjected to SDS-PAGE and Western blotting against the rabbit IgG. The elution efficiency was expressed as percentage of eluted antibody compared to total antibody (n=1).

In the first dynabead experiment, the insoluble pellet of PC12 cells was incubated with anti-GFP-coated dynabeads. For this purpose, 74Q and 23Q cells were both induced with doxycycline for 4 days. Approximately  $1 \times 10^6$  cells

per clone were lysed for 30 minutes on ice in 1% triton lysis buffer containing protease inhibitors and incubated with 100 units benzonase for 30 minutes at 37°C to digest the DNA so that the pellet can be easily resuspended during the following steps. The insoluble pellet was obtained by 2 centrifugation steps of 15 minutes at 13,000 rpm, resuspended in lysis buffer with protease inhibitors and incubated with  $1 \times 10^7$  coated beads per sample for 1 hour at 4°C. The beads were extracted in the magnet and washed twice in PBS/BSA. Then the bound proteins were eluted from the beads with hot SDS sample buffer for 5 minutes at 99°C. All samples collected at different stages of the experiment were analysed by SDS-PAGE and Western blotting against GFP and polyQ. Before elution, a droplet of beads was placed on a microscope slide, mounted in Aqua Polymount, and images were taken with a fluorescent microscope. The eluates were additionally separated by SDS-PAGE and stained with silver.

The Western blot on the left in Fig. 31A shows all samples taken during the procedure, probed for GFP; the samples of 23Q and 74Q cells were run in pairs. The lysate (lanes 1+2) shows both GFP-HttEx1 constructs in the resolving gel; the 74Q sample contains moreover the signal of the aggregates retained in the stacking gel. After centrifugation, all soluble protein was detected in the supernatants. The supernatant S1 (lanes 3+4) shows a very strong signal, whereas S2 (lanes 5+6) is nearly clean. No aggregates were detected in the supernatants S1 and S2. Therefore, the separation of 74Q aggregate and soluble GFP-HttEx1 protein by centrifugation was effective.

After the incubation of the insoluble pellet with dynabeads, the beads were extracted. The resulting supernatant S3 (lanes 7+8) contains the components of the insoluble pellet which did not bind to the beads. The S3 from the 74Q samples shows moreover two faint bands of GFP-HttEx1-74Q in the resolving and in the stacking gel, which result from unbound aggregates that were partly solubilised in the sample buffer. The very low signal intensity indicates that most aggregates were bound to the beads. The last lane contains a control of coated beads, showing the IgG heavy chain at 50 kDa.

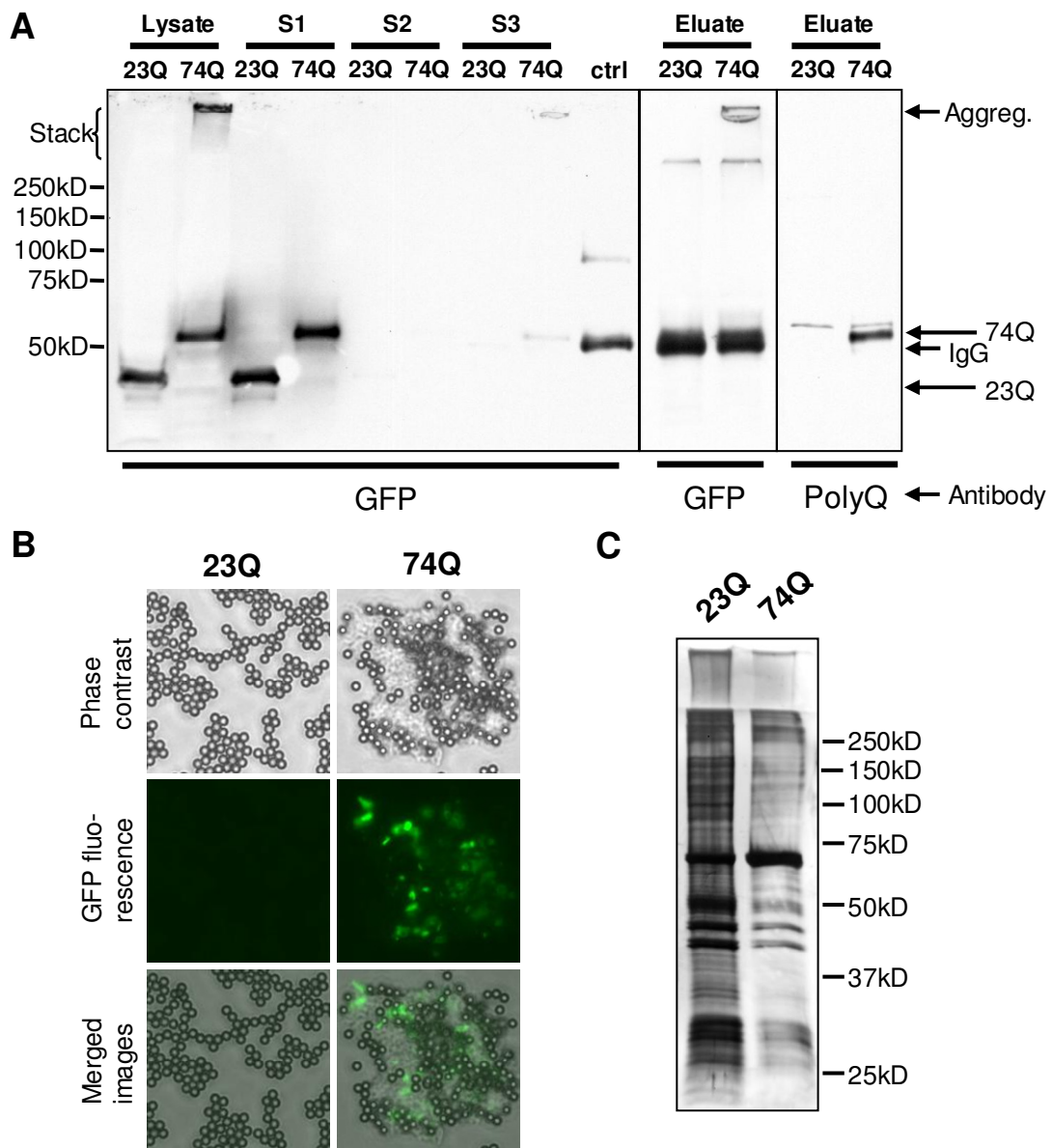


**Fig. 31: Immunomagnetic separation with Dynabeads.**

23Q cells and 74Q cells (clone 72.16) were lysed in 1% triton lysis buffer after 4 d of induction with 1  $\mu$ g/ml dox. Insoluble pellets were resuspended in buffer and incubated with anti-GFP-coated dynabeads for 1 h at 4  $^{\circ}$ C. The dynabeads were extracted, washed, and bound proteins eluted in SDS-SB for 5 min at 99  $^{\circ}$ C.

A) The samples were analysed by SDS-PAGE and Western blotting against GFP and PolyQ. (S1 and S2 = supernatant after centrifugation; S3 = supernatant after incubation with beads; ctrl = coated beads only.) B) Dynabeads before elution were imaged by fluorescence microscopy. Fluorescence of the GFP-HttEx1-74Q aggregates is shown in green. The dynabeads are visible in the phase contrast images. C) Silver stain of all proteins in the 23Q and 74Q eluates.

The other two Western blots in Fig. 31A show the eluates from the 23Q and 74Q cells, probed for GFP (middle) and polyQ (right). The GFP-HttEx1-74Q aggregates were eluted from the beads with SDS-SB at 99 $^{\circ}$ C and mostly

retained in the stacking gel. The insoluble GFP-Htt-74Q in the stacking gel could be detected by the antibody against GFP but not by the antibody against polyQ, as observed before. The polyQ signal in the resolving gel allows the detection of solubilised GFP-Htt-74Q, which is overlaid in the middle blot by the strong signal of the coating-antibody.

The fluorescent images of the dynabeads before the elution confirm that the dynabeads bind the GFP-HttEx1-74Q aggregates (Fig. 31B). The dynabeads are clearly visible in the phase contrast in both samples (top panel). The phase contrast image of the 74Q sample shows also some amorphous material attached to the beads. Fluorescence from the GFP was only detected in the 74Q sample (middle panel). The merged image of the 74Q sample in the bottom panel reveals that not all material which is visible in the phase contrast is also fluorescent, suggesting that other material besides the GFP-HttEx1-74Q aggregates is attached to the beads.

The protein staining of the eluates (Fig. 31C) shows that both eluates contain a large number of proteins. The pattern is approximately the same, but the staining is stronger in the 23Q sample, probably because the amount of each sample was based on cell number and not as usual on protein content. One can conclude that the eluates are very impure, i.e. they contain many proteins that are unspecifically attached to the dynabeads and not through the antibody against GFP.

The experiment was repeated with coated and uncoated beads to test whether the binding of the dynabeads to the aggregates was specific. Before elution, samples were taken for analysis by Western blotting against GFP and PolyQ (Fig. 32). The 23Q samples do not contain any GFP-HttEx1 because only the insoluble pellet was incubated with the beads. The band intensity of the aggregates (in the stacking gel) in the samples with coated and uncoated beads is the same, indicating that the same amount of aggregates was bound to the coated beads as was bound to the uncoated beads. The lack of IgG in lanes 3 and 4 confirms that these dynabeads were in deed uncoated. This experiment reveals that the binding of GFP-HttEx1 aggregates to the dynabeads was

unspecific and not, or only partially, mediated by the rabbit-anti-GFP IgG bound to the beads. Despite the initial positive results, this approach to purification did therefore not give satisfactory results. It raised however the idea that the aggregates have a very sticky nature which might cause artefacts.

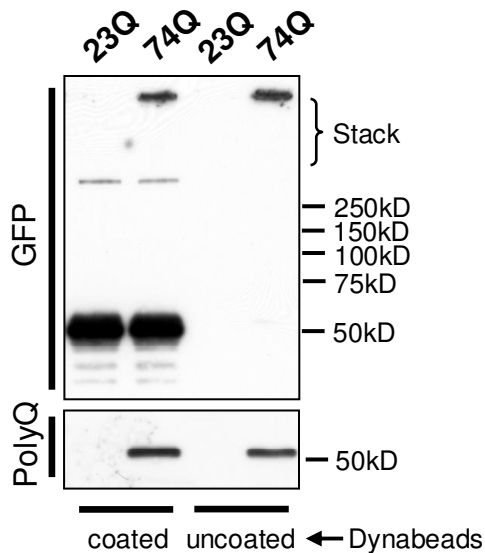


Fig. 32: Immunomagnetic separation with Dynabeads. Insoluble pellets of lysate from induced 23Q cells and 74Q cells (clone 72.16) were incubated with coated and uncoated beads. The beads were extracted, washed and analysed by SDS-PAGE and Western blotting against GFP and PolyQ.

Another attempt to purify GFP-HttEx1 aggregates by immunomagnetic separation was made with a different type of beads, named  $\mu$ MACS (Miltenyi Biotec). They are also referred to as microbeads because they are with a diameter of 50 nm much smaller than the dynabeads. Because of their small size they remain in suspension and cannot be extracted from a solution by placing the tube in a magnet. Instead, the solution has to be passed through a column which contains steel beads in its funnel and is placed in a very strong magnetic field. After several washing steps, the target protein can be eluted from the column with hot elution buffer, while the antibody-conjugated beads remain in the column. The microbeads were in this case already covalently coated with an antibody against GFP, which specifically recognised the GFP-HttEx1-23Q and -74Q proteins. The column, however, through which the solution has to pass, renders this experimental set-up unsuitable for the purification of insoluble proteins because they are mechanically retained in the funnel.

### 3.3.3 Purification of Fibrils

In all the above experiments, mild lysis conditions were used to disrupt the cells in order to avoid damaging the integrity of the aggregates or releasing binding partners. Under these conditions it was impossible to separate the aggregates from the mesh of the cytoskeleton and other cellular components. Therefore, a harsher treatment with SDS was tested.

74Q cells, either induced for 4 days or uninduced, were lysed as before in 1% Triton lysis buffer with protease inhibitors for 1 hour on ice, followed by treatment with benzonase for 30 minutes at 37°C. Lysate containing 18 mg of protein was filled up to volume of 1 ml with a final concentration of 2% SDS and then shaken for 1 hour at 37°C. Subsequently, the sample was centrifuged for 20 minutes at 16,000 g to separate the aggregates from the soluble GFP-HttEx1-74Q. The pellet was resuspended in lysis buffer with 2% SDS, incubated for 30 minutes at 37°C and centrifuged again. This step was repeated one more time, before solubilising the resulting pellets in 100% formic acid for 30 minutes at 37°C, evaporating the formic acid and solubilising the dried pellets in SDS sample buffer. SDS-PAGE and Western blotting against GFP of the pellets and the three supernatants (Fig. 33A, only induced samples shown) revealed that the aggregates did not sediment during the three centrifugation steps at 16,000 g, as they used to do without the SDS-treatment. Instead, they were present in the supernatants S1 and S2.

The treatment with 2% SDS did not solubilise the aggregated huntingtin protein, but it must have affected the aggregates in some way to make them remain mostly in the supernatant S1 during centrifugation. Some aggregates probably pelleted during the first centrifugation step and were then dispersed by the second treatment with SDS, leaving them in the supernatant during the second centrifugation (S2). Only a very small amount of the aggregates pelleted during all three centrifugation steps and became visible after solubilisation in formic acid in the faint signal above 50 kDa in the pellet (P, equal to 11 x S1). The pellets were in addition separated by SDS-PAGE and stained with silver, but nothing was detected, although 4 times the amount of pellet was used in comparison with the Western blot (data not shown).

The supernatants S1 were therefore centrifuged again, but at 100,000 g for 1 hour. The pellet was washed twice in 1% triton lysis buffer with 0.5% SDS and centrifuged again after each wash. The resulting pellet of the induced cells was bright green, the control pellet colourless. After the first spin, the pellets also contained a white material that appeared like mother-of-pearl crystals in suspension (possibly SDS crystals). It was mostly removed during both washing steps, leaving only very small, but visible pellets. As before, the pellets were solubilised in 100% formic acid and dried. The high speed pellet (HP) and the three supernatants (HS1-3) were analysed by SDS-PAGE and Western blotting against GFP, polyQ and ubiquitin (Fig. 33B).

The centrifugation of the supernatant S1 at a higher speed, i.e. 100,000 g, pelleted most insoluble GFP-HttEx1-74Q, as there is only little insoluble protein retained in the stacking gel of HS1 and HS2, and large amounts of solubilised GFP-HttEx1-74Q were detected in the pellet HP (after treatment with formic acid). This supports the hypothesis from above, that the treatment with SDS dispersed the aggregates, but without solubilising the protein. The Western blot against GFP of the pellet HP shows a wide range of bands from 25 kDa into the stacking gel. Most prominent is the band just above 50 kDa plus a strong band just below and three less strong bands above, which could indicate protein ubiquitination. Moreover, there is a band just above 25 kDa. The smears are the strongest at the top of the stacking and the resolving gel.

The pellet HP shows nearly the identical pattern when probed against GFP and against polyQ. Only the band just above 25 kDa is missing in the Western blot against polyQ, possibly the GFP-part of the fusion protein. Interestingly, the polyQ antibody detected in this blot also the huntingtin retained in the top of the stacking and resolving gel, which were usually not detected by this antibody. This might be caused by the treatment with SDS or the large amount of GFP-HttEx1-74Q in this preparation. The Western blot against ubiquitin shows that the protein retained in the top of the stacking and resolving gel is heavily ubiquitinated. The ladder pattern above 50 kDa is detected as well, though the signal is only faint. This finding confirms that the aggregated GFP-HttEx1-74Q is partly ubiquitinated. The strongest band of solubilised GFP-HttEx1-74Q

(above 50 kDa) however is not detected with this antibody, neither is the band of the soluble huntingtin fusion protein in the control (lysate, last lane).

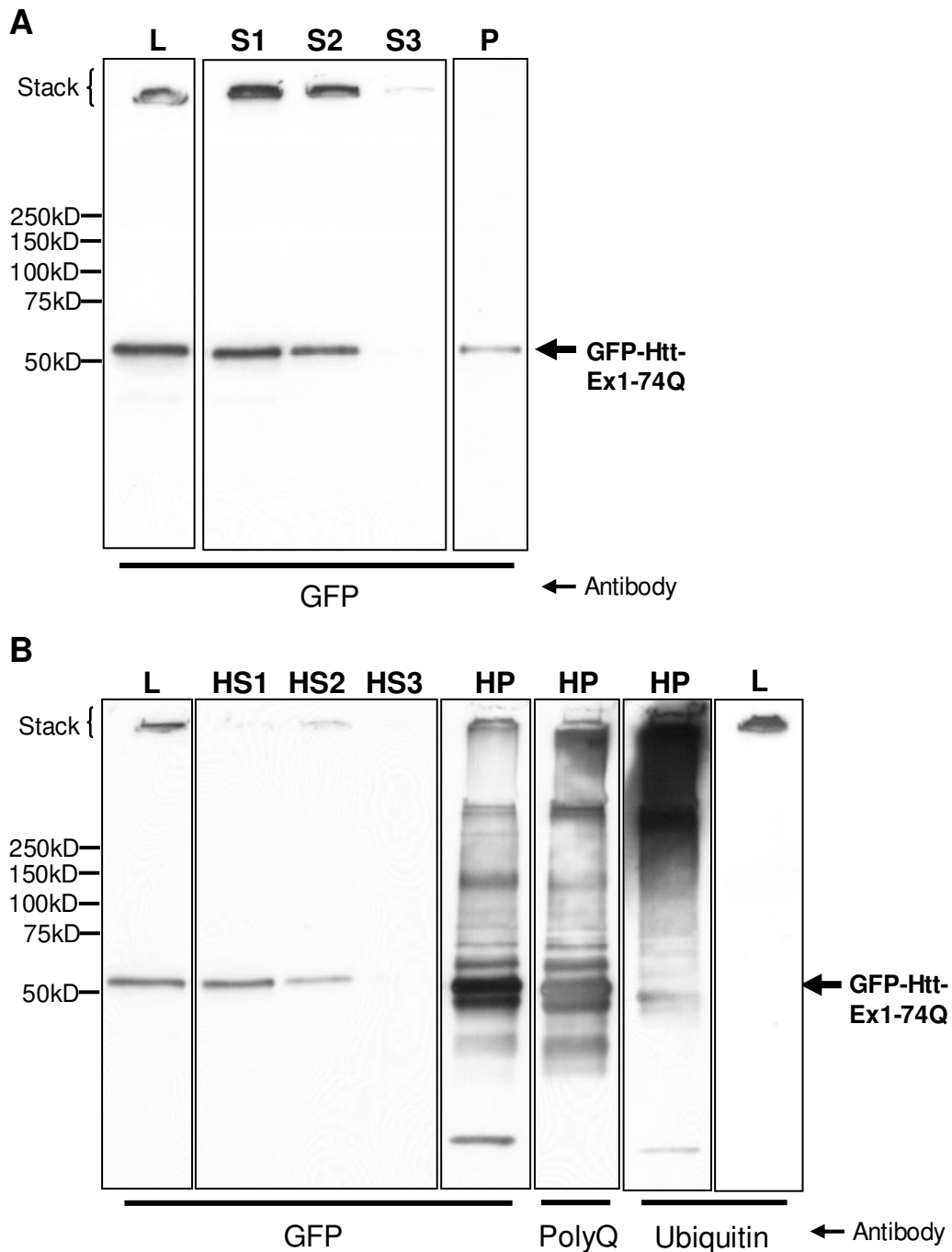


**Fig. 33: SDS-purification of GFP-HttEx1-74Q aggregates.**

Induced 74Q cells (clone 72.16) were lysed and treated with 2% SDS. The treated lysate was centrifuged 3 times at 16,000 g; the resulting first supernatant was centrifuged 3 times at 100,000 g. The samples were analysed by SDS-PAGE and Western blotting against GFP, PolyQ and ubiquitin. (L= lysate)

A) Supernatants S1-S2 and pellet P after low speed centrifugation.

B) Supernatants HS1-HS3 and pellet HP after high speed centrifugation.

The same experiment as above was repeated with the double amount of lysate of 74Q cells, uninduced or induced for 4 days, to analyse the pellet by electron microscopy. This time the SDS-treated lysate was directly centrifuged at 100,000 g. The first wash was performed with 1% triton lysis buffer and 0.5% SDS, the second in ultra pure water which prevented the accumulation of crystals in the pellets. The pellets were then analysed by electron microscopy, which was performed by Dr. David Dinsdale (Fig. 34).

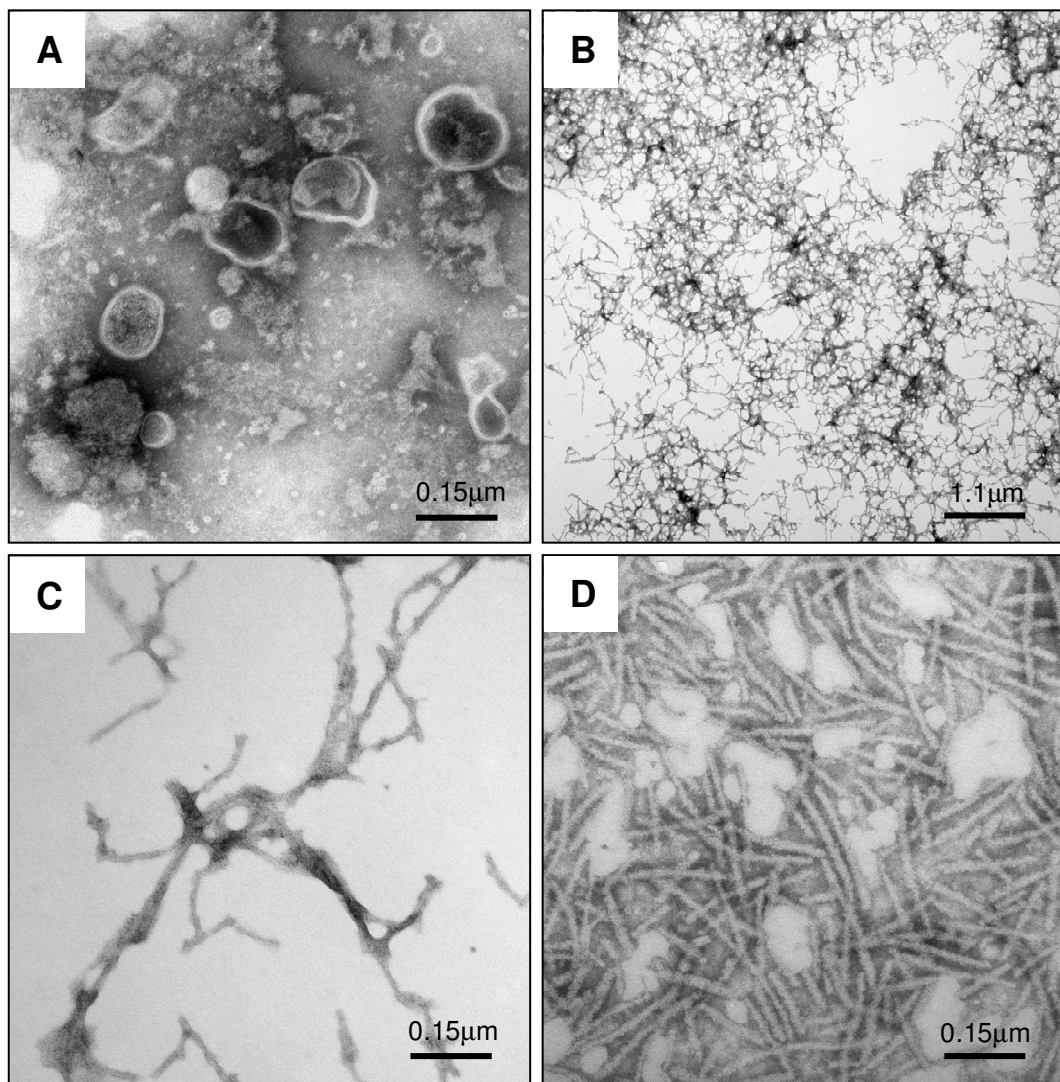


**Fig. 34: GFP-HttEx1-74Q aggregates – Electron Microscopy.**

74Q cells (clone 72.16), which were uninduced or induced for 4 d with 1  $\mu\text{g/ml}$  dox, were lysed and treated with 2% SDS. The treated lysate was centrifuged 3 x at 100,000 g. The samples were analysed by electron microscopy by Dr. D. Dinsdale. Two contrast methods were used, either tungsten or uranium. Images were taken at a magnification of 50,000x. A) 74Q uninduced; tungsten. B) 74Q +Dox; uranium. C) 74Q +Dox; uranium. D) 74Q +Dox; tungsten.

The pellet of the uninduced 74Q cells contained only amorphous material (Fig. 34A), whereas the pellet of the induced 74Q cells contained thousands of fibrils, which are approximately 10 nm thick and of various lengths (Fig. 34B-D).

The GFP-HttEx1-74Q fibrils resemble those formed in vitro by recombinant huntingtin exon-1 with an expanded polyglutamine tract (51Q), which have a diameter of 10-12 nm and vary in length from 100 nm to several micrometers (Scherzinger et al., 1997). Electron micrographs of huntingtin inclusions in human post-mortem brain (Gutekunst et al., 1999) and brain from R6 transgenic mice (Davies et al., 1997; Scherzinger et al., 1997) also reveal filamentous and granular material.

Although this purification method with SDS does not allow any conclusion with regard to other proteins which may be sequestered into inclusion bodies, it presents a simple and effective method to purify SDS-resistant fibrils and could also be tested on tissue samples. In addition, the purified fibrils could be used in cell culture or in vitro experiments, for example to test their toxicity.

## 4 Discussion

### 4.1 The Effect of Huntingtin Aggregates on Endosomal Recycling

The clinical symptoms of Huntington's disease have been initially assumed to be caused by the massive neuronal death in the striatum, which disturbs the physiological function of the basal ganglia in movement control and thus causes chorea and other motor deficits seen in HD. However, the symptoms of the disease begin before overt neuronal loss (Vonsattel and DiFiglia, 1998), and dysfunction rather than cell death may be the underlying cause, in particular of the early symptoms, while cell death may result from long-term dysfunction. In this thesis, I demonstrate a lesion in the exit of cargo from the endosomal recycling centre which is specifically associated with huntingtin aggregates. As endosomal recycling is essential for correct neuronal function, this lesion presents a possible mechanism whereby protein inclusions may cause neuronal dysfunction and contribute to the cognitive and motor deficits seen in HD.

The first project was based on the result of a proteomics study by Dr. Paul Richards and Anna Simpson that Rab11, a protein involved endosomal recycling, is reduced in a PC12 cell culture model of HD. Therefore, I investigated whether the endosomal recycling is affected in PC12 cells expressing a fragment of human GFP-tagged huntingtin exon-1 with an expanded CAG repeat (GFP-HttEx1-74Q) or a normal CAG repeat (GFP-HttEx1-23Q) under the control of the Tet-On promoter (see chapter 3.1).

The endosomal recycling pathway was studied by monitoring the recycling of transferrin, which is described in more detail in chapter 1.3. Transferrin is taken up into the cell by clathrin-mediated endocytosis of the transferrin receptor. As visualised by the live-cell imaging, the transferrin in the medium first attaches to the plasma membrane, is then taken up into vesicles at the cell periphery and finally reaches the endocytic recycling compartment (ERC). Live-cell imaging and quantitative Western blot analysis demonstrated that the uptake of transferrin in this cell culture model is neither affected by the

expression of wild-type or mutant GFP-HttEx1 nor in the presence of GFP-HttEx1-74Q aggregates. The 74Q cells displayed a higher rate of transferrin uptake into the cells compared to the 23Q cells. However, this difference is in all probability independent of transgene expression in both clones, as cells with a low background expression level in the absence of doxycycline display a similar rate of transferrin uptake as cells with high expression levels after 1 or 4 days of induction with doxycycline.

After the release of the transported iron in the sorting endosome, transferrin and its receptor are shuttled back to the plasma membrane via two pathways. The fast recycling pathway leads from the sorting endosome directly back to the plasma membrane, while the slower pathway includes the trafficking from the sorting endosome to the ERC and from the ERC to the plasma membrane. The molecular mechanisms which determine whether recycling occurs through the direct or indirect pathway are not known (Maxfield and McGraw, 2004). However, in PC12 cells recycling through the ERC is predominant (Dr. Paul Richards, personal communication). The extrusion of transferrin from the cell was monitored by quantitative Western blot analysis and confocal microscopy of fixed cells in pulse-chase experiments with labelled transferrin. As before, the uninduced 74Q cells displayed a faster rate of transferrin recycling than the uninduced 23Q cells, and as before, the rate of extrusion in 23Q cells was not significantly different in cells with or without expression of GFP-HttEx1-23Q. In contrast, the rate of extrusion in 74Q cells was significantly reduced in cells after 4 days of induction (when ca. 40% of the cells contain visible aggregates) compared to uninduced cells (low background induction) and cells after only 1 day of induction (i.e. with soluble GFP-HttEx1-74Q, but without aggregates).

Confocal images at the start of the chase show the typical pattern of internalised transferrin, i.e. vesicles are stained throughout the cytoplasm with the highest concentration of transferrin and the highest density of vesicles in the perinuclear region, where the ERC is located. In cells with visible aggregates, this signal at the ERC is stronger than in cells without aggregates, suggesting an accumulation of transferrin in the ERC during the loading with labelled transferrin. During the chase, the transferrin signal at the ERC disappears, and

only dispersed transferrin-positive vesicles remain in the cytoplasm, revealing no apparent difference between the 3 time points of the chase (15, 30 and 60 minutes) or between cells with or without expression of wild-type or mutant GFP-HttEx-1. The fact that the higher level of retained transferrin in 74Q cells after 4 days of induction is only visible in the Western blot analysis and not by confocal microscopy is probably due to the higher sensitivity of Western blotting, which is more suitable for quantitative analysis.

Suggested by the impaired transferrin clearance and the accumulation of transferrin in the ERC of cells containing aggregates, I used the time-lapse data on transferrin uptake in 23Q and 74Q cells to determine the kinetics of the transferrin flux through the ERC. For this purpose, the ERC of each cell was marked as a region of interest, and the fluorescence intensity of labelled transferrin within this region of interest at each time point was calculated. Subsequently, the uptake of transferrin into the ERC for 23Q cells (with or without soluble GFP-HttEx1-23Q) and for 74Q cells (with or without soluble GFP-httEx1-74Q or with aggregates) was plotted over time. The graphs demonstrated that the flux of transferrin through the ERC is not affected by the presence of soluble wild-type or mutant GFP-HttEx1, but that the accumulation of transferrin in cells containing aggregates is significantly higher. Taking into account that there was no impairment in uptake, these data reflect a significant reduction of the export of transferrin from the ERC, which is specifically associated with the presence of huntingtin aggregates.

This defect in endosomal recycling coincided with a decrease of the GTPase Rab11b in cytosolic PC12 fractions, which was discovered in a proteomics screen by Dr. Paul Richards and Anna Simpson. Cytosolic fractions of uninduced and induced 23Q and 74Q cells were prepared for this purpose by mild cell lysis in buffer containing 1% Triton, followed by a short centrifugation step at 16,000 g (5 min). Cytosolic fractions were in addition analysed by Western blotting against Rab11 (a and b), confirming that Rab11 is reduced after 4 days of GFP-HttEx1-74Q expression (see chapter 3.2.1). Later experiments were carried out using the lysates with RIPA buffer, which contains stronger detergents and solubilises more proteins. Western blots against Rab11

with these lysates did not reproduce the reduction of Rab11 in 74Q cells after 4 days of induction (Dr. Paul Richards, personal communication). The different results with both buffers may reflect a change in Rab11 distribution rather than a change in expression levels (or both). Also the confocal images of PC12 cells immuno-stained with antibody against Rab11 (a and b) do not clearly show a loss of Rab11, but a less pronounced signal at the ERC in cells containing GFP-HttEx1-74Q aggregates, which still lies in the range of variation between individual uninduced 23Q and 74Q cells (not quantified). Rab GTPases can switch between an active GTP-bound form and an inactive GDP-bound form, and this switch is also linked to a switch in localisation. Thus, the GDP-bound form is localised in the cytosol, while activation by nucleotide exchange occurs on membranes (Groschans et al., 2006). A loss of Rab11 signal at ERC membranes could therefore suggest that less GTP-bound Rab11 is present in cells containing GFP-HttEx1-74Q aggregates. Based on the Western blot results that a mild detergent extracts less Rab11 in 74Q cells after 4 days induction, however, one would rather expect an increase in membrane-bound Rab11 in cells containing GFP-HttEx1-74Q aggregates.

Rab11 is a Rab GTPase involved in endosomal recycling, which has been shown to mediate trafficking of cargo from the ERC to the plasma membrane (Ullrich et al., 1996; Ren et al., 1998). I silenced Rab11a and Rab11b with specific siRNAs in order to test whether this would affect transferrin recycling. The downregulation of Rab11a, Rab11b or both by siRNA was successful, reducing the amount endogenous protein by about 85-90%. While silencing of Rab11a had no significant effect on transferrin recycling, the silencing of Rab11b significantly reduced the rate of transferrin extrusion in PC12 cells, which resembles the effect seen in 74Q cells which contain GFP-HttEx1-74Q aggregates after 4 days of induction.

There is also evidence in the literature that endosomal recycling is affected in HD. One report from 2006 confirms my finding that the uptake of transferrin by clathrin-mediated endocytosis is not impaired by mutant huntingtin. The study was carried out in primary striatal neurons from transgenic mice (HD72) and in PC12 cells expressing full length huntingtin with 82Q. The extrusion of

transferrin from the cell was not examined. Instead, inhibition of caveolin-1-dependent endocytosis was detected, and intracellular accumulation of cholesterol, which is internalised by caveolin-1-dependent endocytosis, was observed *in vitro* and *in vivo*. In addition, an interaction between caveolin-1 and mutant huntingtin was demonstrated (Trushina et al., 2006).

In another study, a function for huntingtin in the nucleotide exchange on Rab11 and thus in the activation of Rab11 was proposed (Li et al., 2008). More recently, two publications by the same group reported the disruption of Rab11 activity in a knock-in mouse model of HD (140Q) (Li et al., 2009 a) and in fibroblasts from HD patients (Li et al., 2009 b). In mouse brain, reduced GEF (guanine nucleotide exchange factor) activity on Rab11 was detected, leading to insufficient Rab11 activation. The level of Rab11 in mouse striatum was unchanged, but more Rab11 was attached to membranes. This finding is interesting because it agrees with the finding in our group that a reduction of Rab11 was only observed in cytosolic fractions of PC12 cells which were prepared with a mild detergent (see above). The changes in Rab11 activation in knock-in mice occurred before the onset of neuropathology. In addition, mice expressing a dominant-negative Rab11 (GDP-bound) developed neurodegeneration and motor deficits, suggesting that Rab11 has a crucial role in neurons and that defect Rab11 function may contribute to disease pathology in HD mice.

Li and co-workers also investigated transferrin recycling in primary cortical neurons from HD knock-in mice and observed delayed return of transferrin to the plasma membrane (Li et al., 2009, a), confirming my results for 74Q cells. Normal transferrin uptake and delayed return to the plasma membrane was also observed in fibroblasts from HD patients, but transferrin recycling in these cells could be normalised by expression of a dominant-active Rab11 (GTP-bound) (Li et al., 2009, b).

Both studies by Li and co-workers did not examine the role of huntingtin aggregates in their model and did not try to distinguish between the effects of soluble mutant huntingtin and those of inclusion bodies. However, nuclear and neuropil aggregates are present in these knock-in mice before the onset of

abnormal behaviour (Menalled et al., 2003). The authors propose a novel mechanism of HD pathogenesis arising from diminished Rab11 activity at recycling endosomes, but do not specify how mutant huntingtin could cause the loss of Rab11 activity. The proposed function of wild-type huntingtin in nucleotide exchange on Rab11 (Li et al., 2008) rather suggests a loss of function in mutant huntingtin.

In this thesis, I show clearly on the single cell level that the impairment of exit from the ERC specifically correlates with the presence of visible GFP-HttEx1-74Q aggregates and not with soluble GFP-HttEx1-74Q. However, my data do not prove a causal relationship between the two. It is possible that misfolded huntingtin intermediates, which cannot be visualised by microscopy, are present in 74Q cells also containing visible GFP-HttEx1-74Q inclusion bodies, and that these folding intermediates (and not the inclusion bodies) cause the defect in endosomal recycling. The use of molecules which promote or interfere with aggregate formation could give more information about the correlation between huntingtin inclusion bodies and impairment of exit from the ERC, but these molecules may also have unknown effects on the cell or on the folding intermediates, besides their effect on the formation of visible huntingtin inclusion bodies.

Altogether, these data from my thesis and Li and co-workers reveal a deficit of endosomal recycling in HD which is likely to affect the recycling of many receptor proteins and thereby to interfere with neuronal function.

In the human brain, synaptic plasticity plays a key role in learning and memory. It is mediated by long-lasting changes of synaptic strength of excitatory glutamatergic synapses on dendrites which receive and integrate the input from innumerable axon terminals. These synapses are located on dendritic spines, which are small membrane protrusions on the dendrites. An increase in synaptic strength is named long-term potentiation (LTP), while a decrease in synaptic strength is named long-term depression (LTD). The synaptic strength depends on the number and composition of the glutamate receptors at the synapse on the dendritic spine. There are three types of ionotropic glutamate

receptors, which include AMPA receptors (subunits GluR1-4), kainate receptors (subunits GluR5-7, KA1-2) and NMDA receptors (subunits NR1, NR2A-D). AMPA receptors are the main mediators of synaptic strength, while NMDA receptors have a crucial signalling function for synaptic plasticity. (For reviews on synaptic plasticity see Newpher and Ehlers, 2008 and 2009).

Recycling endosomes located at the dendritic spine play a central role in synaptic plasticity by regulating the recycling and delivery of glutamate receptors at the synapse. For example, it has been shown that AMPA receptors are mobilised from recycling endosomes in dendritic spines during LTP stimulation (Park et al., 2004). The recycling endosomes in the dendritic spines have also been implicated in the formation and modelling of dendritic spines during LTP by providing membrane components (Park et al., 2006). In addition, it has been demonstrated that the transport of AMPA receptors from the dendritic shaft into the spine is Rab11-dependent (Park et al., 2004; Brown et al., 2007; Petrini et al., 2009). The Rab11 effectors Rab11-FIP2 and myosin Vb are also involved in this transport process (Wang et al., 2008).

In Huntington's disease, dendritic changes in neurons have been reported, including recurving of dendrites, decreases and increases in density of spines, and changes in size and shape of spines (Vonsattel and DiFiglia, 1998). At the same time, a high frequency of neuropil aggregates before the onset of disease symptoms has been described (Gutekunst et al., 1999). Therefore, the present data provide a mechanism by which huntingtin aggregates could cause the neurological deficits in Huntington's disease.

## 4.2 The Purification of Huntingtin Aggregates

One mechanism by which aggregates could be toxic has been suggested to be the sequestration of proteins into inclusion bodies and the subsequent perturbation of cell function. The term 'sequestration' can also be used for the interaction between specific soluble proteins by which cellular processes are often regulated, but it will not be used in that sense here. Much of the evidence for the sequestration of proteins other than huntingtin into protein inclusions was provided by studies which used fluorescence microscopy to demonstrate the colocalisation of huntingtin inclusions with other proteins (see introduction). This approach, however, has several disadvantages: the core of the aggregate may be inaccessible to the antibody; the antigen may not be in its native conformation; no quantification of the amount of sequestered protein is possible; reliable controls to exclude unspecific binding are missing; and the choice of targets adds bias. As a consequence, it has never been proven that the huntingtin inclusions sequester indeed sufficient amounts of proteins to reduce the levels of the free protein, and to exclude that proteins only bind transiently to the aggregate shell. Therefore, I aimed to purify the huntingtin aggregates from PC12 cells expressing GFP-HttEx1-74Q, to dissolve them in formic acid and to identify their components by mass spectrometry.

First, I attempted to purify the aggregates by density gradient centrifugation in combination with mild detergents which would not release components of the aggregates. Centrifugation of whole cell lysate on a continuous sucrose gradient between 40-70% was carried out. The aggregates were located in the 74Q pellet, but the presence of a pellet in the 23Q pellet indicated that the aggregates in the 74Q were not pure. This assumption was confirmed by the 2D gel analysis of these pellets after dissolving them in 100% formic acid, as the protein spot patterns in both gels of 23Q and 74Q samples were highly similar, except for the GFP-HttEx1-74Q protein in the 74Q gel. Several spots were picked and analysed by mass spectrometry, which identified several heterogeneous nuclear ribonucleoproteins, nuclear RNA-binding proteins, keratins type I and II, and peripherin, a neuronal intermediate filament. It is improbable that these proteins form part of the aggregates since they were also found in the

pellet of the 23Q control. Instead, they may be associated with nuclear components, ribosomal material or cytoskeleton. Interestingly, the study on the composition of aggregates purified by FACS (Hazeki et al., 2002) reported the sequestration of heterogeneous nuclear ribonucleoproteins, which comprise a large group of predominantly nuclear RNA binding proteins, into huntingtin exon-1 aggregates. As this study did not have a control because of its design, it is possible that the ribonucleoproteins only attached to the aggregates during the processes to which the cell lysate was subjected.

Since the previous experiment demonstrated that sucrose was not dense enough to resolve the aggregates in a pure fraction, I tested Nycodenz as an alternative density gradient medium with a higher maximum density than sucrose. Four centrifugation experiments were carried out with induced control and mutant clones with varying gradients. The aggregates were distributed over a relatively large range which indicates a high variation in density, and the fraction, in which the aggregates migrated, contained many other proteins, as demonstrated by the control (data not shown). In the Nycodenz gradient, the aggregates migrated at a lower density ( $1.159 \text{ g/cm}^3$ -  $1.237 \text{ g/cm}^3$ ) than in the sucrose ( $>1.34 \text{ g/cm}^3$ ), which is not unusual, as the density of a protein depends on the medium used for the density gradient. However, the wide distribution of the aggregates in the gradient demonstrated that density gradient centrifugation was not suitable to purify the GFP-HttEx1-74Q aggregates.

Subsequently, I tested immunomagnetic separation with dynabeads to purify GFP-HttEx1 aggregates using the GFP-tag. This method does not require centrifugation steps because the beads can be pulled out from a solution by placing a 1.5 ml tube into a special magnet. The dynabeads are super-paramagnetic beads which were coated with covalently linked to sheep anti rabbit IgG and were additionally coated with rabbit anti GFP IgG.

Many experiments were run with varying sample preparation, incubation and elution conditions. Early results from fluorescence microscopy and Western blotting demonstrated that the dynabeads did bind the aggregates and could pull them out of the sample. However, during further experiments, more and more difficulties became apparent with respect to the high unspecific binding in

the control sample (23Q) and to the lack of effective elution methods other than boiling in sample buffer which damages the dynabeads and is moreover incompatible with 2D gel electrophoresis. Finally, it became evident that the nature of the interaction between aggregates and magnetic beads was unspecific, demonstrated by the fact that also beads that were not coated with the primary antibody against GFP did pull out the aggregates.

All experiments described so far have been carried out on cell lysates in 1% triton buffer, because a mild detergent was preferable in order to purify components of the GFP-HttEx1 protein aggregates. However, it appears that the aggregates are locked in a mesh of cytoskeletal proteins and other proteins, and that it is impossible to obtain pure aggregates from this lysate.

Hence, very harsh treatment with SDS was attempted instead to produce a pure fraction of aggregates. 74Q cells that were either left uninduced or induced for 4 days were lysed as usual in 1% triton lysis buffer, followed by treatment with benzonase. Then, SDS was added to the solution in a final concentration of 2%, and the sample shaken for 1 h at 37°C. After 3 centrifugation steps at 16,000 g, the supernatants and pellets (solubilised in formic acid) were analysed by SDS-PAGE and Western blotting against GFP, which revealed that the aggregates had not pelleted in the centrifugation steps as they used to do before. It appeared that the SDS treatment had disintegrated the aggregates and I therefore centrifuged the supernatant at 100,000 g, which can be used to distinguish between soluble and insoluble protein. Therefore, the aggregates should pellet during this centrifugation if they were truly SDS-insoluble, as often reported. A bright green pellet was obtained and also some crystals that seemed to be precipitated SDS. As before, the pellet (solubilised in formic acid) and supernatants were subjected to Western blotting against GFP and PolyQ plus ubiquitin. The results indicated that the aggregates had pelleted with 100,000 g. This means that the aggregates were dispersed by the treatment with SDS, but had retained their insoluble nature. The Western blot analysis of the formic-acid-treated pellets demonstrated that the huntingtin aggregates in PC12 cells consist of many huntingtin fragments of different sizes which are partly ubiquitinated.

The same experiment was repeated and the pellet subjected to electron microscopy. The pellet of the induced 74Q containing the aggregates proved to contain thousands of fibrils, approximately 10 nm thick and of various lengths. In contrast, the uninduced control showed only amorphous material.

The GFP-HttEx1-74Q fibrils resemble those formed in vitro by recombinant huntingtin exon-1 with an expanded polyglutamine tract (51Q), which have a diameter of 10-12 nm and vary in length from 100 nm to several micrometers (Scherzinger et al., 1997). Electron micrographs of huntingtin inclusions in human post-mortem brain (Gutekunst et al., 1999) and brain from R6 transgenic mice (Davies et al., 1997; Scherzinger et al., 1997) also reveal filamentous and granular material.

One attempt to aggregate purification by CsCl density gradient centrifugation (Suhr et al., 2001) was published in the *Journal of Cell Biology*. The work was carried out on stably transfected cell lines overexpressing GFP-tagged HttEx1 with a polyglutamine tract of either 13 or 96 residues. Whole cell lysate was centrifuged (16,000 g; 5 min), the pellet resuspended in Tris buffer, sonicated and incubated with DnaseI. CsCl density gradient centrifugation was carried out for 24 h at 110,000 g. A greenish band was observed which was subsequently diluted in Tris buffer and centrifuged (3 times at 5,000 g). The resulting pellet was subjected to SDS-PAGE, after which protein bands were cut out and analysed by mass spectrometry (MALDI). Ubiquitin, p53, Hsp70, TBP, actin, 68kD NF and nuclear core components were identified. The main criticism to this study is the absence of a control. Analysis of the corresponding fraction in a CsCl density gradient centrifugation of cells expressing wild-type exon-1 was not shown. Moreover, the aggregates were not solubilised before SDS-PAGE, so they would have been retained in the stacking gel. In this case, sequestered components of the aggregates tightly bound to the mutant Htt exon-1 would not be expected to enter into the resolving gel either. The nature of some of the identified proteins suggests they are nuclear or cytoskeletal proteins which may have pelleted during the centrifugation and co-migrated in the CsCl gradient.

Another attempt to purify aggregates was made by gel filtration (Dyer and McMurray, 2001). This study used material from human brain (HD and control)

and transgenic mice (R6/1) in order to find out whether the aggregates contained only mutant or also wild-type huntingtin and whether the huntingtin was found in form of full length protein or fragments. RIPA buffer extracts of striatal tissue were filtered through cheesecloth and resolved by Sepharose CL2B gel filtration ( $7 \times 10^4$ - $4 \times 10^7$ ). Fractions were eluted with Tris buffer and subjected to Western blot analysis with two different antibodies (2166, anti exon-1; 1C2, anti-PolyQ). Huntingtin was detected in its monomeric form as well as in high mass complexes. The profile of the full length huntingtin was very similar in control and HD brains, suggesting that the wild-type huntingtin in control brains formed high mass complexes of similar size to the mutant huntingtin in HD brains. Both HD and control brain contained wild-type huntingtin N-terminal cleavage products. However, in the HD brains the N-terminal fragments co-eluted with high mass fractions, whereas in control brains they eluted with low mass fractions. The HD brains did not generate N-terminal cleavage products of mutant huntingtin in the collected fractions. The authors conclude that mutant huntingtin is more resistant to proteolysis and that mutant full length huntingtin sequesters N-terminal fragments of wild-type huntingtin. The study draws some misleading conclusions based on selective interpretation of their data. For instance, the similarity of the full length elution profile in control and HD brains indicates that the high mass fractions represent high mass complexes that are also present in the control and therefore distinct from the microscopically visible aggregates, which only appear in HD brains. Moreover, since no solubilisation step was performed, aggregated huntingtin would be mostly retained in the stacking gels, which were not shown in the figures in this publication.

A major obstacle for analysis of aggregate composition is their insolubility which prevents further separation of their components, e.g. by electrophoresis. In the year 2000, a biochemical study was published demonstrating the successful solubilisation of aggregates by concentrated formic acid, assessed by a filter retardation assay (Hazeki et al., 2000). This method was applied in the study on aggregate composition by Hazeki et al., 2002. The study was carried out on a neuronal cell line transiently expressing Htt exon-1 with a 74 CAG repeat. Aggregates were purified by differential centrifugation (300 g for 5 min) of whole

cell lysate, followed by fluorescence-activated cell sorting (FACS). After solubilisation of the aggregates in 100% formic acid for 1 hour at 37°C, the samples were subjected to SDS-PAGE and N-terminal sequencing. The major component of the aggregates was the Htt-exon-1-GFP fusion protein. In addition, heterogeneous ribonucleoproteins F and H, histones and ubiquitin were found to be associated with the aggregates. However, this study lacks a control due to its methodological design.

HttEx1 aggregates have been reported to be purified by cesium chloride density gradient centrifugation (Scherzinger et al., 1999). The aggregate density in caesium chloride was determined as 1.307 g/ml. The aggregate-containing fraction was used to prove the presence of fibrils by electron microscopy in cells expressing HttEx1 with an expanded polyglutamine tract. The authors did not, however, analyse the purity of the fraction which would be necessary to identify components of the aggregates.

Another study used homogenisation and treatment with SDS to purify aggregates from human post-mortem HD brain. The homogenate was dialysed to retain only extremely large proteins and centrifuged at 100,000 g, and the purified fibrils were solubilised by formic acid (Hoffner et al., 2005). This study, however, did not attempt to identify aggregate components as they would have been lost during the SDS-treatment. Instead, they analysed the composition of aggregates with respect to the huntingtin fragments which they consist of. They demonstrated that aggregates in human brain consist of N-terminal fragments between 50 and 150 kDa, in addition to oligomeric and polymeric complexes, indicating that some huntingtin fragments are conjugated by peptide-bonds, which were not dissolved by formic acid.

Judging from my results and the reports of others, the aggregates have such a high affinity for other proteins that it is impossible to separate them from other cellular components without harsh detergent treatment like SDS, which will make it impossible to carry out a quantitative analysis of aggregate components and proteins that may be sequestered into them. The sequestration of proteins into huntingtin inclusions will therefore remain a possible hypothesis.

## 5 References

- Aisen, P., Enns, C. and Wessling-Resnick, M. (2001). Chemistry and biology of eukaryotic iron metabolism. *Int J Biochem Cell Biol.* Vol. 33, pp. 940-59.
- Andrade, M. A. and Bork, P. (1995). HEAT repeats in the Huntington's disease protein. *Nat Genet.* Vol. 11, pp. 115-6.
- Andresen, J. M., Gayan, J., Cherny, S. S., Brocklebank, D., Alkorta-Aranburu, G., Addis, E. A., Cardon, L. R., Housman, D. E., et al. (2007). Replication of twelve association studies for Huntington's disease residual age of onset in large Venezuelan kindreds. *J Med Genet.* Vol. 44, pp. 44-50.
- Andrew, S. E., Goldberg, Y. P., Kremer, B., Telenius, H., Theilmann, J., Adam, S., Starr, E., Squitieri, F., et al. (1993). The relationship between trinucleotide (CAG) repeat length and clinical features of Huntington's disease. *Nat Genet.* Vol. 4, pp. 398-403.
- Arning, L., Kraus, P. H., Valentin, S., Saft, C., Andrich, J. and Epplen, J. T. (2005). NR2A and NR2B receptor gene variations modify age at onset in Huntington disease. *Neurogenetics.* Vol. 6, pp. 25-8.
- Arning, L., Monte, D., Hansen, W., Wieczorek, S., Jagiello, P., Akkad, D. A., Andrich, J., Kraus, P. H., et al. (2008). ASK1 and MAP2K6 as modifiers of age at onset in Huntington's disease. *J Mol Med.* Vol. 86, pp. 485-90.
- Aronin, N., Chase, K., Young, C., Sapp, E., Schwarz, C., Matta, N., Kornreich, R., Landwehrmeyer, B., et al. (1995). CAG expansion affects the expression of mutant Huntingtin in the Huntington's disease brain. *Neuron.* Vol. 15, pp. 1193-201.
- Behrends, C., Langer, C. A., Boteva, R., Bottcher, U. M., Stemp, M. J., Schaffar, G., Rao, B. V., Giese, A., et al. (2006). Chaperonin TRiC promotes the assembly of polyQ expansion proteins into nontoxic oligomers. *Mol Cell.* Vol. 23, pp. 887-97.
- Bence, N. F., Sampat, R. M. and Kopito, R. R. (2001). Impairment of the ubiquitin-proteasome system by protein aggregation. *Science.* Vol. 292, pp. 1552-5.
- Bennett, E. J., Bence, N. F., Jayakumar, R. and Kopito, R. R. (2005). Global impairment of the ubiquitin-proteasome system by nuclear or cytoplasmic

- protein aggregates precedes inclusion body formation. *Mol Cell*. Vol. 17, pp. 351-65.
- Bett, J. S., Cook, C., Petrucelli, L. and Bates, G. P. (2009). The ubiquitin-proteasome reporter GFPu does not accumulate in neurons of the R6/2 transgenic mouse model of Huntington's disease. *PLoS One*. Vol. 4, p. e5128.
- Bhide, P. G., Day, M., Sapp, E., Schwarz, C., Sheth, A., Kim, J., Young, A. B., Penney, J., et al. (1996). Expression of normal and mutant huntingtin in the developing brain. *J Neurosci*. Vol. 16, pp. 5523-35.
- Bizat, N., Hermel, J. M., Boyer, F., Jacquard, C., Creminon, C., Ouary, S., Escartin, C., Hantraye, P., et al. (2003). Calpain is a major cell death effector in selective striatal degeneration induced in vivo by 3-nitropropionate: implications for Huntington's disease. *J Neurosci*. Vol. 23, pp. 5020-30.
- Bjorkqvist, M., Wild, E. J., Thiele, J., Silvestroni, A., Andre, R., Lahiri, N., Raibon, E., Lee, R. V., et al. (2008). A novel pathogenic pathway of immune activation detectable before clinical onset in Huntington's disease. *J Exp Med*. Vol. 205, pp. 1869-77.
- Block-Galarza, J., Chase, K. O., Sapp, E., Vaughn, K. T., Vallee, R. B., DiFiglia, M. and Aronin, N. (1997). Fast transport and retrograde movement of huntingtin and HAP 1 in axons. *Neuroreport*. Vol. 8, pp. 2247-51.
- Brown, T. C., Correia, S. S., Petrok, C. N. and Esteban, J. A. (2007). Functional compartmentalization of endosomal trafficking for the synaptic delivery of AMPA receptors during long-term potentiation. *J Neurosci*. Vol. 27, pp. 13311-5.
- Carmichael, J., Chatellier, J., Woolfson, A., Milstein, C., Fersht, A. R. and Rubinsztein, D. C. (2000). Bacterial and yeast chaperones reduce both aggregate formation and cell death in mammalian cell models of Huntington's disease. *Proc Natl Acad Sci U S A*. Vol. 97, pp. 9701-5.
- Carter, R. J., Lione, L. A., Humby, T., Mangiarini, L., Mahal, A., Bates, G. P., Dunnett, S. B. and Morton, A. J. (1999). Characterization of progressive motor deficits in mice transgenic for the human Huntington's disease mutation. *J Neurosci*. Vol. 19, pp. 3248-57.

- Caviston, J. P. and Holzbaur, E. L. (2009). Huntingtin as an essential integrator of intracellular vesicular trafficking. *Trends Cell Biol.*
- Chandra, S., Shao, J., Li, J. X., Li, M., Longo, F. M. and Diamond, M. I. (2008). A common motif targets huntingtin and the androgen receptor to the proteasome. *J Biol Chem.* Vol. 283, pp. 23950-5.
- Chang, D. T., Rintoul, G. L., Pandipati, S. and Reynolds, I. J. (2006). Mutant huntingtin aggregates impair mitochondrial movement and trafficking in cortical neurons. *Neurobiol Dis.* Vol. 22, pp. 388-400.
- Chattopadhyay, B., Baksi, K., Mukhopadhyay, S. and Bhattacharyya, N. P. (2005). Modulation of age at onset of Huntington disease patients by variations in TP53 and human caspase activated DNase (hCAD) genes. *Neurosci Lett.* Vol. 374, pp. 81-6.
- Chen, W., Feng, Y., Chen, D. and Wandinger-Ness, A. (1998). Rab11 is required for trans-golgi network-to-plasma membrane transport and a preferential target for GDP dissociation inhibitor. *Mol Biol Cell.* Vol. 9, pp. 3241-57.
- Chen, C. Y. and Brodsky, F. M. (2005). Huntingtin-interacting protein 1 (Hip1) and Hip1-related protein (Hip1R) bind the conserved sequence of clathrin light chains and thereby influence clathrin assembly in vitro and actin distribution in vivo. *J Biol Chem.* Vol. 280, pp. 6109-17.
- Colin, E., Regulier, E., Perrin, V., Durr, A., Brice, A., Aebischer, P., Deglon, N., Humbert, S., et al. (2005). Akt is altered in an animal model of Huntington's disease and in patients. *Eur J Neurosci.* Vol. 21, pp. 1478-88.
- Colin, E., Zala, D., Liot, G., Rangone, H., Borrell-Pages, M., Li, X. J., Saudou, F. and Humbert, S. (2008). Huntingtin phosphorylation acts as a molecular switch for anterograde/retrograde transport in neurons. *Embo J.* Vol. 27, pp. 2124-34.
- Cooper, J. K., Schilling, G., Peters, M. F., Herring, W. J., Sharp, A. H., Kaminsky, Z., Masone, J., Khan, F. A., et al. (1998). Truncated N-terminal fragments of huntingtin with expanded glutamine repeats form nuclear and cytoplasmic aggregates in cell culture. *Hum Mol Genet.* Vol. 7, pp. 783-90.

- Cui, L., Jeong, H., Borovecki, F., Parkhurst, C. N., Tanese, N. and Krainc, D. (2006). Transcriptional repression of PGC-1alpha by mutant huntingtin leads to mitochondrial dysfunction and neurodegeneration. *Cell*. Vol. 127, pp. 59-69.
- Davies, S. W., Turmaine, M., Cozens, B. A., DiFiglia, M., Sharp, A. H., Ross, C. A., Scherzinger, E., Wanker, E. E., et al. (1997). Formation of neuronal intranuclear inclusions underlies the neurological dysfunction in mice transgenic for the HD mutation. *Cell*. Vol. 90, pp. 537-48.
- de la Monte, S. M., Vonsattel, J. P. and Richardson, E. P., Jr. (1988). Morphometric demonstration of atrophic changes in the cerebral cortex, white matter, and neostriatum in Huntington's disease. *J Neuropathol Exp Neurol*. Vol. 47, pp. 516-25.
- del Toro, D., Alberch, J., Lazaro-Diequez, F., Martin-Ibanez, R., Xifro, X., Egea, G. and Canals, J. M. (2009). Mutant huntingtin impairs post-Golgi trafficking to lysosomes by delocalizing optineurin/Rab8 complex from the Golgi apparatus. *Mol Biol Cell*. Vol. 20, pp. 1478-92.
- Diaz-Hernandez, M., Valera, A. G., Moran, M. A., Gomez-Ramos, P., Alvarez-Castelao, B., Castano, J. G., Hernandez, F. and Lucas, J. J. (2006). Inhibition of 26S proteasome activity by huntingtin filaments but not inclusion bodies isolated from mouse and human brain. *J Neurochem*. Vol. 98, pp. 1585-96.
- DiFiglia, M., Sapp, E., Chase, K., Schwarz, C., Meloni, A., Young, C., Martin, E., Vonsattel, J. P., et al. (1995). Huntingtin is a cytoplasmic protein associated with vesicles in human and rat brain neurons. *Neuron*. Vol. 14, pp. 1075-81.
- DiFiglia, M., Sapp, E., Chase, K. O., Davies, S. W., Bates, G. P., Vonsattel, J. P. and Aronin, N. (1997). Aggregation of huntingtin in neuronal intranuclear inclusions and dystrophic neurites in brain. *Science*. Vol. 277, pp. 1990-3.
- Dompierre, J. P., Godin, J. D., Charrin, B. C., Cordelieres, F. P., King, S. J., Humbert, S. and Saudou, F. (2007). Histone deacetylase 6 inhibition compensates for the transport deficit in Huntington's disease by increasing tubulin acetylation. *J Neurosci*. Vol. 27, pp. 3571-83.

- Dragileva, E., Hendricks, A., Teed, A., Gillis, T., Lopez, E. T., Friedberg, E. C., Kucherlapati, R., Edelman, W., et al. (2009). Intergenerational and striatal CAG repeat instability in Huntington's disease knock-in mice involve different DNA repair genes. *Neurobiol Dis.* Vol. 33, pp. 37-47.
- Duyao, M., Ambrose, C., Myers, R., Novelletto, A., Persichetti, F., Frontali, M., Folstein, S., Ross, C., et al. (1993). Trinucleotide repeat length instability and age of onset in Huntington's disease. *Nat Genet.* Vol. 4, pp. 387-92.
- Duyao, M. P., Auerbach, A. B., Ryan, A., Persichetti, F., Barnes, G. T., McNeil, S. M., Ge, P., Vonsattel, J. P., et al. (1995). Inactivation of the mouse Huntington's disease gene homolog Hdh. *Science.* Vol. 269, pp. 407-10.
- Dyer, R. B. and McMurray, C. T. (2001). Mutant protein in Huntington disease is resistant to proteolysis in affected brain. *Nat Genet.* Vol. 29, pp. 270-8.
- Engqvist-Goldstein, A. E., Kessels, M. M., Chopra, V. S., Hayden, M. R. and Drubin, D. G. (1999). An actin-binding protein of the Sla2/Huntingtin interacting protein 1 family is a novel component of clathrin-coated pits and vesicles. *J Cell Biol.* Vol. 147, pp. 1503-18.
- Fan, G. H., Lapierre, L. A., Goldenring, J. R., Sai, J. and Richmond, A. (2004). Rab11-family interacting protein 2 and myosin Vb are required for CXCR2 recycling and receptor-mediated chemotaxis. *Mol Biol Cell.* Vol. 15, pp. 2456-69.
- Ferrante, R. J., Kibilus, J. K., Lee, J., Ryu, H., Beesen, A., Zucker, B., Smith, K., Kowall, N. W., et al. (2003). Histone deacetylase inhibition by sodium butyrate chemotherapy ameliorates the neurodegenerative phenotype in Huntington's disease mice. *J Neurosci.* Vol. 23, pp. 9418-27.
- Ferrer, I., Goutan, E., Marin, C., Rey, M. J. and Ribalta, T. (2000). Brain-derived neurotrophic factor in Huntington disease. *Brain Res.* Vol. 866, pp. 257-61.
- Finkbeiner, S., Tavazoie, S. F., Maloratsky, A., Jacobs, K. M., Harris, K. M. and Greenberg, M. E. (1997). CREB: a major mediator of neuronal neurotrophin responses. *Neuron.* Vol. 19, pp. 1031-47.
- Floto, R. A., Sarkar, S., Perlstein, E. O., Kampmann, B., Schreiber, S. L. and Rubinsztein, D. C. (2007). Small molecule enhancers of rapamycin-induced TOR inhibition promote autophagy, reduce toxicity in Huntington's disease models and enhance killing of mycobacteria by

- macrophages. *Autophagy*. Vol. 3, pp. 620-2.
- Gafni, J., Hermel, E., Young, J. E., Wellington, C. L., Hayden, M. R. and Ellerby, L. M. (2004). Inhibition of calpain cleavage of Huntingtin reduces toxicity: Accumulation of calpain/caspase fragments in the nucleus. *J Biol Chem*.
- Garcia-Mata, R., Bebok, Z., Sorscher, E. J. and Sztul, E. S. (1999). Characterization and dynamics of aggresome formation by a cytosolic GFP-chimera. *J Cell Biol*. Vol. 146, pp. 1239-54.
- Gardian, G., Browne, S. E., Choi, D. K., Klivenyi, P., Gregorio, J., Kibilus, J. K., Ryu, H., Langley, B., et al. (2005). Neuroprotective effects of phenylbutyrate in the N171-82Q transgenic mouse model of Huntington's disease. *J Biol Chem*. Vol. 280, pp. 556-63.
- Gauthier, L. R., Charrin, B. C., Borrell-Pages, M., Dompierre, J. P., Rangone, H., Cordelieres, F. P., De Mey, J., MacDonald, M. E., et al. (2004). Huntingtin controls neurotrophic support and survival of neurons by enhancing BDNF vesicular transport along microtubules. *Cell*. Vol. 118, pp. 127-38.
- Gerber, H. P., Seipel, K., Georgiev, O., Hofferer, M., Hug, M., Rusconi, S. and Schaffner, W. (1994). Transcriptional activation modulated by homopolymeric glutamine and proline stretches. *Science*. Vol. 263, pp. 808-11.
- Gervais, F. G., Singaraja, R., Xanthoudakis, S., Gutekunst, C. A., Leavitt, B. R., Metzler, M., Hackam, A. S., Tam, J., et al. (2002). Recruitment and activation of caspase-8 by the Huntingtin-interacting protein Hip-1 and a novel partner Hip1. *Nat Cell Biol*. Vol. 4, pp. 95-105.
- Giorgini, F., Moller, T., Kwan, W., Zwilling, D., Wacker, J. L., Hong, S., Tsai, L. C., Cheah, C. S., et al. (2008). Histone deacetylase inhibition modulates kynurenine pathway activation in yeast, microglia, and mice expressing a mutant huntingtin fragment. *J Biol Chem*. Vol. 283, pp. 7390-400.
- Goffredo, D., Rigamonti, D., Tartari, M., De Micheli, A., Verderio, C., Matteoli, M., Zuccato, C. and Cattaneo, E. (2002). Calcium-dependent cleavage of endogenous wild-type huntingtin in primary cortical neurons. *J Biol Chem*. Vol. 277, pp. 39594-8.
- Graham, R. K., Slow, E. J., Deng, Y., Bissada, N., Lu, G., Pearson, J., Shehadeh, J., Leavitt, B. R., et al. (2006, a). Levels of mutant huntingtin

- influence the phenotypic severity of Huntington disease in YAC128 mouse models. *Neurobiol Dis.* Vol. 21, pp. 444-55.
- Graham, R. K., Deng, Y., Slow, E. J., Haigh, B., Bissada, N., Lu, G., Pearson, J., Shehadeh, J., et al. (2006, b). Cleavage at the caspase-6 site is required for neuronal dysfunction and degeneration due to mutant huntingtin. *Cell.* Vol. 125, pp. 1179-91.
- Graham, R. K., Pouladi, M. A., Joshi, P., Lu, G., Deng, Y., Wu, N. P., Figueroa, B. E., Metzler, M., et al. (2009). Differential susceptibility to excitotoxic stress in YAC128 mouse models of Huntington disease between initiation and progression of disease. *J Neurosci.* Vol. 29, pp. 2193-204.
- Graveland, G. A., Williams, R. S. and DiFiglia, M. (1985). Evidence for degenerative and regenerative changes in neostriatal spiny neurons in Huntington's disease. *Science.* Vol. 227, pp. 770-3.
- Grosshans, B. L., Ortiz, D. and Novick, P. (2006). Rabs and their effectors: achieving specificity in membrane traffic. *Proc Natl Acad Sci U S A.* Vol. 103, pp. 11821-7.
- Guidetti, P., Bates, G. P., Graham, R. K., Hayden, M. R., Leavitt, B. R., MacDonald, M. E., Slow, E. J., Wheeler, V. C., et al. (2006). Elevated brain 3-hydroxykynurenine and quinolinate levels in Huntington disease mice. *Neurobiol Dis.* Vol. 23, pp. 190-7.
- Gusella, J. F., Wexler, N. S., Conneally, P. M., Naylor, S. L., Anderson, M. A., Tanzi, R. E., Watkins, P. C., Ottina, K., et al. (1983). A polymorphic DNA marker genetically linked to Huntington's disease. *Nature.* Vol. 306, pp. 234-8.
- Gusella, J. F. and MacDonald, M. E. (2000). Molecular genetics: unmasking polyglutamine triggers in neurodegenerative disease. *Nat Rev Neurosci.* Vol. 1, pp. 109-15.
- Gusella, J. F. and Macdonald, M. E. (2009). Huntington's disease: the case for genetic modifiers. *Genome Med.* Vol. 1, p. 80.
- Gutkunst, C. A., Levey, A. I., Heilman, C. J., Whaley, W. L., Yi, H., Nash, N. R., Rees, H. D., Madden, J. J., et al. (1995). Identification and localization of huntingtin in brain and human lymphoblastoid cell lines with anti-fusion protein antibodies. *Proc Natl Acad Sci U S A.* Vol. 92, pp. 8710-4.

- Gutekunst, C. A., Li, S. H., Yi, H., Mulroy, J. S., Kuemmerle, S., Jones, R., Rye, D., Ferrante, R. J., et al. (1999). Nuclear and neuropil aggregates in Huntington's disease: relationship to neuropathology. *J Neurosci*. Vol. 19, pp. 2522-34.
- Hackam, A. S., Singaraja, R., Wellington, C. L., Metzler, M., McCutcheon, K., Zhang, T., Kalchman, M. and Hayden, M. R. (1998). The influence of huntingtin protein size on nuclear localization and cellular toxicity. *J Cell Biol*. Vol. 141, pp. 1097-105.
- Hackam, A. S., Hodgson, J. G., Singaraja, R., Zhang, T., Gan, L., Gutekunst, C. A., Hersch, S. M. and Hayden, M. R. (1999). Evidence for both the nucleus and cytoplasm as subcellular sites of pathogenesis in Huntington's disease in cell culture and in transgenic mice expressing mutant huntingtin. *Philos Trans R Soc Lond B Biol Sci*. Vol. 354, pp. 1047-55.
- Hackam, A. S., Yassa, A. S., Singaraja, R., Metzler, M., Gutekunst, C. A., Gan, L., Warby, S., Wellington, C. L., et al. (2000). Huntingtin interacting protein 1 induces apoptosis via a novel caspase-dependent death effector domain. *J Biol Chem*. Vol. 275, pp. 41299-308.
- Hales, C. M., Griner, R., Hobdy-Henderson, K. C., Dorn, M. C., Hardy, D., Kumar, R., Navarre, J., Chan, E. K., et al. (2001). Identification and characterization of a family of Rab11-interacting proteins. *J Biol Chem*. Vol. 276, pp. 39067-75.
- Hales, C. M., Vaerman, J. P. and Goldenring, J. R. (2002). Rab11 family interacting protein 2 associates with Myosin Vb and regulates plasma membrane recycling. *J Biol Chem*. Vol. 277, pp. 50415-21.
- Hansson, O., Castilho, R. F., Korhonen, L., Lindholm, D., Bates, G. P. and Brundin, P. (2001, a). Partial resistance to malonate-induced striatal cell death in transgenic mouse models of Huntington's disease is dependent on age and CAG repeat length. *J Neurochem*. Vol. 78, pp. 694-703.
- Hansson, O., Guatteo, E., Mercuri, N. B., Bernardi, G., Li, X. J., Castilho, R. F. and Brundin, P. (2001, b). Resistance to NMDA toxicity correlates with appearance of nuclear inclusions, behavioural deficits and changes in calcium homeostasis in mice transgenic for exon 1 of the huntington gene. *Eur J Neurosci*. Vol. 14, pp. 1492-504.

- Hansson, O., Nylandsted, J., Castilho, R. F., Leist, M., Jaattela, M. and Brundin, P. (2003). Overexpression of heat shock protein 70 in R6/2 Huntington's disease mice has only modest effects on disease progression. *Brain Res.* Vol. 970, pp. 47-57.
- Harjes, P. and Wanker, E. E. (2003). The hunt for huntingtin function: interaction partners tell many different stories. *Trends Biochem Sci.* Vol. 28, pp. 425-33.
- Harper, P. S. (1991). Huntington's disease. Saunders, W. B., London.
- Harper, P. S. (1992). The epidemiology of Huntington's disease. *Hum Genet.* Vol. 89, pp. 365-76.
- Hayden, M. R. (1981) Huntington's Chorea. Springer-Verlag, New York.
- Hazeki, N., Tukamoto, T., Goto, J. and Kanazawa, I. (2000). Formic acid dissolves aggregates of an N-terminal huntingtin fragment containing an expanded polyglutamine tract: applying to quantification of protein components of the aggregates. *Biochem Biophys Res Commun.* Vol. 277, pp. 386-93.
- Hazeki, N., Tsukamoto, T., Yazawa, I., Koyama, M., Hattori, S., Someki, I., Iwatsubo, T., Nakamura, K., et al. (2002). Ultrastructure of nuclear aggregates formed by expressing an expanded polyglutamine. *Biochem Biophys Res Commun.* Vol. 294, pp. 429-40.
- Heng, M. Y., Detloff, P. J. and Albin, R. L. (2008). Rodent genetic models of Huntington disease. *Neurobiol Dis.* Vol. 32, pp. 1-9.
- Hermel, E., Gafni, J., Propp, S. S., Leavitt, B. R., Wellington, C. L., Young, J. E., Hackam, A. S., Logvinova, A. V., et al. (2004). Specific caspase interactions and amplification are involved in selective neuronal vulnerability in Huntington's disease. *Cell Death Differ.* Vol. 11, pp. 424-38.
- Ho, L. W., Brown, R., Maxwell, M., Wytenbach, A. and Rubinsztein, D. C. (2001). Wild type Huntingtin reduces the cellular toxicity of mutant Huntingtin in mammalian cell models of Huntington's disease. *J Med Genet.* Vol. 38, pp. 450-2.
- Hodges, A., Strand, A. D., Aragaki, A. K., Kuhn, A., Sengstag, T., Hughes, G., Elliston, L. A., Hartog, C., et al. (2006). Regional and cellular gene expression changes in human Huntington's disease brain. *Hum Mol*

- Genet.* Vol. 15, pp. 965-77.
- Hodgson, J. G., Agopyan, N., Gutekunst, C. A., Leavitt, B. R., LePiane, F., Singaraja, R., Smith, D. J., Bissada, N., et al. (1999). A YAC mouse model for Huntington's disease with full-length mutant huntingtin, cytoplasmic toxicity, and selective striatal neurodegeneration. *Neuron*. Vol. 23, pp. 181-92.
- Hoffner, G., Kahlem, P. and Djian, P. (2002). Perinuclear localization of huntingtin as a consequence of its binding to microtubules through an interaction with beta-tubulin: relevance to Huntington's disease. *J Cell Sci*. Vol. 115, pp. 941-8.
- Hoffner, G., Island, M. L. and Djian, P. (2005). Purification of neuronal inclusions of patients with Huntington's disease reveals a broad range of N-terminal fragments of expanded huntingtin and insoluble polymers. *J Neurochem*. Vol. 95, pp. 125-36.
- Holbert, S., Denghien, I., Kiechle, T., Rosenblatt, A., Wellington, C., Hayden, M. R., Margolis, R. L., Ross, C. A., et al. (2001). The Gln-Ala repeat transcriptional activator CA150 interacts with huntingtin: neuropathologic and genetic evidence for a role in Huntington's disease pathogenesis. *Proc Natl Acad Sci U S A*. Vol. 98, pp. 1811-6.
- Humbert, S., Bryson, E. A., Cordelieres, F. P., Connors, N. C., Datta, S. R., Finkbeiner, S., Greenberg, M. E. and Saudou, F. (2002). The IGF-1/Akt pathway is neuroprotective in Huntington's disease and involves Huntingtin phosphorylation by Akt. *Dev Cell*. Vol. 2, pp. 831-7.
- Huntington, G. (1872). On chorea. *Med Surg Reporter*. Vol. 26, pp. 320-21.
- Iwata, A., Riley, B. E., Johnston, J. A. and Kopito, R. R. (2005). HDAC6 and microtubules are required for autophagic degradation of aggregated huntingtin. *J Biol Chem*. Vol. 280, pp. 40282-92.
- Jana, N. R., Zemskov, E. A., Wang, G. and Nukina, N. (2001). Altered proteasomal function due to the expression of polyglutamine-expanded truncated N-terminal huntingtin induces apoptosis by caspase activation through mitochondrial cytochrome c release. *Hum Mol Genet*. Vol. 10, pp. 1049-59.
- Jiang, H., Nucifora, F. C., Jr., Ross, C. A. and DeFranco, D. B. (2003). Cell death triggered by polyglutamine-expanded huntingtin in a neuronal cell

- line is associated with degradation of CREB-binding protein. *Hum Mol Genet.* Vol. 12, pp. 1-12.
- Jiang, H., Poirier, M. A., Liang, Y., Pei, Z., Weiskittel, C. E., Smith, W. W., DeFranco, D. B. and Ross, C. A. (2006). Depletion of CBP is directly linked with cellular toxicity caused by mutant huntingtin. *Neurobiol Dis.* Vol. 23, pp. 543-51.
- Johnston, J. A., Ward, C. L. and Kopito, R. R. (1998). Aggresomes: a cellular response to misfolded proteins. *J Cell Biol.* Vol. 143, pp. 1883-98.
- Kalchman, M. A., Koide, H. B., McCutcheon, K., Graham, R. K., Nichol, K., Nishiyama, K., Kazemi-Esfarjani, P., Lynn, F. C., et al. (1997). HIP1, a human homologue of *S. cerevisiae* Sla2p, interacts with membrane-associated huntingtin in the brain. *Nat Genet.* Vol. 16, pp. 44-53.
- Kawaguchi, Y., Kovacs, J. J., McLaurin, A., Vance, J. M., Ito, A. and Yao, T. P. (2003). The deacetylase HDAC6 regulates aggresome formation and cell viability in response to misfolded protein stress. *Cell.* Vol. 115, pp. 727-38.
- Kegel, K. B., Kim, M., Sapp, E., McIntyre, C., Castano, J. G., Aronin, N. and DiFiglia, M. (2000). Huntingtin expression stimulates endosomal-lysosomal activity, endosome tubulation, and autophagy. *J Neurosci.* Vol. 20, pp. 7268-78.
- Kim, M., Velier, J., Chase, K., Laforet, G., Kalchman, M. A., Hayden, M. R., Won, L., Heller, A., et al. (1999). Forskolin and dopamine D1 receptor activation increase huntingtin's association with endosomes in immortalized neuronal cells of striatal origin. *Neuroscience.* Vol. 89, pp. 1159-67.
- Kim, Y. J., Yi, Y., Sapp, E., Wang, Y., Cuiffo, B., Kegel, K. B., Qin, Z. H., Aronin, N., et al. (2001). Caspase 3-cleaved N-terminal fragments of wild-type and mutant huntingtin are present in normal and Huntington's disease brains, associate with membranes, and undergo calpain-dependent proteolysis. *Proc Natl Acad Sci U S A.* Vol. 98, pp. 12784-9.
- Kim, S., Nollen, E. A., Kitagawa, K., Bindokas, V. P. and Morimoto, R. I. (2002). Polyglutamine protein aggregates are dynamic. *Nat Cell Biol.* Vol. 4, pp. 826-31.

- Kitamura, A., Kubota, H., Pack, C. G., Matsumoto, G., Hirayama, S., Takahashi, Y., Kimura, H., Kinjo, M., et al. (2006). Cytosolic chaperonin prevents polyglutamine toxicity with altering the aggregation state. *Nat Cell Biol.* Vol. 8, pp. 1163-70.
- Kovtun, I. V. and McMurray, C. T. (2001). Trinucleotide expansion in haploid germ cells by gap repair. *Nat Genet.* Vol. 27, pp. 407-11.
- Kuemmerle, S., Gutekunst, C. A., Klein, A. M., Li, X. J., Li, S. H., Beal, M. F., Hersch, S. M. and Ferrante, R. J. (1999). Huntington aggregates may not predict neuronal death in Huntington's disease. *Ann Neurol.* Vol. 46, pp. 842-9.
- Kuhn, A., Goldstein, D. R., Hodges, A., Strand, A. D., Sengstag, T., Kooperberg, C., Becanovic, K., Pouladi, M. A., et al. (2007). Mutant huntingtin's effects on striatal gene expression in mice recapitulate changes observed in human Huntington's disease brain and do not differ with mutant huntingtin length or wild-type huntingtin dosage. *Hum Mol Genet.* Vol. 16, pp. 1845-61.
- Landwehrmeyer, G. B., McNeil, S. M., Dure, L. S. t., Ge, P., Aizawa, H., Huang, Q., Ambrose, C. M., Duyao, M. P., et al. (1995). Huntington's disease gene: regional and cellular expression in brain of normal and affected individuals. *Ann Neurol.* Vol. 37, pp. 218-30.
- Lapierre, L. A., Kumar, R., Hales, C. M., Navarre, J., Bhartur, S. G., Burnette, J. O., Provance, D. W., Jr., Mercer, J. A., et al. (2001). Myosin vb is associated with plasma membrane recycling systems. *Mol Biol Cell.* Vol. 12, pp. 1843-57.
- Leavitt, B. R., Guttman, J. A., Hodgson, J. G., Kimel, G. H., Singaraja, R., Vogl, A. W. and Hayden, M. R. (2001). Wild-type huntingtin reduces the cellular toxicity of mutant huntingtin in vivo. *Am J Hum Genet.* Vol. 68, pp. 313-24.
- Lee, W. C., Yoshihara, M. and Littleton, J. T. (2004). Cytoplasmic aggregates trap polyglutamine-containing proteins and block axonal transport in a *Drosophila* model of Huntington's disease. *Proc Natl Acad Sci U S A.* Vol. 101, pp. 3224-9.
- Legendre-Guillemain, V., Metzler, M., Lemaire, J. F., Philie, J., Gan, L., Hayden, M. R. and McPherson, P. S. (2005). Huntington interacting protein 1

- (HIP1) regulates clathrin assembly through direct binding to the regulatory region of the clathrin light chain. *J Biol Chem*. Vol. 280, pp. 6101-8.
- Li, H., Li, S. H., Cheng, A. L., Mangiarini, L., Bates, G. P. and Li, X. J. (1999). Ultrastructural localization and progressive formation of neuropil aggregates in Huntington's disease transgenic mice. *Hum Mol Genet*. Vol. 8, pp. 1227-36.
- Li, S. H., Schilling, G., Young, W. S., 3rd, Li, X. J., Margolis, R. L., Stine, O. C., Wagster, M. V., Abbott, M. H., et al. (1993). Huntington's disease gene (IT15) is widely expressed in human and rat tissues. *Neuron*. Vol. 11, pp. 985-93.
- Li, S. H. and Li, X. J. (1998). Aggregation of N-terminal huntingtin is dependent on the length of its glutamine repeats. *Hum Mol Genet*. Vol. 7, pp. 777-82.
- Li, S. H. and Li, X. J. (2004). Huntingtin-protein interactions and the pathogenesis of Huntington's disease. *Trends Genet*. Vol. 20, pp. 146-54.
- Li, X., Sapp, E., Valencia, A., Kegel, K. B., Qin, Z. H., Alexander, J., Masso, N., Reeves, P., et al. (2008). A function of huntingtin in guanine nucleotide exchange on Rab11. *Neuroreport*. Vol. 19, pp. 1643-7.
- Li, X., Sapp, E., Chase, K., Comer-Tierney, L. A., Masso, N., Alexander, J., Reeves, P., Kegel, K. B., et al. (2009, a). Disruption of Rab11 activity in a knock-in mouse model of Huntington's disease. *Neurobiol Dis*. Vol. 36, pp. 374-83.
- Li, X., Standley, C., Sapp, E., Valencia, A., Qin, Z. H., Kegel, K. B., Yoder, J., Comer-Tierney, L. A., et al. (2009, b). Mutant huntingtin impairs vesicle formation from recycling endosomes by interfering with Rab11 activity. *Mol Cell Biol*. Vol. 29, pp. 6106-16.
- Lin, S. X., Gundersen, G. G. and Maxfield, F. R. (2002). Export from pericentriolar endocytic recycling compartment to cell surface depends on stable, detyrosinated (glu) microtubules and kinesin. *Mol Biol Cell*. Vol. 13, pp. 96-109.
- Lonze, B. E. and Ginty, D. D. (2002). Function and regulation of CREB family transcription factors in the nervous system. *Neuron*. Vol. 35, pp. 605-23.

- Lunkes, A. and Mandel, J. L. (1998). A cellular model that recapitulates major pathogenic steps of Huntington's disease. *Hum Mol Genet.* Vol. 7, pp. 1355-61.
- Luo, S., Vacher, C., Davies, J. E. and Rubinsztein, D. C. (2005). Cdk5 phosphorylation of huntingtin reduces its cleavage by caspases: implications for mutant huntingtin toxicity. *J Cell Biol.* Vol. 169, pp. 647-56.
- Luthi-Carter, R., Strand, A., Peters, N. L., Solano, S. M., Hollingsworth, Z. R., Menon, A. S., Frey, A. S., Spektor, B. S., et al. (2000). Decreased expression of striatal signaling genes in a mouse model of Huntington's disease. *Hum Mol Genet.* Vol. 9, pp. 1259-71.
- Lyon, I. W. (1863). Chronic hereditary chorea. *Amer med Times.* Vol. 7, p. 289.
- MacDonald, M. E., Vonsattel, J. P., Shrinidhi, J., Couropmitree, N. N., Cupples, L. A., Bird, E. D., Gusella, J. F. and Myers, R. H. (1999). Evidence for the GluR6 gene associated with younger onset age of Huntington's disease. *Neurology.* Vol. 53, pp. 1330-2.
- Mangiarini, L., Sathasivam, K., Seller, M., Cozens, B., Harper, A., Hetherington, C., Lawton, M., Trotter, Y., et al. (1996). Exon 1 of the HD gene with an expanded CAG repeat is sufficient to cause a progressive neurological phenotype in transgenic mice. *Cell.* Vol. 87, pp. 493-506.
- Manley, K., Shirley, T. L., Flaherty, L. and Messer, A. (1999). Msh2 deficiency prevents in vivo somatic instability of the CAG repeat in Huntington disease transgenic mice. *Nat Genet.* Vol. 23, pp. 471-3.
- Martindale, D., Hackam, A., Wieczorek, A., Ellerby, L., Wellington, C., McCutcheon, K., Singaraja, R., Kazemi-Esfarjani, P., et al. (1998). Length of huntingtin and its polyglutamine tract influences localization and frequency of intracellular aggregates. *Nat Genet.* Vol. 18, pp. 150-4.
- Maxfield, F. R. and McGraw, T. E. (2004). Endocytic recycling. *Nat Rev Mol Cell Biol.* Vol. 5, pp. 121-32.
- Menalled, L. B., Sison, J. D., Dragatsis, I., Zeitlin, S. and Chesselet, M. F. (2003). Time course of early motor and neuropathological anomalies in a knock-in mouse model of Huntington's disease with 140 CAG repeats. *J Comp Neurol.* Vol. 465, pp. 11-26.

- Metzger, S., Bauer, P., Tomiuk, J., Laccone, F., Didonato, S., Gellera, C., Mariotti, C., Lange, H. W., et al. (2006). Genetic analysis of candidate genes modifying the age-at-onset in Huntington's disease. *Hum Genet.* Vol. 120, pp. 285-92.
- Metzger, S., Rong, J., Nguyen, H. P., Cape, A., Tomiuk, J., Soehn, A. S., Propping, P., Freudenberg-Hua, Y., et al. (2008). Huntingtin-associated protein-1 is a modifier of the age-at-onset of Huntington's disease. *Hum Mol Genet.* Vol. 17, pp. 1137-46.
- Miller, V. M., Nelson, R. F., Gouvion, C. M., Williams, A., Rodriguez-Lebron, E., Harper, S. Q., Davidson, B. L., Rebagliati, M. R., et al. (2005). CHIP suppresses polyglutamine aggregation and toxicity in vitro and in vivo. *J Neurosci.* Vol. 25, pp. 9152-61.
- Mitra, S., Tsvetkov, A. S. and Finkbeiner, S. (2009). Single neuron ubiquitin-proteasome dynamics accompanying inclusion body formation in huntington disease. *J Biol Chem.* Vol. 284, pp. 4398-403.
- Muchowski, P. J., Ning, K., D'Souza-Schorey, C. and Fields, S. (2002). Requirement of an intact microtubule cytoskeleton for aggregation and inclusion body formation by a mutant huntingtin fragment. *Proc Natl Acad Sci U S A.* Vol. 99, pp. 727-32.
- Nasir, J., Floresco, S. B., O'Kusky, J. R., Diewert, V. M., Richman, J. M., Zeisler, J., Borowski, A., Marth, J. D., et al. (1995). Targeted disruption of the Huntington's disease gene results in embryonic lethality and behavioral and morphological changes in heterozygotes. *Cell.* Vol. 81, pp. 811-23.
- Naze, P., Vuillaume, I., Destee, A., Pasquier, F. and Sablonniere, B. (2002). Mutation analysis and association studies of the ubiquitin carboxy-terminal hydrolase L1 gene in Huntington's disease. *Neurosci Lett.* Vol. 328, pp. 1-4.
- Neuwald, A. F. and Hirano, T. (2000). HEAT repeats associated with condensins, cohesins, and other complexes involved in chromosome-related functions. *Genome Res.* Vol. 10, pp. 1445-52.
- Newpher, T. M. and Ehlers, M. D. (2008). Glutamate receptor dynamics in dendritic microdomains. *Neuron.* Vol. 58, pp. 472-97.

- Newpher, T. M. and Ehlers, M. D. (2009). Spine microdomains for postsynaptic signaling and plasticity. *Trends Cell Biol.* Vol. 19, pp. 218-27.
- Nucifora, F. C., Jr., Sasaki, M., Peters, M. F., Huang, H., Cooper, J. K., Yamada, M., Takahashi, H., Tsuji, S., et al. (2001). Interference by huntingtin and atrophin-1 with cbp-mediated transcription leading to cellular toxicity. *Science.* Vol. 291, pp. 2423-8.
- Ordway, J. M., Tallaksen-Greene, S., Gutekunst, C. A., Bernstein, E. M., Cearley, J. A., Wiener, H. W., Dure, L. S. t., Lindsey, R., et al. (1997). Ectopically expressed CAG repeats cause intranuclear inclusions and a progressive late onset neurological phenotype in the mouse. *Cell.* Vol. 91, pp. 753-63.
- Owen, B. A., Yang, Z., Lai, M., Gajec, M., Badger, J. D., 2nd, Hayes, J. J., Edelmann, W., Kucherlapati, R., et al. (2005). (CAG)(n)-hairpin DNA binds to Msh2-Msh3 and changes properties of mismatch recognition. *Nat Struct Mol Biol.* Vol. 12, pp. 663-70.
- Pallos, J., Bodai, L., Lukacsovich, T., Purcell, J. M., Steffan, J. S., Thompson, L. M. and Marsh, J. L. (2008). Inhibition of specific HDACs and sirtuins suppresses pathogenesis in a Drosophila model of Huntington's disease. *Hum Mol Genet.* Vol. 17, pp. 3767-75.
- Panov, A. V., Gutekunst, C. A., Leavitt, B. R., Hayden, M. R., Burke, J. R., Strittmatter, W. J. and Greenamyre, J. T. (2002). Early mitochondrial calcium defects in Huntington's disease are a direct effect of polyglutamines. *Nat Neurosci.* Vol. 5, pp. 731-6.
- Park, M., Penick, E. C., Edwards, J. G., Kauer, J. A. and Ehlers, M. D. (2004). Recycling endosomes supply AMPA receptors for LTP. *Science.* Vol. 305, pp. 1972-5.
- Park, M., Salgado, J. M., Ostroff, L., Helton, T. D., Robinson, C. G., Harris, K. M. and Ehlers, M. D. (2006). Plasticity-induced growth of dendritic spines by exocytic trafficking from recycling endosomes. *Neuron.* Vol. 52, pp. 817-30.
- Pavese, N., Gerhard, A., Tai, Y. F., Ho, A. K., Turkheimer, F., Barker, R. A., Brooks, D. J. and Piccini, P. (2006). Microglial activation correlates with severity in Huntington disease: a clinical and PET study. *Neurology.* Vol. 66, pp. 1638-43.

- Perutz, M. F., Johnson, T., Suzuki, M. and Finch, J. T. (1994). Glutamine repeats as polar zippers: their possible role in inherited neurodegenerative diseases. *Proc Natl Acad Sci U S A*. Vol. 91, pp. 5355-8.
- Perutz, M. F., Finch, J. T., Berriman, J. and Lesk, A. (2002). Amyloid fibers are water-filled nanotubes. *Proc Natl Acad Sci U S A*. Vol. 99, pp. 5591-5.
- Petersen, A., Chase, K., Puschban, Z., DiFiglia, M., Brundin, P. and Aronin, N. (2002). Maintenance of susceptibility to neurodegeneration following intrastriatal injections of quinolinic acid in a new transgenic mouse model of Huntington's disease. *Exp Neurol*. Vol. 175, pp. 297-300.
- Petrini, E. M., Lu, J., Cognet, L., Lounis, B., Ehlers, M. D. and Choquet, D. (2009). Endocytic trafficking and recycling maintain a pool of mobile surface AMPA receptors required for synaptic potentiation. *Neuron*. Vol. 63, pp. 92-105.
- Pratt, G. and Rechsteiner, M. (2008). Proteasomes cleave at multiple sites within polyglutamine tracts: activation by PA28gamma(K188E). *J Biol Chem*. Vol. 283, pp. 12919-25.
- Qin, Z. H., Wang, Y., Kegel, K. B., Kazantsev, A., Apostol, B. L., Thompson, L. M., Yoder, J., Aronin, N., et al. (2003). Autophagy Regulates the Processing of Amino Terminal Huntingtin Fragments. *Hum Mol Genet*.
- Rangone, H., Poizat, G., Troncoso, J., Ross, C. A., MacDonald, M. E., Saudou, F. and Humbert, S. (2004). The serum- and glucocorticoid-induced kinase SGK inhibits mutant huntingtin-induced toxicity by phosphorylating serine 421 of huntingtin. *Eur J Neurosci*. Vol. 19, pp. 273-9.
- Ravikumar, B., Duden, R. and Rubinsztein, D. C. (2002). Aggregate-prone proteins with polyglutamine and polyalanine expansions are degraded by autophagy. *Hum Mol Genet*. Vol. 11, pp. 1107-17.
- Ravikumar, B., Vacher, C., Berger, Z., Davies, J. E., Luo, S., Oroz, L. G., Scaravilli, F., Easton, D. F., et al. (2004). Inhibition of mTOR induces autophagy and reduces toxicity of polyglutamine expansions in fly and mouse models of Huntington disease. *Nat Genet*. Vol. 36, pp. 585-95.
- Ren, M., Xu, G., Zeng, J., De Lemos-Chiarandini, C., Adesnik, M. and Sabatini, D. D. (1998). Hydrolysis of GTP on rab11 is required for the direct

- delivery of transferrin from the pericentriolar recycling compartment to the cell surface but not from sorting endosomes. *Proc Natl Acad Sci U S A*. Vol. 95, pp. 6187-92.
- Ridley, R. M., Frith, C. D., Crow, T. J. and Conneally, P. M. (1988). Anticipation in Huntington's disease is inherited through the male line but may originate in the female. *J Med Genet*. Vol. 25, pp. 589-95.
- Rigamonti, D., Bauer, J. H., De-Fraja, C., Conti, L., Sipione, S., Sciorati, C., Clementi, E., Hackam, A., et al. (2000). Wild-type huntingtin protects from apoptosis upstream of caspase-3. *J Neurosci*. Vol. 20, pp. 3705-13.
- Rigamonti, D., Sipione, S., Goffredo, D., Zuccato, C., Fossale, E. and Cattaneo, E. (2001). Huntingtin's neuroprotective activity occurs via inhibition of procaspase-9 processing. *J Biol Chem*. Vol. 276, pp. 14545-8.
- Rong, J., McGuire, J. R., Fang, Z. H., Sheng, G., Shin, J. Y., Li, S. H. and Li, X. J. (2006). Regulation of intracellular trafficking of huntingtin-associated protein-1 is critical for TrkA protein levels and neurite outgrowth. *J Neurosci*. Vol. 26, pp. 6019-30.
- Ross, C. A. and Poirier, M. A. (2004). Protein aggregation and neurodegenerative disease. *Nat Med*. Vol. 10 Suppl, pp. S10-7.
- Rubinsztein, D. C., Leggo, J., Coles, R., Almqvist, E., Biancalana, V., Cassiman, J. J., Chotai, K., Connarty, M., et al. (1996). Phenotypic characterization of individuals with 30-40 CAG repeats in the Huntington disease (HD) gene reveals HD cases with 36 repeats and apparently normal elderly individuals with 36-39 repeats. *Am J Hum Genet*. Vol. 59, pp. 16-22.
- Rubinsztein, D. C., Leggo, J., Chiano, M., Dodge, A., Norbury, G., Rosser, E. and Craufurd, D. (1997). Genotypes at the GluR6 kainate receptor locus are associated with variation in the age of onset of Huntington disease. *Proc Natl Acad Sci U S A*. Vol. 94, pp. 3872-6.
- Ryu, H., Lee, J., Hagerty, S. W., Soh, B. Y., McAlpin, S. E., Cormier, K. A., Smith, K. M. and Ferrante, R. J. (2006). ESET/SETDB1 gene expression and histone H3 (K9) trimethylation in Huntington's disease. *Proc Natl Acad Sci U S A*. Vol. 103, pp. 19176-81.
- Sapp, E., Kegel, K. B., Aronin, N., Hashikawa, T., Uchiyama, Y., Tohyama, K., Bhide, P. G., Vonsattel, J. P., et al. (2001). Early and progressive

- accumulation of reactive microglia in the Huntington disease brain. *J Neuropathol Exp Neurol*. Vol. 60, pp. 161-72.
- Sarkar, S., Perlstein, E. O., Imarisio, S., Pineau, S., Cordenier, A., Maglathlin, R. L., Webster, J. A., Lewis, T. A., et al. (2007). Small molecules enhance autophagy and reduce toxicity in Huntington's disease models. *Nat Chem Biol*. Vol. 3, pp. 331-8.
- Sarkar, S., Ravikumar, B., Floto, R. A. and Rubinsztein, D. C. (2009). Rapamycin and mTOR-independent autophagy inducers ameliorate toxicity of polyglutamine-expanded huntingtin and related proteinopathies. *Cell Death Differ*. Vol. 16, pp. 46-56.
- Scherzinger, E., Lurz, R., Turmaine, M., Mangiarini, L., Hollenbach, B., Hasenbank, R., Bates, G. P., Davies, S. W., et al. (1997). Huntingtin-encoded polyglutamine expansions form amyloid-like protein aggregates in vitro and in vivo. *Cell*. Vol. 90, pp. 549-58.
- Scherzinger, E., Sittler, A., Schweiger, K., Heiser, V., Lurz, R., Hasenbank, R., Bates, G. P., Lehrach, H., et al. (1999). Self-assembly of polyglutamine-containing huntingtin fragments into amyloid-like fibrils: implications for Huntington's disease pathology. *Proc Natl Acad Sci U S A*. Vol. 96, pp. 4604-9.
- Schilling, B., Gafni, J., Torcassi, C., Cong, X., Row, R. H., LaFevre-Bernt, M. A., Cusack, M. P., Ratovitski, T., et al. (2006). Huntingtin phosphorylation sites mapped by mass spectrometry. Modulation of cleavage and toxicity. *J Biol Chem*. Vol. 281, pp. 23686-97.
- Schmidt, M. R. and Haucke, V. (2007). Recycling endosomes in neuronal membrane traffic. *Biol Cell*. Vol. 99, pp. 333-42.
- Schwarcz, R., Whetsell, W. O., Jr. and Mangano, R. M. (1983). Quinolinic acid: an endogenous metabolite that produces axon-sparing lesions in rat brain. *Science*. Vol. 219, pp. 316-8.
- Sharp, A. H., Loev, S. J., Schilling, G., Li, S. H., Li, X. J., Bao, J., Wagster, M. V., Kotzuk, J. A., et al. (1995). Widespread expression of Huntington's disease gene (IT15) protein product. *Neuron*. Vol. 14, pp. 1065-74.
- Shelbourne, P. F., Keller-McGandy, C., Bi, W. L., Yoon, S. R., Dubeau, L., Veitch, N. J., Vonsattel, J. P., Wexler, N. S., et al. (2007). Triplet repeat mutation length gains correlate with cell-type specific vulnerability in

- Huntington disease brain. *Hum Mol Genet.* Vol. 16, pp. 1133-42.
- Shimojo, M. (2008). Huntingtin regulates RE1-silencing transcription factor/neuron-restrictive silencer factor (REST/NRSF) nuclear trafficking indirectly through a complex with REST/NRSF-interacting LIM domain protein (RILP) and dynactin p150 Glued. *J Biol Chem.* Vol. 283, pp. 34880-6.
- Sikorski, P. and Atkins, E. (2005). New model for crystalline polyglutamine assemblies and their connection with amyloid fibrils. *Biomacromolecules.* Vol. 6, pp. 425-32.
- Sittler, A., Lurz, R., Lueder, G., Priller, J., Lehrach, H., Hayer-Hartl, M. K., Hartl, F. U. and Wanker, E. E. (2001). Geldanamycin activates a heat shock response and inhibits huntingtin aggregation in a cell culture model of Huntington's disease. *Hum Mol Genet.* Vol. 10, pp. 1307-15.
- Slow, E. J., van Raamsdonk, J., Rogers, D., Coleman, S. H., Graham, R. K., Deng, Y., Oh, R., Bissada, N., et al. (2003). Selective striatal neuronal loss in a YAC128 mouse model of Huntington disease. *Hum Mol Genet.* Vol. 12, pp. 1555-67.
- Slow, E. J., Graham, R. K., Osmand, A. P., Devon, R. S., Lu, G., Deng, Y., Pearson, J., Vaid, K., et al. (2005). Absence of behavioral abnormalities and neurodegeneration in vivo despite widespread neuronal huntingtin inclusions. *Proc Natl Acad Sci U S A.* Vol. 102, pp. 11402-7.
- Snell, R. G., MacMillan, J. C., Cheadle, J. P., Fenton, I., Lazarou, L. P., Davies, P., MacDonald, M. E., Gusella, J. F., et al. (1993). Relationship between trinucleotide repeat expansion and phenotypic variation in Huntington's disease. *Nat Genet.* Vol. 4, pp. 393-7.
- Squitieri, F., Gellera, C., Cannella, M., Mariotti, C., Cislighi, G., Rubinsztein, D. C., Almqvist, E. W., Turner, D., et al. (2003). Homozygosity for CAG mutation in Huntington disease is associated with a more severe clinical course. *Brain.* Vol. 126, pp. 946-55.
- Stack, E. C., Kubilus, J. K., Smith, K., Cormier, K., Del Signore, S. J., Guelin, E., Ryu, H., Hersch, S. M., et al. (2005). Chronology of behavioral symptoms and neuropathological sequela in R6/2 Huntington's disease transgenic mice. *J Comp Neurol.* Vol. 490, pp. 354-70.

- Stack, E. C., Del Signore, S. J., Luthi-Carter, R., Soh, B. Y., Goldstein, D. R., Matson, S., Goodrich, S., Markey, A. L., et al. (2007). Modulation of nucleosome dynamics in Huntington's disease. *Hum Mol Genet.* Vol. 16, pp. 1164-75.
- Steffan, J. S., Kazantsev, A., Spasic-Boskovic, O., Greenwald, M., Zhu, Y. Z., Gohler, H., Wanker, E. E., Bates, G. P., et al. (2000). The Huntington's disease protein interacts with p53 and CREB-binding protein and represses transcription. *Proc Natl Acad Sci U S A.* Vol. 97, pp. 6763-8.
- Steffan, J. S., Bodai, L., Pallos, J., Poelman, M., McCampbell, A., Apostol, B. L., Kazantsev, A., Schmidt, E., et al. (2001). Histone deacetylase inhibitors arrest polyglutamine-dependent neurodegeneration in *Drosophila*. *Nature.* Vol. 413, pp. 739-43.
- Stenmark, H. (2009). Rab GTPases as coordinators of vesicle traffic. *Nat Rev Mol Cell Biol.* Vol. 10, pp. 513-25.
- St-Pierre, J., Drori, S., Uldry, M., Silvaggi, J. M., Rhee, J., Jager, S., Handschin, C., Zheng, K., et al. (2006). Suppression of reactive oxygen species and neurodegeneration by the PGC-1 transcriptional coactivators. *Cell.* Vol. 127, pp. 397-408.
- Strong, T. V., Tagle, D. A., Valdes, J. M., Elmer, L. W., Boehm, K., Swaroop, M., Kaatz, K. W., Collins, F. S., et al. (1993). Widespread expression of the human and rat Huntington's disease gene in brain and nonneural tissues. *Nat Genet.* Vol. 5, pp. 259-65.
- Sugars, K. L., Brown, R., Cook, L. J., Swartz, J. and Rubinsztein, D. C. (2004). Decreased cAMP response element-mediated transcription: an early event in exon 1 and full-length cell models of Huntington's disease that contributes to polyglutamine pathogenesis. *J Biol Chem.* Vol. 279, pp. 4988-99.
- Suhr, S. T., Senut, M. C., Whitelegge, J. P., Faull, K. F., Cuizon, D. B. and Gage, F. H. (2001). Identities of sequestered proteins in aggregates from cells with induced polyglutamine expression. *J Cell Biol.* Vol. 153, pp. 283-94.
- Taherzadeh-Fard, E., Saft, C., Andrich, J., Wieczorek, S. and Arning, L. (2009). PGC-1alpha as modifier of onset age in Huntington disease. *Mol Neurodegener.* Vol. 4, p. 10.

- Tai, Y. F., Pavese, N., Gerhard, A., Tabrizi, S. J., Barker, R. A., Brooks, D. J. and Piccini, P. (2007). Microglial activation in presymptomatic Huntington's disease gene carriers. *Brain*. Vol. 130, pp. 1759-66.
- Tam, S., Geller, R., Spiess, C. and Frydman, J. (2006). The chaperonin TRiC controls polyglutamine aggregation and toxicity through subunit-specific interactions. *Nat Cell Biol*. Vol. 8, pp. 1155-62.
- Taylor, J. P., Tanaka, F., Robitschek, J., Sandoval, C. M., Taye, A., Markovic-Plese, S. and Fischbeck, K. H. (2003). Aggresomes protect cells by enhancing the degradation of toxic polyglutamine-containing protein. *Hum Mol Genet*. Vol. 12, pp. 749-57.
- Telenius, H., Kremer, H. P., Theilmann, J., Andrew, S. E., Almqvist, E., Anvret, M., Greenberg, C., Greenberg, J., et al. (1993). Molecular analysis of juvenile Huntington disease: the major influence on (CAG)<sub>n</sub> repeat length is the sex of the affected parent. *Hum Mol Genet*. Vol. 2, pp. 1535-40.
- Telenius, H., Kremer, B., Goldberg, Y. P., Theilmann, J., Andrew, S. E., Zeisler, J., Adam, S., Greenberg, C., et al. (1994). Somatic and gonadal mosaicism of the Huntington disease gene CAG repeat in brain and sperm. *Nat Genet*. Vol. 6, pp. 409-14.
- Telenius, H., Almqvist, E., Kremer, B., Spence, N., Squitieri, F., Nichol, K., Grandell, U., Starr, E., et al. (1995). Somatic mosaicism in sperm is associated with intergenerational (CAG)<sub>n</sub> changes in Huntington disease. *Hum Mol Genet*. Vol. 4, pp. 189-95.
- The Huntington's Disease Collaborative Research Group (1993). A novel gene containing a trinucleotide repeat that is expanded and unstable on Huntington's disease chromosomes. *Cell*. Vol. 72, pp. 971-83.
- Thomas, E. A., Coppola, G., Desplats, P. A., Tang, B., Soragni, E., Burnett, R., Gao, F., Fitzgerald, K. M., et al. (2008). The HDAC inhibitor 4b ameliorates the disease phenotype and transcriptional abnormalities in Huntington's disease transgenic mice. *Proc Natl Acad Sci U S A*. Vol. 105, pp. 15564-9.
- Torres-Peraza, J. F., Giralt, A., Garcia-Martinez, J. M., Pedrosa, E., Canals, J. M. and Alberch, J. (2008). Disruption of striatal glutamatergic transmission induced by mutant huntingtin involves remodeling of both postsynaptic density and NMDA receptor signaling. *Neurobiol Dis*. Vol.

29, pp. 409-21.

- Trischler, M., Stoorvogel, W. and Ullrich, O. (1999). Biochemical analysis of distinct Rab5- and Rab11-positive endosomes along the transferrin pathway. *J Cell Sci.* Vol. 112 ( Pt 24), pp. 4773-83.
- Trottier, Y., Devys, D., Imbert, G., Saudou, F., An, I., Lutz, Y., Weber, C., Agid, Y., et al. (1995). Cellular localization of the Huntington's disease protein and discrimination of the normal and mutated form. *Nat Genet.* Vol. 10, pp. 104-10.
- Trushina, E., Dyer, R. B., Badger, J. D., 2nd, Ure, D., Eide, L., Tran, D. D., Vrieze, B. T., Legendre-Guillemain, V., et al. (2004). Mutant huntingtin impairs axonal trafficking in mammalian neurons in vivo and in vitro. *Mol Cell Biol.* Vol. 24, pp. 8195-209.
- Trushina, E., Singh, R. D., Dyer, R. B., Cao, S., Shah, V. H., Parton, R. G., Pagano, R. E. and McMurray, C. T. (2006). Mutant huntingtin inhibits clathrin-independent endocytosis and causes accumulation of cholesterol in vitro and in vivo. *Hum Mol Genet.* Vol. 15, pp. 3578-91.
- Ullrich, O., Reinsch, S., Urbe, S., Zerial, M. and Parton, R. G. (1996). Rab11 regulates recycling through the pericentriolar recycling endosome. *J Cell Biol.* Vol. 135, pp. 913-24.
- Van Raamsdonk, J. M., Pearson, J., Rogers, D. A., Bissada, N., Vogl, A. W., Hayden, M. R. and Leavitt, B. R. (2005). Loss of wild-type huntingtin influences motor dysfunction and survival in the YAC128 mouse model of Huntington disease. *Hum Mol Genet.* Vol. 14, pp. 1379-92.
- Van Raamsdonk, J. M., Pearson, J., Murphy, Z., Hayden, M. R. and Leavitt, B. R. (2006). Wild-type huntingtin ameliorates striatal neuronal atrophy but does not prevent other abnormalities in the YAC128 mouse model of Huntington disease. *BMC Neurosci.* Vol. 7, p. 80.
- Velier, J., Kim, M., Schwarz, C., Kim, T. W., Sapp, E., Chase, K., Aronin, N. and DiFiglia, M. (1998). Wild-type and mutant huntingtins function in vesicle trafficking in the secretory and endocytic pathways. *Exp Neurol.* Vol. 152, pp. 34-40.
- Venkatraman, P., Wetzel, R., Tanaka, M., Nukina, N. and Goldberg, A. L. (2004). Eukaryotic proteasomes cannot digest polyglutamine sequences and release them during degradation of polyglutamine-containing

- proteins. *Mol Cell*. Vol. 14, pp. 95-104.
- Vetter, I. R., Arndt, A., Kutay, U., Gorlich, D. and Wittinghofer, A. (1999). Structural view of the Ran-Importin beta interaction at 2.3 Å resolution. *Cell*. Vol. 97, pp. 635-46.
- Volpicelli, L. A., Lah, J. J., Fang, G., Goldenring, J. R. and Levey, A. I. (2002). Rab11a and myosin Vb regulate recycling of the M4 muscarinic acetylcholine receptor. *J Neurosci*. Vol. 22, pp. 9776-84.
- Vonsattel, J. P., Myers, R. H., Stevens, T. J., Ferrante, R. J., Bird, E. D. and Richardson, E. P., Jr. (1985). Neuropathological classification of Huntington's disease. *J Neuropathol Exp Neurol*. Vol. 44, pp. 559-77.
- Vonsattel, J. P. and DiFiglia, M. (1998). Huntington disease. *J Neuropathol Exp Neurol*. Vol. 57, pp. 369-84.
- Waelter, S., Boeddrich, A., Lurz, R., Scherzinger, E., Lueder, G., Lehrach, H. and Wanker, E. E. (2001). Accumulation of mutant huntingtin fragments in aggresome-like inclusion bodies as a result of insufficient protein degradation. *Mol Biol Cell*. Vol. 12, pp. 1393-407.
- Wang, Z., Edwards, J. G., Riley, N., Provance, D. W., Jr., Karcher, R., Li, X. D., Davison, I. G., Ikebe, M., et al. (2008). Myosin Vb mobilizes recycling endosomes and AMPA receptors for postsynaptic plasticity. *Cell*. Vol. 135, pp. 535-48.
- Warby, S. C., Chan, E. Y., Metzler, M., Gan, L., Singaraja, R. R., Crocker, S. F., Robertson, H. A. and Hayden, M. R. (2005). Huntingtin phosphorylation on serine 421 is significantly reduced in the striatum and by polyglutamine expansion in vivo. *Hum Mol Genet*. Vol. 14, pp. 1569-77.
- Warby, S. C., Doty, C. N., Graham, R. K., Shively, J., Singaraja, R. R. and Hayden, M. R. (2009). Phosphorylation of huntingtin reduces the accumulation of its nuclear fragments. *Mol Cell Neurosci*. Vol. 40, pp. 121-7.
- Waters, C. O. (1848). Letter on chorea. In *The Practice of Medicine*, by R. Dunglison, 3rd ed., Vol. 2, p. 216. Lea and Blanchard, Philadelphia.
- Webb, J. L., Ravikumar, B. and Rubinsztein, D. C. (2004). Microtubule disruption inhibits autophagosome-lysosome fusion: implications for studying the roles of aggresomes in polyglutamine diseases. *Int J Biochem Cell Biol*. Vol. 36, pp. 2541-50.

- Wellington, C. L., Singaraja, R., Ellerby, L., Savill, J., Roy, S., Leavitt, B., Cattaneo, E., Hackam, A., et al. (2000). Inhibiting caspase cleavage of huntingtin reduces toxicity and aggregate formation in neuronal and nonneuronal cells. *J Biol Chem*. Vol. 275, pp. 19831-8.
- Wexler, N. S., Young, A. B., Tanzi, R. E., Travers, H., Starosta-Rubinstein, S., Penney, J. B., Snodgrass, S. R., Shoulson, I., et al. (1987). Homozygotes for Huntington's disease. *Nature*. Vol. 326, pp. 194-7.
- Wexler, N. S., Lorimer, J., Porter, J., Gomez, F., Moskowitz, C., Shackell, E., Marder, K., Penchaszadeh, G., et al. (2004). Venezuelan kindreds reveal that genetic and environmental factors modulate Huntington's disease age of onset. *Proc Natl Acad Sci U S A*. Vol. 101, pp. 3498-503.
- Weydt, P., Pineda, V. V., Torrence, A. E., Libby, R. T., Satterfield, T. F., Lazarowski, E. R., Gilbert, M. L., Morton, G. J., et al. (2006). Thermoregulatory and metabolic defects in Huntington's disease transgenic mice implicate PGC-1alpha in Huntington's disease neurodegeneration. *Cell Metab*. Vol. 4, pp. 349-62.
- Weydt, P., Soyal, S. M., Gellera, C., Didonato, S., Weidinger, C., Oberkofler, H., Landwehrmeyer, G. B. and Patsch, W. (2009). The gene coding for PGC-1alpha modifies age at onset in Huntington's Disease. *Mol Neurodegener*. Vol. 4, p. 3.
- Wheeler, V. C., Lebel, L. A., Vrbanac, V., Teed, A., te Riele, H. and MacDonald, M. E. (2003). Mismatch repair gene Msh2 modifies the timing of early disease in Hdh(Q111) striatum. *Hum Mol Genet*. Vol. 12, pp. 273-81.
- White, J. K., Auerbach, W., Duyao, M. P., Vonsattel, J. P., Gusella, J. F., Joyner, A. L. and MacDonald, M. E. (1997). Huntingtin is required for neurogenesis and is not impaired by the Huntington's disease CAG expansion. *Nat Genet*. Vol. 17, pp. 404-10.
- Wilcke, M., Johannes, L., Galli, T., Mayau, V., Goud, B. and Salamero, J. (2000). Rab11 regulates the compartmentalization of early endosomes required for efficient transport from early endosomes to the trans-golgi network. *J Cell Biol*. Vol. 151, pp. 1207-20.
- Wytenbach, A., Carmichael, J., Swartz, J., Furlong, R. A., Narain, Y., Rankin, J. and Rubinsztein, D. C. (2000). Effects of heat shock, heat shock protein 40 (HDJ-2), and proteasome inhibition on protein aggregation in cellular

- models of Huntington's disease. *Proc Natl Acad Sci U S A*. Vol. 97, pp. 2898-903.
- Wytttenbach, A., Swartz, J., Kita, H., Thykjaer, T., Carmichael, J., Bradley, J., Brown, R., Maxwell, M., et al. (2001). Polyglutamine expansions cause decreased CRE-mediated transcription and early gene expression changes prior to cell death in an inducible cell model of Huntington's disease. *Hum Mol Genet*. Vol. 10, pp. 1829-45.
- Yu, Z. X., Li, S. H., Nguyen, H. P. and Li, X. J. (2002). Huntingtin inclusions do not deplete polyglutamine-containing transcription factors in HD mice. *Hum Mol Genet*. Vol. 11, pp. 905-14.
- Zala, D., Colin, E., Rangone, H., Liot, G., Humbert, S. and Saudou, F. (2008). Phosphorylation of mutant huntingtin at S421 restores anterograde and retrograde transport in neurons. *Hum Mol Genet*. Vol. 17, pp. 3837-46.
- Zeitlin, S., Liu, J. P., Chapman, D. L., Papaioannou, V. E. and Efstratiadis, A. (1995). Increased apoptosis and early embryonic lethality in mice nullizygous for the Huntington's disease gene homologue. *Nat Genet*. Vol. 11, pp. 155-63.
- Zeng, J., Ren, M., Gravotta, D., De Lemos-Chiarandini, C., Lui, M., Erdjument-Bromage, H., Tempst, P., Xu, G., et al. (1999). Identification of a putative effector protein for rab11 that participates in transferrin recycling. *Proc Natl Acad Sci U S A*. Vol. 96, pp. 2840-5.
- Zerial, M. and McBride, H. (2001). Rab proteins as membrane organizers. *Nat Rev Mol Cell Biol*. Vol. 2, pp. 107-17.
- Zeron, M. M., Hansson, O., Chen, N., Wellington, C. L., Leavitt, B. R., Brundin, P., Hayden, M. R. and Raymond, L. A. (2002). Increased sensitivity to N-methyl-D-aspartate receptor-mediated excitotoxicity in a mouse model of Huntington's disease. *Neuron*. Vol. 33, pp. 849-60.
- Zhang, Y., Leavitt, B. R., van Raamsdonk, J. M., Dragatsis, I., Goldowitz, D., MacDonald, M. E., Hayden, M. R. and Friedlander, R. M. (2006). Huntingtin inhibits caspase-3 activation. *Embo J*. Vol. 25, pp. 5896-906.
- Zoghbi, H. Y. and Orr, H. T. (2000). Glutamine repeats and neurodegeneration. *Annu Rev Neurosci*. Vol. 23, pp. 217-47.
- Zuccato, C., Ciammola, A., Rigamonti, D., Leavitt, B. R., Goffredo, D., Conti, L., MacDonald, M. E., Friedlander, R. M., et al. (2001). Loss of huntingtin-

mediated BDNF gene transcription in Huntington's disease. *Science*. Vol. 293, pp. 493-8.

Zuccato, C., Tartari, M., Crotti, A., Goffredo, D., Valenza, M., Conti, L., Cataudella, T., Leavitt, B. R., et al. (2003). Huntingtin interacts with REST/NRSF to modulate the transcription of NRSE-controlled neuronal genes. *Nat Genet*. Vol. 35, pp. 76-83.

Zuccato, C., Belyaev, N., Conforti, P., Ooi, L., Tartari, M., Papadimou, E., MacDonald, M., Fossale, E., et al. (2007). Widespread disruption of repressor element-1 silencing transcription factor/neuron-restrictive silencer factor occupancy at its target genes in Huntington's disease. *J Neurosci*. Vol. 27, pp. 6972-83.